Analysis of Low Temperature Trapping And Recombination In II—VI Compounds Using Photodielectric Techniques

By

James J. Hinds and William H. Hartwig
Department of Electrical Engineering

Technical Report No. 90
June 19, 1970

SOLID STATE ELECTRONICS RESEARCH LABORATORY

ELECTRONICS RESEARCH CENTER
The University of Texas at Austin
Austin, Texas 78712

The Electronics Research Center at The University of Texas at Austin constitutes interdisciplinary laboratories in which graduate faculty members and graduate candidates from numerous academic disciplines conduct research.

Research conducted for this technical report was supported in part by the Department of Defense's JOINT SERVICES ELECTRONICS PROGRAM (U.S. Army, U.S. Navy, and the U.S. Air Force) through the Research Grant AF-AFOSR 69-1792A. This program is monitored by the Department of Defense's JSEP Technical Advisory Committee consisting of representatives from the U.S. Army Electronics Command, U.S. Army Research Office, Office of Naval Research, and the U.S. Air Force Office of Scientific Research.

Additional support of specific projects by other Federal Agencies, Foundations, and The University of Texas at Austin is acknowledged in footnotes to the appropriate sections.

ANALYSIS OF LOW TEMPERATURE TRAPPING AND RECOMBINATION IN II-VI COMPOUNDS USING PHOTODIELECTRIC TECHNIQUES*

By

James J. Hinds and William H. Hartwig
Department of Electrical Engineering

Technical Report No. 90
June 19, 1970

Grant NGR 44-012-104
National Aeronautics and Space Administration

SOLID STATE ELECTRONICS RESEARCH LABORATORY

ELECTRONICS RESEARCH CENTER
THE UNIVERSITY OF TEXAS AT AUSTIN
Austin, Texas 78712

*Research sponsored in part by the Joint Services Electronics Program under Research Grant AFOSR 69-1792.

ANALYSIS OF LOW TEMPERATURE TRAPPING AND
RECOMBINATION IN II-VI COMPOUNDS USING
PHOTODIELECTRIC TECHNIQUES

ABSTRACT

In II-VI compounds at cryogenic temperatures, the photodielectric (PD) effect is the result of optically-induced changes in the densities of free and trapped carriers. Changes in both the real and imaginary parts of the complex dielectric constant are observable when the semiconductor is placed in a superconducting microwave cavity and irradiated with light. A change in the real part of the dielectric constant results in a sizeable change in the cavity resonant frequency, while a change in the imaginary part of the dielectric constant produces a change in the microwave power absorbed by the semiconductor. Equations are presented which relate the frequency change and power absorption change to the densities and binding energies of trapped carriers, and to the density of free carriers. The PD technique gives a direct measurement of both the free carrier density and the trapped carrier density.

Models involving trapping and recombination centers with selected properties are analyzed to reveal the relations between carrier

densities and other physical characteristics of the sample. Equations are written in forms which allow capture cross sections, recombination cross sections, trap ionization energies, and trap densities to be calculated from the time and temperature variations of the free and trapped carrier densities.

Samples of CdS:Al, CdS:Ag, CdTe, and ZnTe are analyzed, both with PD techniques and with other techniques such as thermally stimulated conductivity, and values for trap depths, densities, and capture cross sections are obtained and compared. In most cases where a comparison of methods is possible, results from the different techniques agree. In the remainder of the cases, photodielectric data, which gives a direct observation of trapped carrier behavior, gives significantly improved accuracy compared to the other techniques where trapped carrier behavior is only obtained indirectly. Results presented demonstrate that PD response spectra yield values for bandgaps and trap ionization energies. The time variation of the photodielectric response is used to reveal several traps which exist in one sample, and to separate trapped carrier effects from free carrier behavior. The direct observation of trap filling and emptying yields sufficient data to calculate trap depths, densities, and cross sections. The temperature dependence of the PD response gives additional information concerning trap ionization energies and cross sections. Data from the variation of the response with respect to light intensity greatly simplifies the choice of an energy band model.

It is demonstrated that in some cases, a photodielectric experiment is clearly more sensitive than other techniques, such as photoconductivity analysis, applied to the same material. The PD method is contactless, eliminating all of the problems associated with making

ohmic contacts. The successful application of PD techniques to a powdered sample is demonstrated. Even when the PD method is applied to single crystal samples, the fact that the behavior of trapped carriers is directly observed means that the method greatly improves an experimenter's ability to analyze and measure trapping and recombination parameters.

TABLE OF CONTENTS

LIST OF FIGURES

Figure | Page

LIST OF TABLES

CHAPTER I

INTRODUCTION

METHODS OF STUDYING CARRIER DYNAMICS

The recombination and trapping dynamics of semiconductors and insulators determine the behavior of many solid state devices. For example, the operation of photocells, radiation detectors, semiconductor lasers, and luminescent phosphors, as well as junction devices, such as transistors and diodes, is very sensitive to the type, density, ionization energy, and capture cross section of localized imperfections. Attempts to improve existing solid state devices or to create new ones are therefore certain to involve a study of the imperfection sites.

No single universal method exists for analyzing defect sites. Dozens of different experimental techniques have been put to use under various circumstances, but all are subject to restrictions in the type of sample, sensitivity and applicability of the measurement equipment, and in theoretical considerations. Bube[1] lists some of the schemes which are commonly applied in trapping and recombination studies; they may be divided into two groups, depending on whether direct electrical contact to the sample is made. In many cases, an experiment requiring ohmic contact is phenomenologically similar to one of the contactless procedures.

When ohmic contact may be made to a sample, some standard measurements are the variation of current with temperature, Hall effect, growth and decay of photoconductivity, thermally stimulated conductivity, photoconductivity spectra and quenching of conductivity, variation of photosensitivity with temperature or light intensity, space charge limited current dependence on voltage, and others. The variation of current

with temperature is a widely used method of determining donor and acceptor energies and the bandgap. The rate of ionization from a level to one of the bands is related to the Boltzmann factor, $e^{-E/kT}$. Tubota[2] and Segall, et al.[3] show that many of the acceptor levels found in ZnTe and CdTe are obtained using this technique. Materials must be relatively free of traps so that ionization of the donor or acceptor is not masked. Either the Hall effect or the Seebeck thermoelectric effect may be used to determine the conductivity type of the thermally freed carrier.

An analysis of the growth and decay of photoconductivity is the subject of three chapters of reference 1 by Bube. The rate equations for the interactions of carriers at various energy levels are obtained and are generally nonlinear and quite difficult to work with until considerably simplified for special cases. If a suitable model describing the states in the forbidden band is chosen, Bube, et al.[4] show that it is often possible to calculate imperfection densities and capture cross sections for the model. However, since the conductivity measurement only gives an indirect look at the behavior of trapped carriers, the selection of a proper model is subject to considerable error. It is often the case that several different models involving different trap distributions can affect the photoconductivity in identical ways.

The thermally stimulated conductivity technique (TSC), described by Haering and Adams[5] and Bube, et al.[6], is probably the most popular method of studying traps, but the interpretation of results is often made difficult when closely spaced levels and donors and acceptors exist in the sample. The traps are filled at a low temperature, and the

amount of thermally stimulated conductivity during warming is related to the rate of trap emptying and the recombination lifetime. Only a fraction of the forbidden band may be surveyed because of temperature limitations at both extremes. Other disadvantages of the technique are that properties of the trap can only be evaluated at one temperature, and the failure to know the degree of saturation of a trap can lead to errors in the results. In more favorable situations, however, TSC yields the depth, capture cross sections and approximate density of a trap.

The direct ionization energy of any level may be found by observing a photoconductivity spectrum and relating the photon energy to the ionization energy. The depth of a quenching level is found in the same manner from a spectrum of photoconductivity quenching. Data from Lambe, et al.[7] and Hemila and Bube[8] shows that neither technique is very sensitive unless the absorption is strong and the lifetime or response time is long enough to insure an observable free carrier density change. Peaks tend to spread, and therefore may be difficult to locate, when the light is not monochromatic or when phonon aborption or emission is a part of the transition. In general, very accurate values for the ionization energy are obtained, but calculation of other parameters of the level is not possible. The measurement is usually insensitive to imperfections with small densities.

Variations in photosensitivity $d\sigma/dT$ with changes in light intensity or temperature can be analyzed to locate carrier traps. When traps become filled, any given site is more likely to act as a recombination center than a trap; the Fermi level rises. The trap is located by calculating the Fermi level when the sensitivity changes. For best

results, the level should be monoenergetic since the movement of the Fermi level through a random distribution of traps is not easily analyzed.

Rose[9] gives a complete treatment of the relation between a distribution of traps and the variation of the space charge limited current in the crystal when the applied field and temperature are varied. The current is related to the charge required to fill the traps, and thus depends on the characteristics of the traps. The result is that simple trap distributions give easily recognized effects, and the total trap density may be estimated. It is also possible to find the depth of a single level. For complex distributions, the analysis is extremely complex, and hence this technique has not been widely used.

The experiments discussed above all have a common drawback: the need for ohmic contacts. In general, it is not easy to make ohmic contact to II-VI compounds[1]. For example, neutral contact to CdS reliably occurs only with In and Ga metals, which both melt at relatively low temperatures. In some instances, contacts of Al are also ohmic, and forming techniques frequently work. It is always necessary to test the contact to insure it behaves as expected. The difficulty of making ohmic contact to p-CdTe and ZnTe at low temperatures is well documented by Aven and Segall[10] and Schiozawa, et al.[11]. Furthermore, most of the II-VI compounds have very high resistivities at low temperatures, making characterization of the contacts difficult.

Methods requiring ohmic contacts are not easily applied to irregularly shaped crystals or to powders. Thus, some samples are analyzed using primarily the contactless methods. In samples which produce luminescence, very accurate measurements of energetic transitions are obtained

by relating the optical wavelength to the photon energy. When this technique may be used, very precise values of binding energies result, and it is also possible to determine the nature of the defect responsible for the emission. For example, Lambe[12,13] studied the effects of silver in CdS, Kulp, et al.[14] mapped the variation of binding energy in CdS due to temperature changes, and Blount, et al.[15] investigated effects of annealing in ZnS, all using luminescence data. Halsted[16] derived the expected ionization energies of various combinations of carriers bound at imperfections, using the hydrogen atom approximation, and applied the results to interpreting edge emission in II-VI compounds.

Garlick and Gibson[17] used thermally stimulated luminescence experiments to study trapping in sulfide and silicate phosphors. This technique is analogous to TSC, and has an advantage over luminescence spectra experiments in that the attempt-to-escape frequency of the trap may be found, and it is possible to judge whether retrapping at the luminescence center is important. Similarly, quenching of luminescence is analogous to photoconductivity quenching (see Broser[18], for example), and fluorescence growth and decay curves are analyzed in a manner similar to the investigation of photoconductivity growth and decay[17].

Although luminescence data yields valuable results in studying certain samples, there are many situations where these techniques are of little value. There is no simple method of finding densities of levels and their cross sections, and if the crystal exhibits a low fluorescence efficiency due to a relatively high degree of imperfection or due to the presence of "killer centers" (which allow the energy to decay in multiphonon processes rather than being emitted as photons), little or no luminescence results[18].

The absorption of light may be considered the inverse of luminescence, and absorption spectra may be analyzed in ways similar to those used to evaluate luminescence data. Segall[19] and Marple[20] have developed the relationships between the absorption coefficient and transition energies and applied them to CdTe in the absorption edge region. Lambe, et al.[7] and Halperin and Garlick[21] have used absorption measurements to investigate deeper levels. A related experiment is the measurement of reflectivity spectra, and Bube[22] has shown that this method is applicable to powders. Absorption and reflectivity curves do not yield values for densities and cross sections, and tend to be insensitive for levels with small concentrations.

From the preceding section, it should be clear that all of the standard experimental methods of analyzing trapping and recombination in II-VI compounds suffer from one or more disadvantages, and several of the techniques must be applied to a sample to extract all of the trapping and recombination parameters. Recent interest in the photodielectric effect, stimulated by Hartwig and co-workers[23-30], brought about this study of the use of the low temperature photodielectric effect as an alternate method of measuring trapping and recombination parameters in II-VI compounds.

HISTORY OF THE PHOTODIELECTRIC EFFECT

Before 1960, very little was known about the photodielectric effect in semiconductors and insulators. The experiments performed up to that time are summarized by Bube[1]. He lists three hypotheses used to explain apparent changes in the dielectric constants of photosensitive materials: (1) It is simply another way to detect a conductivity increase, with the enhanced conductivity effectively lessening the distance between

the plates of a dielectric filled capacitor and making it appear that a dielectric change has occurred. (2) It is a real dielectric constant change brought about by an increase in the sample polarizability as would occur when electrons are trapped. (3) It is a real change in the dielectric constant of non-single-crystal samples due to the existence of space charge trapped at grain boundaries.

Each theory had its supporters, although few experimenters found it desirable to perform the experiments. Measurements on CdS crystals by Kallman, et al.[31,32] led them to adopt the first theory because the capacitance change they observed decayed rapidly even though a deep trap existed. Broser, Brum, and Reuber[33] arrived at the same conclusion using CdS and making measurements at 78°K and 300 kHz; the results are explained with an equivalent circuit consisting of two capacitors and two photoresistors. Garlick and Gibson[34] found evidence for the second hypothesis in several powdered phosphors, including ZnS, but failed to observe any change in single crystals of ZnS and CdS. Garlick[35] then concluded that photodielectric changes occurred only in powders.

These early experiments suffered from lack of sensitivity due to the low measurement frequencies and high temperatures used. In 1961, Hartwig[23] and Genz[24] proposed use of the photodielectric effect at higher frequencies to detect infrared light. Experiments performed with Si and Ge samples in a 400 MHz coaxial cavity operated at 77°K revealed that the thermally generated carriers masked the effects of optically generated carriers. Arndt[25] then repeated the attempts to observe a photodielectric effect in semiconductors, and succeeded by using a superconducting cavity operating at 4.2°K. Stone[26] increased the measurement frequency

to ∿ 1 GHz and demonstrated a wide band optical detector and a tuneable tunnel diode oscillator, both relying on the photodielectric effect. More recently, work by Hinds[27] has been directed at improving detector sensitivity by using CdS as the active material, and Baker[28] thoroughly investigated means of characterizing the semiconductor sample in terms of material parameters pertinent to the photodielectric effect. Hartwig and Hinds[29] described the direct observation of electron trapping in CdS, and Stone, Hartwig and Baker[30] reported the use of the photodielectric effect in an optical feedback tuning system for a superconducting cavity.

Since carrier trapping effects were clearly seen in reference 27 and 29, it was felt that the photodielectric detector system could be used as a research tool in place of some of the standard methods of measuring trapping and recombination mentioned previously. The purpose of the work reported herein is to investigate the use of photodielectric techniques in analyzing low temperature trapping and recombination in II-VI compounds, and to compare photodielectric methods with the standard methods. Some of the pertinent characteristics of II-VI compounds, expected to have a bearing on the outcome, are listed in the following sections.

PROPERTIES OF CdS

Cadmium sulfide is probably the most widely studied II-VI compound. It exists mainly in the hexagonal wurtzite structure[36] and always exhibits n-type conductivity[37] because acceptor defects tend to be compensated by native defects. The hexagonal structure causes the energy bands to be anisotropic at k = 0 and, therefore, most of the transport properties are anisotropic. Some properties are listed in Table I-1, and average values are taken for the anisotropic parameters.

Table I-1

Properties of CdS, CdTe, and ZnTe

(Taken in part from Devlin[38])

Property	Units	Temperature	CdS	Reference	CdTe	Reference	ZnTe	Reference
E_g	eV	300	2.31	59	1.44	65	2.26	71
		77	2.54	60	1.59	66		
		4.2	2.58	61	1.606	20	2.391	58
m_e^*/m	-	-	0.204	61	0.096	67		
m_e^*/m	-	-	5.0 $\parallel c$	61	0.35	68	0.60	10
			0.7 $\perp c$	61				
μ_e	$cm^2/V\text{-}sec$	300	350	62	1050	3	340	72
		4.2	~ 10	40				
μ_h	$cm^2/V\text{-}sec$	300	15	63	80	65	110	10
		4.2			~ 300	65	~ 2200	11
τ_e	sec	4.2	$\sim 10^{-15}$					
τ_h	sec	4.2			2×10^{-13}		7.5×10^{-13}	
ϵ_r	-	300	7.7 @ 44 MHz	64	10.6 (static)	69	10.1 (static)	73
n	-	-	2.28	11	2.69	70	2.70	70
R	-	-	0.152		0.21		0.212	

τ is the momentum relaxation time, n is the refractive index, and R is the reflection coefficient. τ is calculated using the values given for μ and m^*; R is calculated from the value of n.

Donor and defect levels have been reported throughout the forbidden band (see Devlin[28]). The large number of levels observed and the tendency of the material to form defect centers have prevented correlating most of the levels with types of defects. Undoubtedly, the most important defect characteristic of CdS is the compensated acceptor which normally acts as a hole trap. It appears about 1 eV above the valence band, but this apparently varies from sample to sample; it is generally attributed to either a Cd vacancy or Cd vacancy-impurity complex, according to Bube[39]. Other levels often seen are given in Table I-2 with the probable defect involved.

The compensated acceptor level is the key to the high photosensitivity of CdS and similar materials. When it results from a cation vacancy, it initially has a double negative charge and therefore has a very large capture cross section for holes and small subsequent capture cross section for electrons[1]. The great difference in capture cross sections greatly hinders the recombination process, resulting in long free electron lifetimes and enhanced photosensitivity. For this reason, many observers also refer to this type of center as a sensitizing center. The level is normally compensated at room temperature, and Kulp[40], and Litton and Reynolds[41,42] show that excitation of electrons from the level is achieved with sub-bandgap light.

The sensitizing center is responsible for three effects seen in CdS. In some crystals at low temperatures, the acceptor levels have a large density compared to deep electron traps. Photogenerated holes are permanently trapped, and after the electron traps saturate, a very high density of free electrons results. For reasons which are not clear,

TABLE I-2

Energy Levels Often Found in CdS, CdTe, and ZnTe

CdS			CdTe			ZnTe		
E_t	Ref	Type	E_t	Ref	Type	E_t	Ref	Type
0.007	74	D	0.011	3	D	0.034*	2	A; V_c^-
0.014	74	D	0.022	68	D (In)	0.048*	10	A; V_c^-
0.032	62	D	0.05*	80	A; V_c^-	0.11*	10	A (Ag)
0.049	63	t	0.056	79	D	0.11*	81	A (Cu)
0.05	78	t	0.06	80	A; V_c^{--}	0.14*	10	A; V_c^{--}
0.14	78	t	0.15*	68	A; V_c^-	0.15*	10	A (Cu)
0.16	75,76	t, V_a	0.20*	65	A	0.22*	10	A (Au)
0.24	76	t	0.3-0.4*	68	A (Au, Ag, Cu)	0.24*	2	A; V_c^{--}
0.25	78	t						
0.41	78	t	0.6*	68	A; V_c^{--}			
0.45	78	t						
0.63	76,78	D, t						
0.82	76	D						
1.1*	39	S						
1.2	39	t						
1.56	78	t						
1.98	78	t						

Energies are measured from the conduction band in eV, except (*), measured from the valence band.
Symbols: D = donor, A = acceptor, t = trap, V_a = anion vacancy, V_c = cation vacancy, S = sensitizing center.

recombination does not take place, and free electrons may be "stored" in the conduction band; samples which exhibit this behavior are called storage crystals. Examples of this behavior are presented by Kulp[40] and Eastman and Brodie[43].

Some CdS crystals display the tap effect, which is the emission of luminescence and a sharp reduction in conductivity when the crystal is mechanically stimulated[40,41]. The reason for this behavior is still open to discussion[16], but the most widely accepted explanation is that the tap generates a sufficient quantity of phonons to free holes from the sensitizing center and make them available for radiative recombination with trapped electrons[27,40]. Infrared quenching is a related phenomenon in which the holes are optically freed from the sensitizing center, producing the blue and green luminescence seen by Lambe and Klick[45] and reducing the conductivity[8]. Woods[46] has shown that photosensitivity may be increased by heating CdS in a vacuum, increasing the density of sensitizing centers.

PROPERTIES OF CdTe

Cadmium telluride normally crystallizes in the cubic zincblende structure[47], may be doped to give either conductivity type and is the most pure II-VI compound available[48]. There has been considerable discussion about whether the conduction band minimum lies at $k = 0$, but most of the evidence favors the existence of a direct gap[38]. Values of the transport properties are listed in Table I-1.

Native defect levels tend to dominate in the behavior of high purity CdTe, and several experimenters agree that singly and doubly ionized cadmium vacancies both introduce acceptor levels, although there is disagreement about the energies of the levels (see Table I-2). "Killer"

centers of unknown origin tend to exist near the middle of the forbidden band; they act as recombination centers and limit the efficiency of luminescence processes[37]. Measurements requiring ohmic contact are hindered by the fact that low resistance contacts to p-type CdTe have not been achieved[37].

PROPERTIES OF ZnTe

Zinc telluride usually crystallizes in the zincblende crystal form[47] and is normally p-type, although high resistivity n-type crystals have been reported[38]. It is probably the least studied II-VI compound because it is not very photosensitive. According to Aven and Segall[10] and Shiozawa, et al.[11], contacts to ZnTe tend to become non-ohmic for temperatures below 100°K. Donors in ZnTe tend to be completely compensated by holes from singly and doubly ionized Zn vacancies[37]. The quantum efficiency of luminescence processes is usually quite low, and emission may be completely quenched at room temperature[37].

Transport properties of ZnTe are listed in Table I-1 and some commonly seen defect levels are given in Table I-2. As in the case of CdTe, there is a lack of agreement on the energies of sites due to Zn vacancies, but the presence of two such levels is widely accepted.

OTHER II-VI COMPOUNDS

Cadmium selenide has not been widely studied because its behavior is very similar to the behavior of CdS[38]. It is always n-type and crystallizes in the wurtzite structure. Both ZnS and ZnSe are commonly grown in both the wurtzite and zincblende crystal forms, and may be made either n-type or p-type[38]. These two materials are very similar to each other in most ways, differing mainly in the values of their transport

properties. Furthermore, the behavior of the zinc and cadmium sulfides and selenides are generally more similar than dissimilar[38,39].

Because of these overall similarities, CdS was chosen as a representative of the group of ZnS, CdS, ZnSe, and CdSe for the studies reported herein. The behavior of CdS is considered the most interesting because of its ability to display the storage, tap, and quenching effects. ZnTe and CdTe samples were also selected for testing because of their tendency to be p-type, because they often respond unfavorably in tests requiring ohmic contacts, and because their general photostimulated behavior differs from the behaviors of the other four II-VI compounds.

CHAPTER II

Theory of Photodielectric Measurements

INTRODUCTION

Several detailed papers are available which treat various aspects of the photodielectric study of semiconductors. Arndt[25] analyzed the cavity perturbation model to describe the effects of changes in the complex dielectric constant on the behavior of a re-entrant coaxial cavity containing the semiconductor. Hartwig[23], Arndt[25], and Stone[26] derived and applied the relations describing how the existence of excess free carriers in the semiconductor affects the dielectric constant, and Baker[28] extended these investigations to allow calculation of the filling factor of the sample and measurement of the sample relaxation time. Hinds[27] analyzed the relations between bound carriers and the complex dielectric constant. The following consists of a brief summary of the essential results of these reports, laying the groundwork for the analysis to follow. The reader seeking more details is advised to refer to the references given above.

MICROWAVE CAVITY BEHAVIOR

A sensitive scheme for observing photodielectric effects in semiconductors, originally proposed by Hartwig[23] and Genz[24], is to place the semiconductor sample in the high field region of a microwave cavity and monitor the resonant frequency and relative amount of microwave power absorbed by the sample. A re-entrant cavity was chosen because of the favorable geometry; a full size cutaway view of the cavity used to make the measurements reported here is shown in Fig. IV-2. The cavity may be viewed as a length of transmission line with one end shorted and the

other end capacitively terminated. The resonant frequency is determined by both the characteristic impedance of the line and by the capacitive termination. It is clear that changing the dielectric constant of the capacitance, either by introducing a semiconductor wafer or changing ε_r for the semiconductor, changes the cavity resonant frequency and the relative amount of energy absorbed by the termination. Arndt[25] used a cavity perturbation model to calculate the effects of changes in the semiconductor dielectric constant on the cavity behavior, and his primary results are given here with the necessary assumptions involved.

When a semiconductor sample is first placed in the cavity, the resonant frequency will change by the amount

$$\frac{\Delta f}{f_1} = \frac{(\varepsilon_o-\varepsilon_1)\int_{V_s} E_o E_1 dV + (\mu_1-\mu_o)\int_{V_s} H_o H_1 dV}{\int_{V_c} (\varepsilon_o E_o^2 + \mu_o H_o^2) dV} \qquad [2.1]$$

Here, f is the frequency, ε is the dielectric constant, μ is the permeability, E is the electric field, H is the magnetic field, V_s is the sample volume, V_c is the cavity volume, the subscript 0 refers to values before the sample is included, and 1 refers to values with the sample in place. Assumptions are that $V_s << V_c$ and the sample only slightly alters the fields and the frequency.

The ratio of integrals on the right side of equation [2.1] is a measure of the fraction of the electromagnetic energy in the cavity which is stored in the sample. This factor is commonly called the geometry factor or filling factor, and is represented by the symbol G. Thus, equation [2.1] is rewritten

$$\frac{\Delta f}{f_1} = \frac{\varepsilon_o - \varepsilon_1}{\varepsilon_1} G \qquad [2.2]$$

The geometry factor is not easily calculated from the results of the cavity perturbation model. Baker[28] used a transmission line model of the cavity-sample system to calculate an expression for G in terms of the sample and cavity parameters,

$$G = \frac{f_o b}{\varepsilon_o A Z_o \pi^2 f^2} \left[\frac{\cos^2 \frac{\pi f}{2 f_o}}{1 + \frac{f_o}{\pi f} \sin \frac{\pi f}{f_o}} \right] \qquad [2.3]$$

where f_o is the unloaded cavity frequency, f is the loaded cavity frequency, b is the sample thickness, A is its area, and Z_o is the characteristic impedance of the cavity.

The filling factor G may either be calculated using Eq. [2.3] or measured, using Eq. [2.2]. Baker[28] found that the calculated value tended to be somewhat higher than the measured value and concluded that the assumptions used in the perturbation method may be invalid when measuring the G factor of large samples. On the other hand, the magnitude of the term in brackets in Eq. [2.3] is very sensitive to small changes in the two frequencies. It is possible than an inaccuracy involved in determining f_o, which must be calculated from the dimensions of the cavity, ignoring the presence of coupling ports or probes, could easily account for the difference between theory and observation. The best method of accurately finding G still appears to be the perturbation measurement.

Once G is known, changes in the sample dielectric constant may be related to changes in the cavity resonant frequency and changes in

the relative amount of microwave power absorbed in the sample. In a sinusoidally varying field, the complex dielectric constant may be expressed as

$$\varepsilon^* = \varepsilon + \frac{\sigma}{j\omega} = \varepsilon_o(\varepsilon'_r + \frac{\sigma}{j\omega\varepsilon_o}) = \varepsilon_o(\varepsilon'_r - j\varepsilon''_r) \qquad [2.4]$$

For a lossy insulator, with $\varepsilon' >> \varepsilon''$, it may be shown that a change in the dielectric constant causes the cavity frequency to change according to the relation

$$\frac{f_2 - f_1}{f_2} = \varepsilon_o G \left[\frac{1}{\varepsilon'_2} - \frac{1}{\varepsilon'_1}\right] \qquad [2.5]$$

where the subscript 2 denotes the value of a quantity after the change has occurred. If the change in ε' is small, this reduces to

$$\frac{\Delta f}{f} = \frac{-G\Delta\varepsilon'_r}{\varepsilon^2_r} \qquad [2.6]$$

The well known expression for microwave power absorbed in an insulator, when placed in a field E_e with a frequency f is

$$P_{abs} = \sigma E_e^2/2 = \pi f \varepsilon'' E_e^2 \qquad [2.7]$$

The change in absorbed power due to a change in ε''_r is simply

$$\Delta P_{abs} = \pi f \varepsilon_o E_e^2 \Delta\varepsilon''_r \qquad [2.8]$$

Thus, $\Delta\varepsilon''_r$ may be measured by determining the power absorbed by the sample. Baker[28] shows that it also may be determined by measuring the cavity Q, using the relation

$$Q = \left[\frac{Q_o}{1 + \frac{2GQ_o\varepsilon_r''}{\varepsilon_r^2}} \right] \qquad [2.9]$$

where Q_o is the initial cavity Q.

COMPLEX DIELECTRIC CONSTANT THEORY

The dielectric constant of a material is defined as the proportionality constant between the electric field $\vec{E}$ and the resultant electric flux density $\vec{D}$ within the material,

$$\vec{D} = \varepsilon_o \varepsilon_r \vec{E} \qquad [2.10]$$

Within the material, the external field induces an electric dipole moment whose density per unit volume is $\vec{P}$, the polarization of the material, related to $\vec{E}$, $\vec{D}$, and ε_r by

$$\vec{D} = \varepsilon_o \vec{E} + \vec{P} = \varepsilon_o \vec{E} + \varepsilon_o \chi_e \vec{E} \qquad [2.11]$$

where the electric susceptability χ_e is a measure of the ability of the field to induce polarization in the material and therefore it depends on the physical properties of the material. The dielectric constant and susceptability are related by

$$\chi_e = \varepsilon_r - 1 = \vec{M}/V\vec{E}\varepsilon_o \qquad [2.12]$$

The quantity $\vec{M}$ is the total dipole moment for a sample of volume V . If the material contains no permanent dipole moments due to orientational polarization of molecules, $\vec{M}$ may be calculated by summing, for all charged particles, the products of the charge q_i times the displacement from equilibrium $\vec{r}_i$; thus,

$$\vec{M} = \sum_i q_i \vec{r}_i \qquad [2.13]$$

The expression for $\vec{r}_i$ in the presence of an internal ac electric field is found by solving the equation of motion

$$\frac{d^2\vec{r}}{dt^2} + \frac{1}{\tau}\frac{d\vec{r}}{dt} + \frac{k\vec{r}}{m^*} = \frac{q\vec{E}_i}{m^*} e^{j\omega t} \qquad [2.14]$$

where $\vec{E}_i e^{j\omega t}$ is the internal field, τ is the momentum relaxation time, and m^* is the effective mass. The relaxation time is given by $\tau = m^*\mu/e$ for free electrons[49]. After replacing k/m^* with ω_o^2 [50], solving the preceding equation, and discarding the transient component, the solution is

$$\vec{r} = \frac{q}{m^*} \vec{E}_i e^{j\omega t} \frac{(\omega_o^2-\omega^2-j\omega/\tau)}{(\omega_o^2-\omega^2)^2+(\omega/\tau)^2} \qquad [2.15]$$

It is apparent that ω_o is the natural resonant frequency of the system. It was shown in reference 27 that ω_o is related to the energy E which binds the charge to its equilibrium position by the relation

$$\begin{aligned} \omega_o^2 &= \frac{2}{m^*} \frac{(4\pi\varepsilon_o)^2}{e^4} E^3 \\ &= 1.70\times10^{29}(m/m^*)E^3(eV) \end{aligned} \qquad [2.16]$$

The notation E(eV) means that the energy has the units of electron volts.

Substituting Eq. [2.15] back into the preceding expressions yields the result

$$\varepsilon_r = \sum_i \frac{q_i^2}{m_i^* V \varepsilon_o}\left[\frac{\omega_o^2-\omega^2-j\omega/\tau}{(\omega_o^2-\omega^2)^2+(\omega/\tau)^2}\right]_i + 1 \qquad [2.17]$$

To further simplify the problem, we consider only changes in ε_r caused by moving a density of electrons among sites with different binding energies. Letting the index j represent different possible states and Δn_j represent the net density of electrons added to that energy state, we get

$$\Delta\varepsilon_r = \frac{e^2}{m^*\varepsilon_o} \sum_j \Delta n_j \left[\frac{\omega_o^2-\omega^2-j\omega/\tau}{(\omega_o^2-\omega^2)^2+(\omega/\tau)^2}\right]_j \qquad [2.18]$$

If $\Delta\varepsilon_r = \Delta\varepsilon_r' - j\Delta\varepsilon_r''$, the real and imaginary parts are

$$\Delta\varepsilon_r' = \frac{e^2}{m^*\varepsilon_o} \sum_j \Delta n_j \left[\frac{\omega_o^2-\omega^2}{(\omega_o^2-\omega^2)^2+(\omega/\tau)^2}\right]_j \qquad [2.19]$$

$$\Delta\varepsilon_r'' = \frac{e}{m^*\varepsilon_o\omega} \sum_j \Delta n_j \left[\frac{\omega^2/\tau}{(\omega_o^2-\omega^2)^2+(\omega/\tau)^2}\right]_j \qquad [2.20]$$

It is convenient at this point to assign a symbol to the bracketed quantities in the preceding equations, as follows:

$$B'(j) \equiv \left[\frac{\omega_o^2-\omega^2}{(\omega_o^2-\omega^2)^2+(\omega/\tau)^2}\right]_j \qquad [2.21]$$

$$B''(j) \equiv \left[\frac{\omega^2/\tau}{(\omega_o^2-\omega^2)^2+(\omega/\tau)^2}\right]_j \qquad [2.22]$$

B' and B'' represent the relative size of the contribution to the real and imaginary dielectric changes due to a single electron at the level j.

Figures II-1 and II-2 are asymptotic approximations of the variation of B' and B" with electron binding energy for $\omega = 5 \times 10^9$ and 5×10^{10} rad/sec, and $\tau = 10^{-15}$, 2×10^{-13}, and 2×10^{-10} sec, assuming $m^*/m = 0.2$. It has been shown in reference 27 that for the special case of a free electron, setting $E = 0 = \omega_o$ gives the same results obtained by Arndt[25] in treating only the free carrier case.

Four regions of differing behaviors appear in Figs. II-1 and II-2. In the first, for levels with large binding energies, $\omega_o^2 >> \omega^2$ and $\omega_o^2 >> \omega/\tau$, so

$$B' = 1/\omega_o^2 \qquad [2.23]$$

$$B'' = \omega^2/\tau\omega_o^4 \qquad [2.24]$$

Both B' and B" rise as the binding energy drops. In the second region, however, B' decreases as the binding energy is reduced, but B" stays at a constant value. Here, $\omega/\tau >> \omega_o^2$, and

$$B' = \omega_o^2\tau^2/\omega^2 \qquad [2.25]$$

$$B'' = \tau \qquad [2.26]$$

In the third region, seen only in B', the quantity $\omega_o^2 - \omega^2$ goes from a positive to a negative value. The denominator is still controlled by ω/τ, so

$$B' = (\omega_o^2-\omega^2)\tau^2/\omega^2 \qquad [2.27]$$

$$B'' = \tau \qquad [2.28]$$

The fourth region applies for very lightly bound and free carriers. Since $\omega^2 >> \omega_o^2$, we find

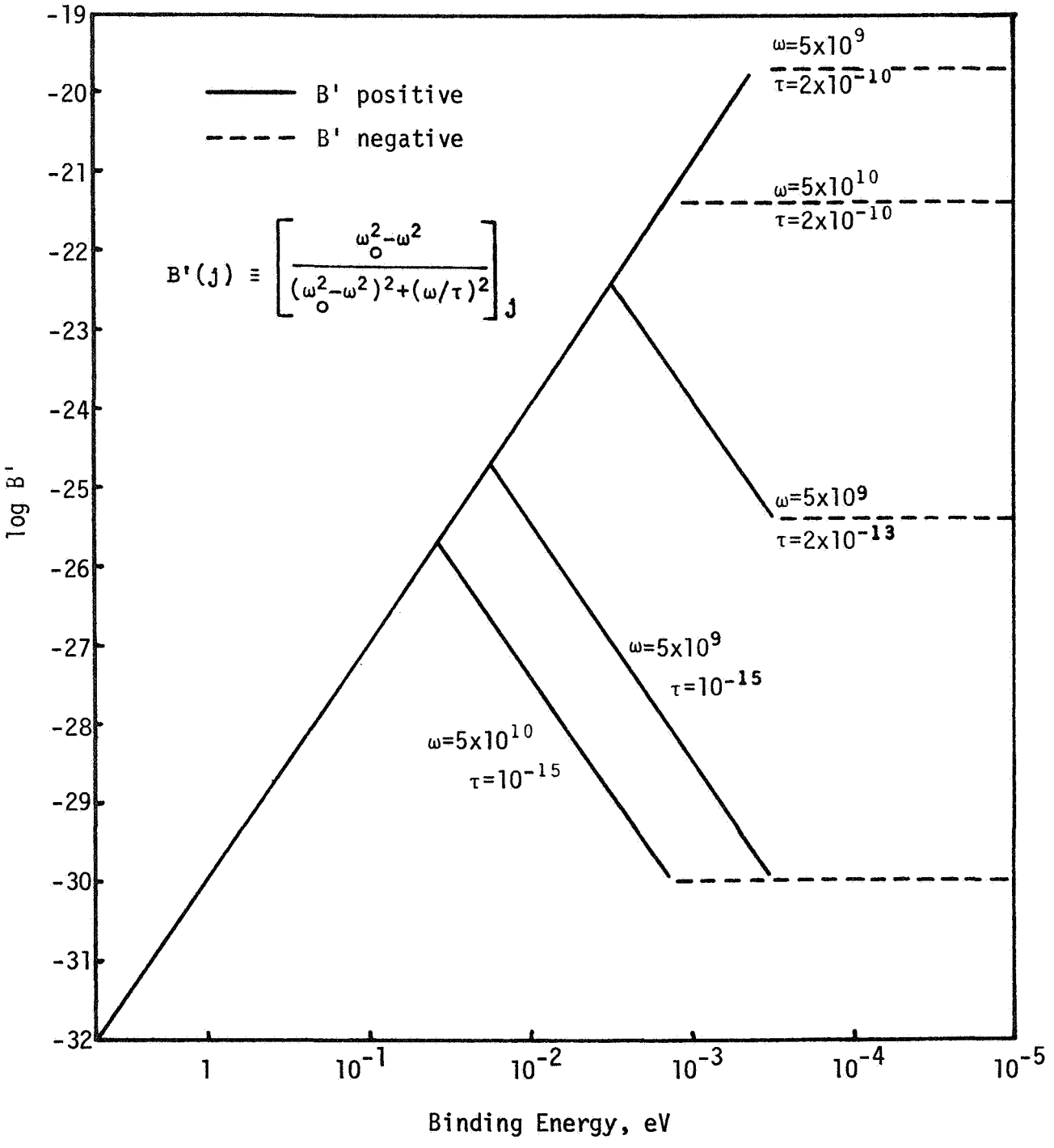

Figure II-1. Asymptotic dependence of B' on the binding energy of an electron state, calculated for m*/m = 0.2.

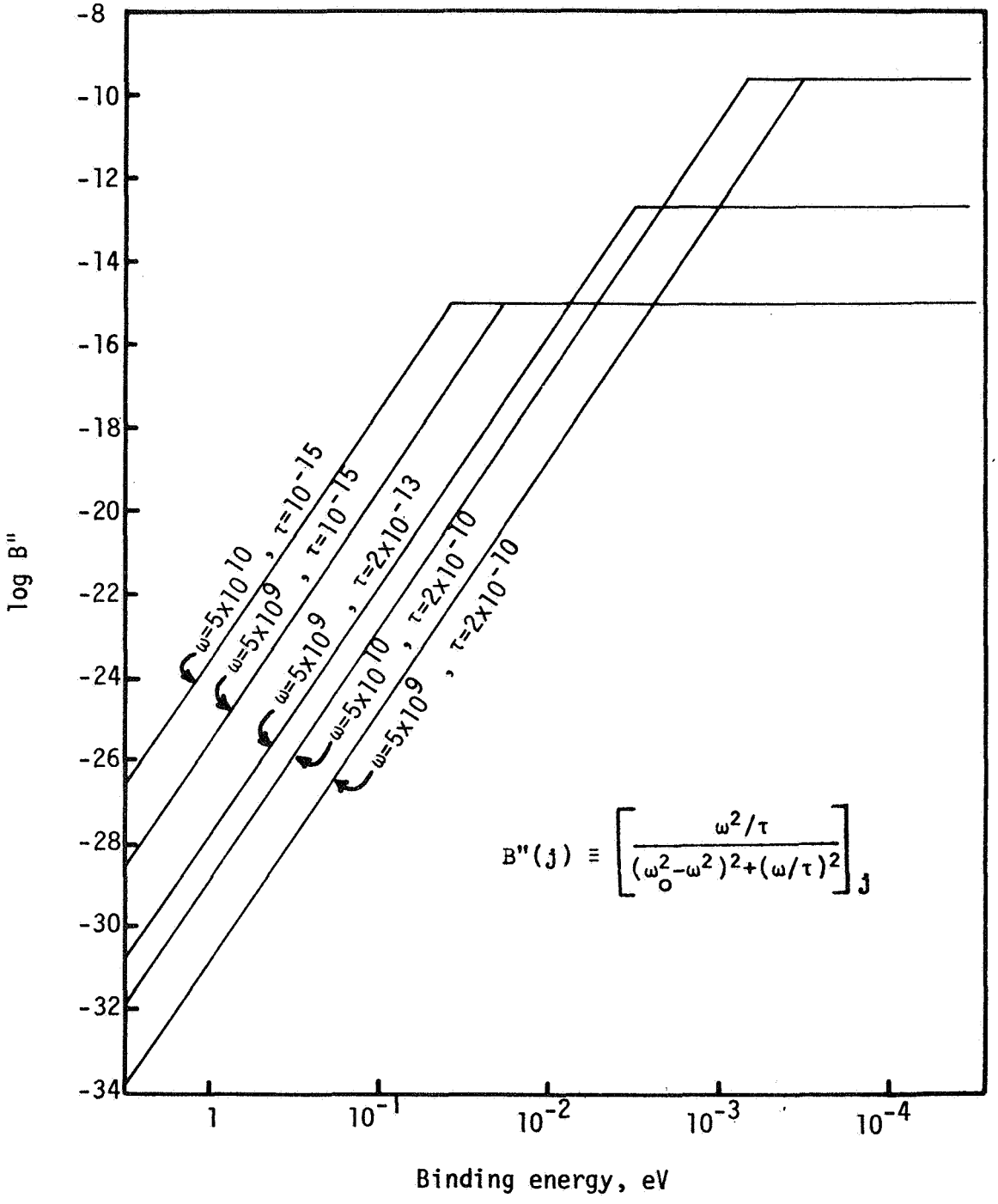

Figure II-2. Asymptotic dependence of B" on the binding energy of an electron state, calculated for m*/m = 0.2.

$$B' = -\tau^2/(1+\omega^2\tau^2) \qquad [2.29]$$

$$B'' = \tau \qquad [2.30]$$

Here, B' is negative, as denoted in the figure by the dotted line.

In cases where $\omega \geq 1/\tau$, the second region does not appear. The break between positive and negative values of B' occurs at $\omega_o^2 = \omega^2$.

The result shows that in crystals with low mobilities, bound carriers may have a larger value of B' than free carriers. For high mobility samples, B' for free electrons is always larger. B" is always larger for free carriers. The highest B' for free carriers is available when $\omega = 1/\tau$, but the highest B" for bound carriers is achieved at the highest frequency.

A combination of equations [2.6], [2.19], and [2.21] now gives

$$\Delta f = -1.59\text{x}10^{10}\ \frac{fG}{\varepsilon_r^2}\ \Delta nB' \qquad [2.31]$$

The measureable quantity $\Delta P_{abs}/P_o$ is obtained from [2.8],[2.20], and [2.22] as

$$\frac{\Delta P_{abs}}{P_o} = \frac{e^2}{\sigma_o m^*}\ \Delta nB'' \qquad [2.32]$$

where the units for Δn are m^{-3}.

ELECTRIC FIELD CONSIDERATIONS

In the preceding discussion, the electric field which has been implied is the local field in the region of the individual atoms or dipoles. In the work reported in Chapter V, the actual value of the local electric field is not involved, and therefore distinctions between local and applied fields are not required. If, however, the foregoing

equations which directly involve the electric field are to be used, the different types of electric fields existing in the insulator must be considered. The local field differs from the applied field because of surface and volume dipoles induced in the material by the applied field. One lucid explanation of the electric field corrections which must be considered is given by Wang[49]. The local field at a reference point in a dielectric material is calculated by first assuming that an imaginary spherical boundary surrounds the point. The radius of the boundary is chosen such that the region outside appears as a continuum with dielectric constant ε_r, while the atomic structure of the region inside the boundary must be taken into account. The microscopic local field is given as the vector sum

$$\vec{E}_{loc} = \vec{E}_0 + \vec{E}_1 + \vec{E}_2 + \vec{E}_3 \qquad [2.33]$$

where $\vec{E}_0$ is the applied field. Kittel[51] describes $\vec{E}_1$ as the field of the polarization charges inside the spherical boundary, $\vec{E}_2$ is the depolarization field due to charges induced on the surface of the specimen, and $\vec{E}_3$ is the contribution induced by charges on the boundary, otherwise known as the Lorentz field*.

The microscopic internal field $\vec{E}_i$ in the dielectric differs from the local field in that $\vec{E}_i$ does not directly include $\vec{E}_0$. In other words,

$$\vec{E}_i = \vec{E}_1 + \vec{E}_2 + \vec{E}_3 = \vec{E}_{loc} - \vec{E}_0$$

The macroscopic electric field which exists within the dielectric is denoted as E_e: [49]

* Wang and Kittel use different notation; that of Wang is followed here.

$$\vec{E}_e = \vec{E}_0 + \vec{E}_2 \qquad [2.34]$$

Nozieres and Pines[54] have demonstrated in a quantum mechanical treatment of the dielectric constants of solids that microscopic local field corrections are not necessary for highly polarizable insulators and semiconductors; that is, Eq. [2.34] describes the correct local field.

The depolarizing field $\vec{E}_2$ results from charges induced on the surface of the sample. The component of $\vec{E}_2$ in any given direction (in particular, in the direction of the applied field) is dependent on the shape and orientation of the sample in the field. The depolarizing factor L accounts for the relationship between the internal polarizing field and the geometry of the sample relative to the external field. It may be shown[51] that the field $\vec{E}_e$ is related to the external field $\vec{E}_0$ and the dielectric polarization $\vec{P}$ by

$$\vec{E}_e = \vec{E}_0 - L\vec{P}$$

Values of L for various geometries are given by Dresselhaus, Kip, and Kittel[52]; the value ranges from 0 to $1/\varepsilon_o$, depending on the axial ratio of the sample when it is treated as an ellipsoid. For a thin slab or disc infinitely extended in the x and y directions, $L = 1/\varepsilon_o$ when the field is applied in the z direction, while the value is $1/3\varepsilon_o$ for a spherical sample. The calculation of L for a real sample with a thickness-to-diameter ratio less than 10 is a very difficult problem, but the value clearly should be close to $1/\varepsilon_o$. Any attempted correlation between photodielectric behavior and the external field must take the depolarization field into account.

PLASMA EFFECTS

The preceding theory describes the change in the dielectric

constant brought about by a change of energy of a single carrier. When the effects of many carriers are taken together, the interactions between carriers must be considered. Dresselhaus, Kip, and Kittel[52,55] have considered plasma effects in solids with high free carrier densities, subjected to rf fields. They have shown that the depolarizing effect is equivalent to a harmonic restoring force, with a force constant given by

$$\text{Force Constant} = \frac{Lne^2}{(1+L\chi_e)} \qquad [2.35]$$

This term alters the equation of motion for electrons, and the net influence of plasma depolarization is taken into account by substituting $\omega' = \omega - \omega_p^2/\omega$ in place of ω in the preceding equations, where ω_p is the plasma frequency given by

$$\omega_p = \left[\frac{Lne^2}{(1+L\chi_e)m^*}\right]^{1/2} \qquad [2.36]$$

Clearly $\omega' = \omega$ for $\omega_p << \omega$(that is, for low free carrier densities.)

It is also concluded[55] that the behavior of minority carriers in another band is not affected by the presence of the majority carrier plasma. Since the effect of a plasma of free electrons is to stiffen the electron motion, we may conclude that the behavior of trapped carriers is not affected by the plasma because the motion of trapped carriers is already limited to a very great extent, and because the behaviors of the two types of carriers are independent.

Plasma effects are not considered further here because II-VI compounds tend to have low free carrier densities at low temperatures, even while illuminated. When the rf frequency is about 10^9 Hz, plasma

effects are not appreciable until n reaches about 10^{16} cm^{-3}. For discussions of plasma effects in photodielectric experiments, see Stone[26] and Baker[28].

CHAPTER III

Trapping and Recombination

INTRODUCTION

The preceding chapter described how the redistribution of electrons among the energy states of a semiconductor can lead to a change in the dielectric constant. Electron densities at various energy levels are determined by the properties of the semiconductor, and in this chapter, relations between densities and other parameters are developed. The equations presented are intended to represent low temperature situations.

The treatment will refer mainly to electrons, but may be made applicable to holes by the usual obvious substitutions of $n \rightarrow p$, $m_e^* \rightarrow m_h^*$, $E_c \rightarrow E_v$, etc. The discrete levels in the forbidden band are all referred to as traps, rather than separating them into traps and recombination centers as Bube[1] and Rose[9] normally do for photoconductors at room temperature, because whether or not recombination takes place at a level depends on many parameters not related to the trap, such as the temperature.

Pioneering work on trapping and recombination in semiconductors was performed by Shockley and Read[56] and Hall[57], and the analysis presented here follows the extension of their work given by Bube[1]. It is assumed here that the divergence of the drift and diffusion components of the current density are negligible.

In a photoconductor the density of free carriers may be altered in several ways, as shown in figure III-1. Electrons may be added to the conduction band by optical excitation from the valence band or from a trap, or by thermal generation from a lower level. The density is

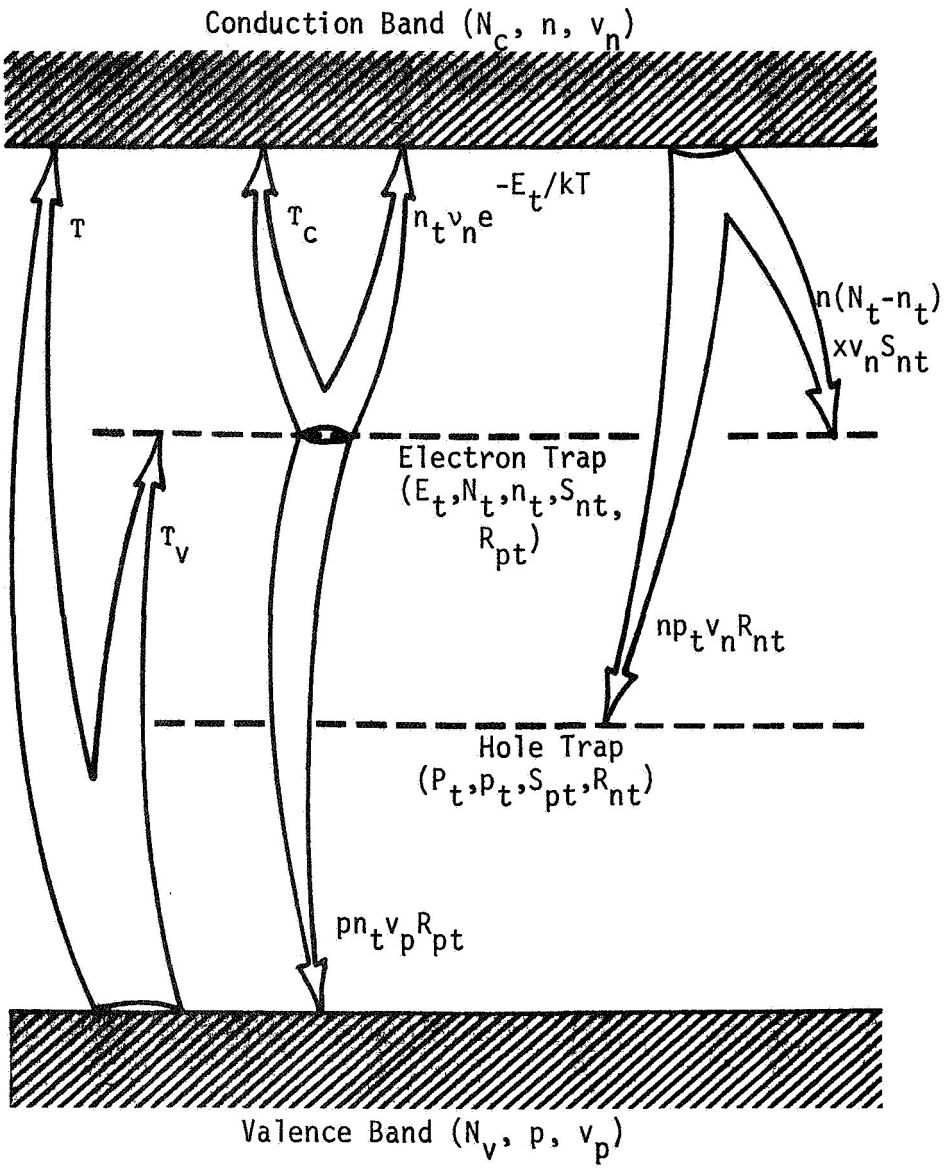

Figure III-1. General model for electron trapping and recombination, neglecting direct band-to-band recombination. The rate equations implied are

$$\frac{dn}{dt} = T + T_c + n_t v_n e^{-E_t/kT} - np_t v_n R_{nt} - n(N_t-n_t)v_n S_{nt}$$

$$\frac{dn_t}{dt} = n(N_t-n_t)v_n S_{nt} + T_v - n_t v_n e^{-E_t/kT} - T_c - pn_t v_p R_{pt}.$$

decreased by recombination or through trapping. Thus the time rate of change of n, with terms listed in the order mentioned, is

$$\frac{dn}{dt} = T + n_t \nu_n e^{-E_t/kT} - np_t v_n R_{nt} - n(N_t - n_t) v_n S_{nt} \qquad [3.1]$$

Here n, p, and t refer to electrons, holes, and traps, respectively. T is the absorbed light flux density in photons/cm^3-sec, ν is the attempt-to-escape frequency, E_t is the trap depth measured relative to the conduction band, v is the thermal velocity, S is the capture cross section of an empty trap, R is the recombination cross section for one type of carrier at a level already containing the other type of carrier, and N_t is the density of traps. It is assumed that all recombination occurs via traps (or recombination centers), because at low carrier densities and low temperatures, direct band-to-band and Auger recombination are not likely processes[1].

Electrons may normally be added to shallow traps either by decay from the conduction band or direct optical excitation from the valence band. It is assumed that direct excitation or decay from other traps and thermal generation from the valence band are negligible. The density is decreased by thermal or optical excitation to the conduction band or by recombination with a free hole. The net rate of change, where the terms are listed in the order mentioned, is

$$\frac{dn_t}{dt} = n(N_t - n_t) v_n S_{nt} + T_v - n_t \nu_n e^{-E_t/kT} - T_c - pn_t v_p R_{pt} \qquad [3.2]$$

If thermal emission to the conduction band is negligible for carriers in deep traps, the rate equation is

$$\frac{dn_t}{dt} = n(N_t - n_t)v_n S_{nt} + T_v - T_c - pn_t v_p R_{pt} \qquad [3.3]$$

where the terms represent filling from the conduction band, optical excitation from the valence band, optical freeing, and recombination by hole capture.

The quantities ν, v, and N_c may be expressed in terms of the other parameters as follows:

$$\nu_n = N_c v_n S_{nt} \qquad [3.4]$$

$$v = \left(\frac{2kT}{m^*}\right)^{1/2} \qquad [3.5]$$

$$N_c = 2\left(\frac{2\pi m^* kT}{h^2}\right)^{3/2} \qquad [3.6]$$

All other parameters have the usual meanings.

It is quite difficult and not advantageous to solve equations [3.1] through [3.3] for the general case. They are more useful when solved for certain special cases in which simplifying assumptions may be made. The initial value of dn/dt is easily found by letting $n_t \to 0$ and $n \to 0$, so that at $t \simeq 0$,

$$\frac{dn}{dt} \simeq T$$

The early time variation of n is given by

$$n = T\tau_L(1 - e^{-t/\tau_L}) \qquad [3.7]$$

where $\tau_L = 1/N_t v_n S_{nt}$. If more than one trap or recombination level exists, τ_L is corrected by replacing $N_t S_{nt}$ with the sum of the NS products.

When the steady state is reached and only one electron trap dominates in the behavior, $dn/dt = 0$ and

$$n = \frac{T + n_t \nu_n e^{-E_t/kT}}{(N_t - n_t) v_n S_{nt}} \qquad [3.8]$$

The initial variation of n_t is also easily found when n_t is very small.

$$n_t \simeq T[t - \tau_L(1 - e^{-t/\tau_L})] \qquad [3.9]$$

This expression is valid for cases when recombination at the trap by hole capture and thermal freeing are negligible and the trap is not near saturation. At steady state,

$$n_t = \frac{n/\tau_L}{n v_n S_{nt} + p v_p R_{pt} + \nu_n e^{-E_t/kT}} \qquad [3.10]$$

Further simplifications result for special cases. In the following sections, combinations of discrete states are assumed and analyzed; the combinations are those expected to be encountered in photodielectric experiments at low temperatures.

SINGLE ELECTRON TRAP

If only one shallow electron state exists in the forbidden band, and both the temperature and band gap light intensity are low, the

photogenerated electrons are quickly trapped and soon recombine with free electrons. If the trap is deep enough that $T >> n_t \nu_n \exp(-E_t/kT)$ and fast recombination keeps $n_t << N_t$, equation [3.7] is always valid, and after a few τ_L have elapsed, $n = T\tau_L$. The energy level diagram which is applicable is shown in figure III-2.

Equation [3.9] for n_t is valid only as long as recombination is negligible, which is a very short time. However, steady state is established within a few microseconds, with all of the photogenerated carriers going to supply the recombination. Since $p = n + n_t$ and $n_t >> n$, $p \simeq n_t$; thus

$$T \simeq n_t^2 v_p R_{pt} \qquad [3.11]$$

$$n \simeq \frac{n_t^2 v_p R_{pt}}{N_t v_n S_{nt}} = \frac{T}{N_t v_n S_{nt}} \qquad [3.12]$$

$$n_t(\infty) \simeq \frac{T}{p v_p R_{pt}} \qquad [3.13]$$

where $n_t(\infty)$ is the steady state value of n_t. When the light is removed, the decay of n is exponential with a decay time of $\tau = (N_t v_n S_{nt})^{-1}$:

$$n(t) = n(\infty) e^{-t/\tau}$$

The decay of n_t follows equation [3.2] with all but the last term negligible; the solution is

$$n_t(t) = \frac{n_t(\infty)}{1 + [n_t(\infty) v_p R_{pt}]t} \qquad [3.14]$$

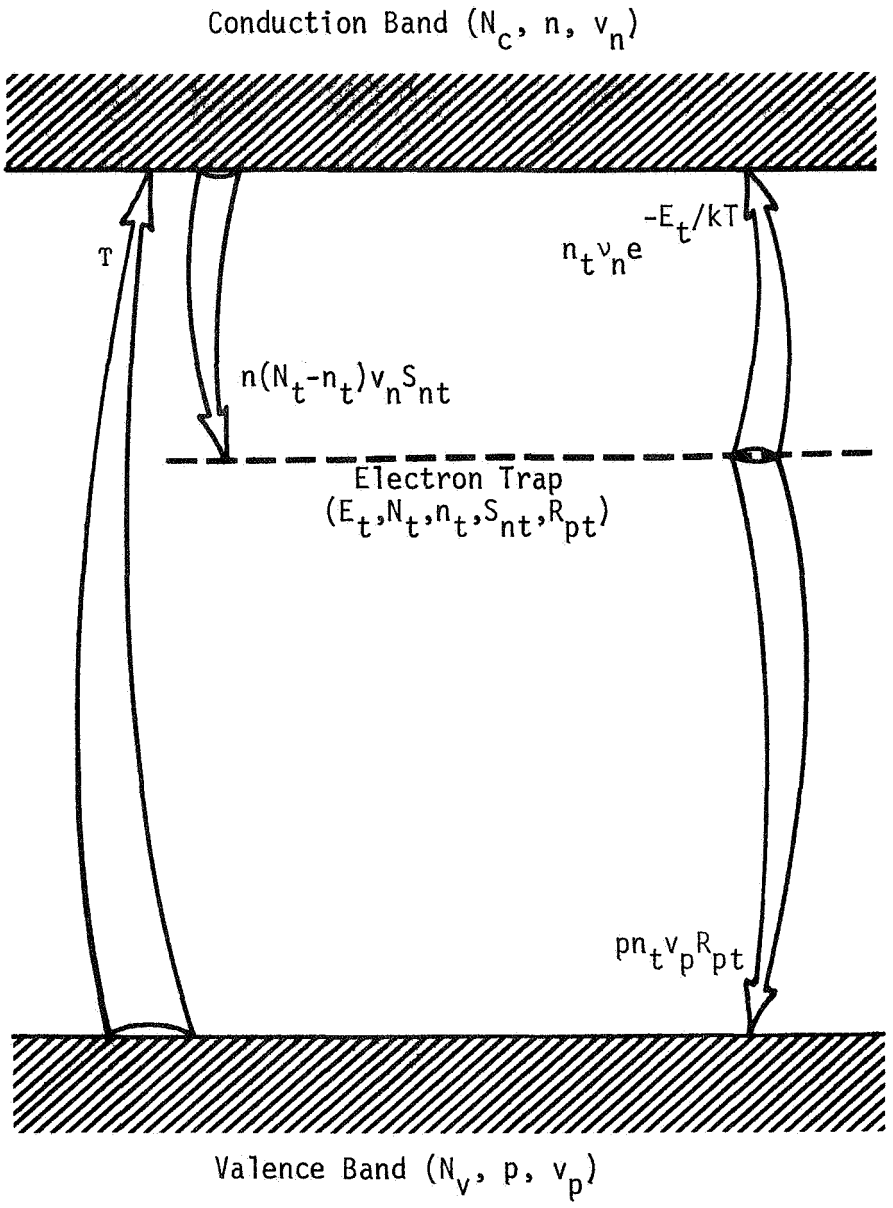

Figure III-2. Shown is the energy level model for use when only a single electron trap exists in the forbidden band. Sub-bandgap optical excitation is neglected. The rate equations are

$$\frac{dn}{dt} = T + n_t \nu_n e^{-E_t/kT} - n(N_t-n_t)v_n S_{nt}$$

$$\frac{dn_t}{dt} = n(N_t-n_t)v_n S_{nt} - n_t \nu_n e^{-E_t/kT} - pn_t v_p R_{pt}.$$

Application of sub-bandgap light, which excites electrons from the valence band to the trap, alters the rate equations by placing the T term in equation [3.2] rather than in Eq. [3.1]. At equilibrium

$$n \simeq \left(\frac{N_c}{N_t}\right) n_t e^{-E_t/kT} \qquad [3.15]$$

Eq. [3.13] is still correct for n_t.

When the light is removed and thermal excitation from the trap to the conduction band becomes important, the second term of Eq. [3.1] predominates and Eq. [3.15] is then the correct expression for $n(\infty)$. In that case, the decay of n is governed by the replentishing from the trap, and the decay time is

$$\tau_d = \left[N_c v_n S_{nt} e^{-E_t/kT} \right]^{-1} \qquad [3.16]$$

All parameters of the trap may be calculated from data taken from the equilibrium or decay conditions given in this section. Assuming $n(t)$, $n_t(t)$, and $T(t)$ are known, Eq. [3.11] gives R_{pt}. E_t is found by measuring $n(\infty)$ at two different temperatures and altering Eq. [3.15] as follows:

$$\ell n\left(\frac{n_1}{N_{c1}}\right) - \ell n\left(\frac{n_2}{N_{c2}}\right) = \frac{E_t}{k}\left(\frac{1}{T_2} - \frac{1}{T_1}\right) \qquad [3.17]$$

Then N_t comes from Eq. [3.15]. If thermal emptying of the trap is negligible, S_t is found from Eq. [3.12], while Eq. [3.16] is used when the emptying is not negligible.

SINGLE ELECTRON TRAP AND SINGLE SENSITIZING CENTER WITH SLOW HOLE TRAPPING

Some crystals have sensitizing centers with a large capture cross section for holes and a small subsequent capture cross section for electrons. Photogenerated holes may either be trapped at the sensitizing center or recombine with trapped electrons, where we assume that direct band-to-band recombination is negligible. The relative fraction of holes which proceeds to each level depends on the density of empty sites and the cross section governing the entrance of holes into the level. A portion of the photogenerated holes recombines quickly, but those which are trapped cannot interact with electrons again until they are thermally or optically freed. The electrons remain in the traps and the conduction band, with the relative density in each being determined by the properties of the trap. The situation is pictured in figure III-3.

The rate equations for free holes and trapped holes are

$$\frac{dp}{dt} = T - p(P_t - p_t)v_p S_{pt} - pn_t v_p R_{pt} \qquad [3.18]$$

$$\frac{dp_t}{dt} = p(P_t - p_t)v_p S_{pt} \qquad [3.19]$$

Here, P_t represents the density of hole traps. As long as p_t and n_t are small, p has the form

$$p = T\tau_p(1 - e^{-t/\tau_p}) \qquad [3.20]$$

where $\tau_p = (P_t v_p S_{pt})^{-1}$. Therefore, p_t initially rises at a constant rate, after a few τ_p have elapsed:

$$p_t = Tt \qquad [3.21]$$

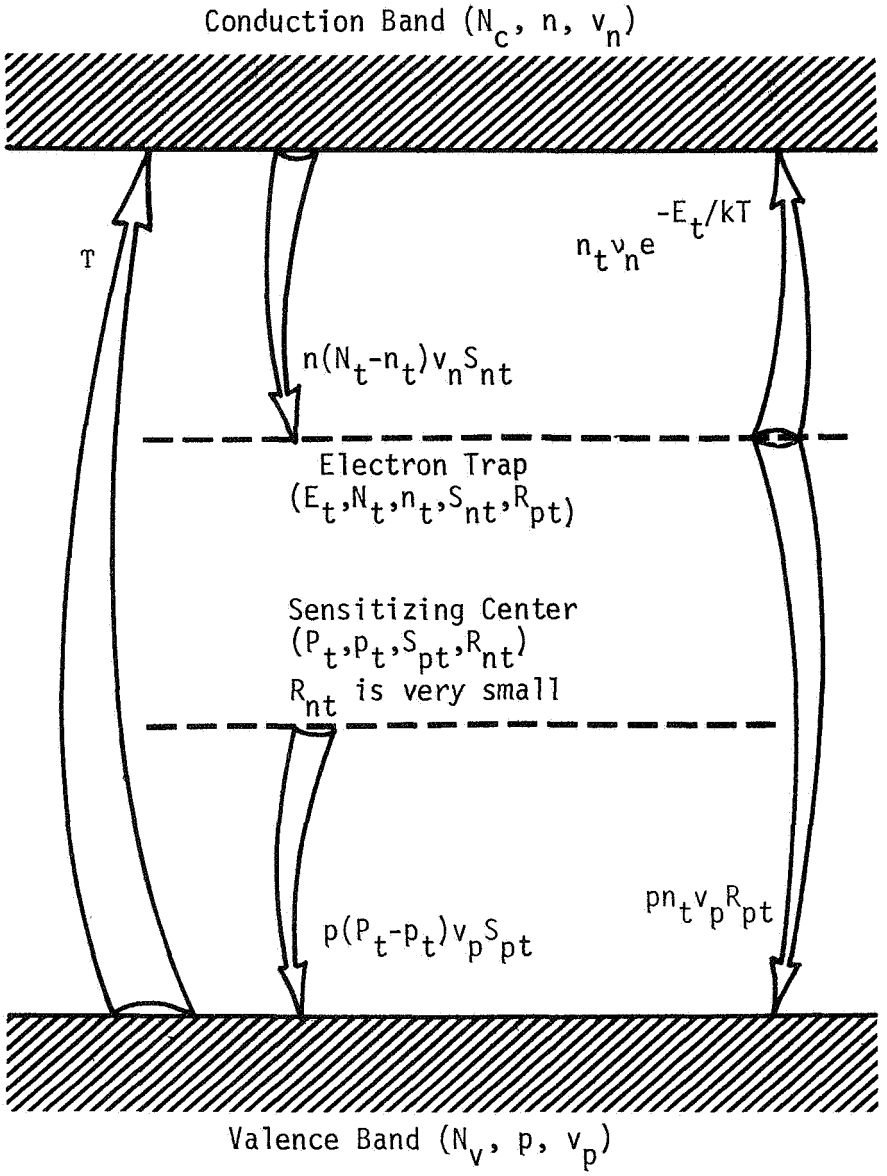

Figure III-3. Shown is the energy level model for use when a single electron trap and a single sensitizing center with slow hole trapping exist. Recombination at the sensitizing center, thermal emission from the sensitizing center, and sub-bandgap optical excitation are neglected. The rate equations for electrons are

$$\frac{dn}{dt} = T + n_t \nu_n e^{-E_t/kT} - n(N_t-n_t)v_n S_{nt}$$

$$\frac{dn_t}{dt} = n(N_t-n_t)v_n S_{nt} - n_t \nu_n e^{-E_t/kT} - pn_t v_p R_{pt}.$$

The initial variation of n is given by

$$n = T\tau_n(1 - e^{-t/\tau_n}) \qquad [3.22]$$

and $\tau_n = (N_t v_n S_{nt})^{-1}$. The early variation of n_t, assuming negligible thermal freeing compared to T and constant values of n and p, is

$$n_t = \frac{P_t v_p S_{pt}}{v_n R_{pt}} (1 - e^{-t/\tau_i}) \qquad [3.23]$$

where the initial response time τ_i, given by

$$\tau_i = P_t v_p S_{pt}/T v_n R_{pt} \qquad [3.24]$$

can easily be many hours at low light levels. For $t << \tau_i$, n_t may be further simplified by using the series expansion for e^{-t/τ_i} and keeping only the first terms, $1 - t/\tau_i$. This gives for the early variation of n_t,

$$n_t \simeq Tt \qquad [3.25]$$

The only time steady state is possible with this model occurs when the hole traps saturate and p rises to a high enough value for $(pn_t v_p R_{pt})$ to balance T; this is seen by setting dp_t/dt and dp/dt equal to zero in Eq. [3.18] and Eq. [3.19]. If the electron traps saturate before the hole traps, the excess electrons remain in the conduction band. This would allow band-to-band recombination to become important, and the rate equations given for n and p would no longer be valid.

Assuming n is still small when the hole traps saturate, the following steady state conditions hold:

$$pn_t v_p R_{pt} = T = n(N_t - n_t) v_n S_{nt} - n_t \nu_n e^{-E_t/kT} \qquad [3.26]$$

$$P_t = p_t \qquad [3.27]$$

$$n + n_t = p + p_t \qquad [3.28]$$

When the light is removed after saturation, the excess holes quickly recombine; the decay is exponential with $\tau_L = (n_t v_p R_{pt})^{-1}$ if $n_t >> p$ so that n_t does not change appreciably. Meanwhile, the excess conduction electrons are trapped, and the density of free electrons reaches the value

$$n = \frac{N_c n_t e^{-E_t/kT}}{(N_t - n_t)} \qquad [3.29]$$

The response time for the decay of n is the inverse of the probability of escape from the trap, which is given by

$$\text{Probability} = N_c v_n S_{nt} e^{-E_t/kT} = 1/\tau_d \qquad [3.30]$$

The decay is exponential if the number of electrons involved in the decay is small compared to n_t.

Parameters of both traps may be calculated from values of T, n, and n_t taken for the situations discussed above. E_t and N_t are found by applying Eq. [3.29] at two or more temperatures; E_t may also be found by rewriting Eq. [3.30] as

$$E_t = kT \, \ell n(\tau_d N_c v_n S_{nt}) \qquad [3.31]$$

Use of Eq. [3.31] with data from two different temperatures gives E_t and S_{nt}.

The density P_t is found directly from Eq. [3.27] and Eq. [3.28] when the hole traps are saturated. The values of S_{pt} and R_{pt} are found using Eqs. [3.23] and [3.24] to analyze the early variation of n_t. The initial free electron lifetime is $1/(N_t v_n S_{nt})$ according to Eq. [3.22]; the lifetime and decay time are related by

$$\tau_L/\tau_d = n/n_t \qquad [3.32]$$

SINGLE ELECTRON TRAP AND SINGLE SENSITIZING CENTER WITH FAST HOLE TRAPPING

If the hole traps have a high density and large capture cross section for holes, and the trap is separated from the valence band by many kT, the free hole density during illumination can not become significant until the traps are saturated. As a consequence, recombination effects at electron traps may be neglected prior to the saturation of hole traps. Under these conditions, Eqs. [3.21], [3.22], and [3.25] are valid until saturation is reached. After saturation has been reached, the remainder of the analysis in the preceding section holds true. Figure III-4 illustrates the situation.

If $P_t > N_t$, the density n_t for deep electron traps rises linearly with time until saturation is approached. The current remains at a constant low value and then begins rising at a linear rate when saturation comes. If a shallow trap is present, its electron occupancy also increases linearly, but the current has both constant and linearly rising components; the rate of growth jumps upward when saturation is achieved. When the traps are all filled and the light is removed, the

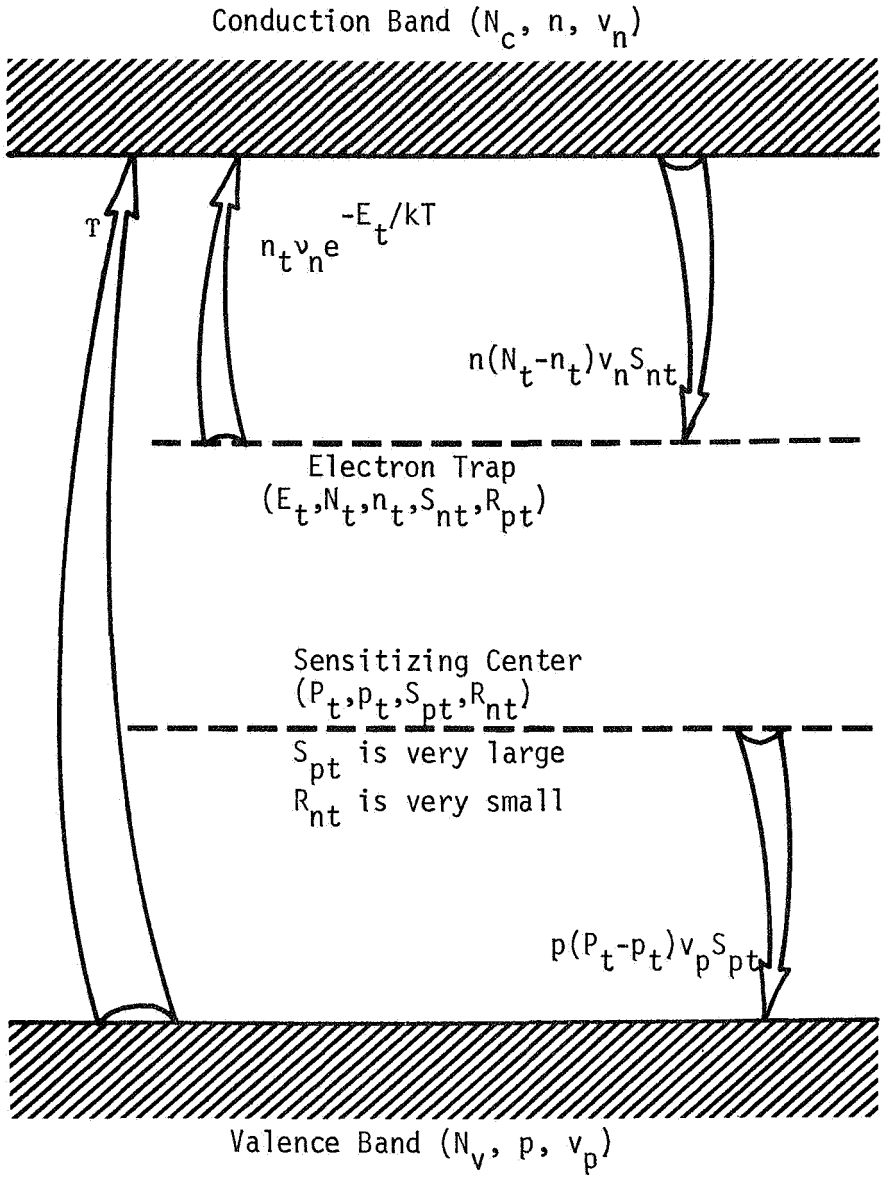

Figure III-4. Shown is the energy level scheme for use when a single electron trap and a single sensitizing center with fast hole trapping exist. Direct band-to-band recombination, thermal emission from the sensitizing center, and sub-bandgap optical excitation are neglected. The rate equations for electrons are

$$\frac{dn}{dt} = T + n_t v_n e^{-E_t/kT} - n(N_t-n_t)v_n S_{nt}$$

$$\frac{dn_t}{dt} = n(N_t-n_t)v_n S_{nt} - n_t v_n e^{-E_t/kT}.$$

current does not decay because recombination of electrons with trapped holes is not favorable.

If $N_t > P_t$, both types of traps fill at the constant electron-hole generation rate until $p_t \simeq P_t$. The availability of free holes after that time prevents the electron traps from filling completely, because of the fast recombination. For this reason, the free hole density remains small. Electrons in the conduction band and shallow traps decay into deeper traps when the excitation is removed.

If electrons are removed from a trap by long wavelength light, the excess density of free electrons is $\Delta n = T\tau_L$, where $1/\tau_L = (N_t - n_t)v_n S_{nt}$, and Δn decays exponentially with a characteristic time of τ_L when the light is removed:

$$\Delta n(t) = \Delta n_o e^{-t/\tau_L}$$

If several electron traps exist, electrons in the shallow traps decay into deep traps when the excitation is removed. The response time of this redistribution is governed by the rate at which electrons leave the traps, and is given by Eq. [3.30] since $\tau_d >> \tau_L$.

SINGLE ELECTRON TRAP AND SINGLE HOLE TRAP

If both hole traps and electron traps exist, recombination is possible at both levels. The rate equations are all non-linear and very difficult to work with. Bube[1] treats several cases of this situation after making extensive assumptions. A situation not treated in that reference is when recombination is very fast for one type of carrier and relatively slow for the other type. This case may be treated as an extension of the previous sections if we assume that free holes are quickly trapped or recombine with trapped electrons. Free electrons have a much greater probability for being captured at electron traps

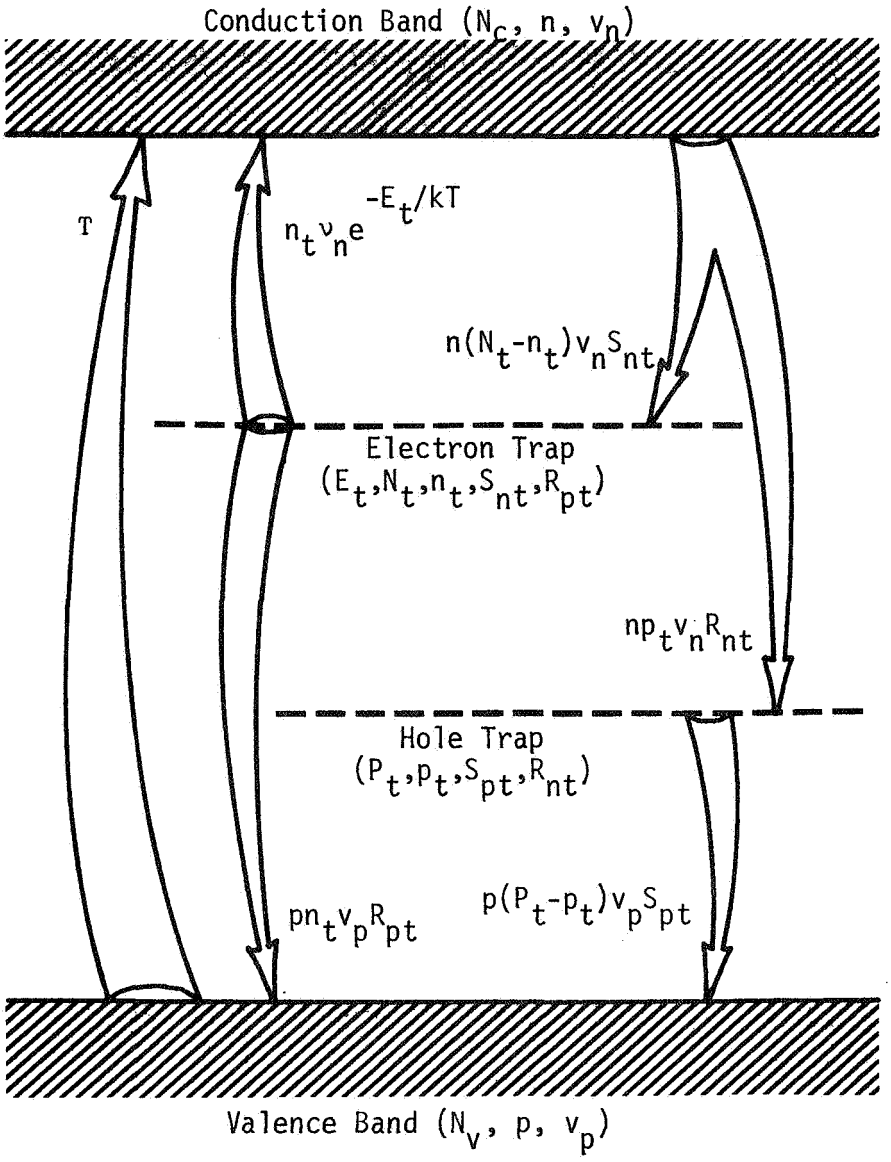

Figure III-5. Shown is the energy level model for use when both hole and electron traps exist. Direct band-to-band recombination, thermal emission from the hole trap, and sub-bandgap optical excitation are neglected. The rate equations are

$$\frac{dn}{dt} = T + n_t v_n e^{-E_t/kT} - n(N_t-n_t)v_n S_{nt} - np_t v_n R_{nt}$$

$$\frac{dn_t}{dt} = n(N_t-n_t)v_n S_{nt} - n_t v_n e^{-E_t/kT} - pn_t v_p R_{pt}$$

$$\frac{dp}{dt} = T - pn_t v_p R_{pt} - p(P_t-p_t)v_p S_{pt}$$

$$\frac{dp_t}{dt} = p(P_t-p_t)v_p S_{pt} - np_t v_n R_{nt}.$$

than for recombining with trapped holes. The energy band model appears in figure III-5.

The effect of slow recombination at hole traps is to include a small subtractive term in the rate equation for n. It leads to no significant changes in the initial rise, excitation steady state, and early decay relations for the carrier densities. It does affect the long term decay, however, where the rate of decay is

$$\frac{dn}{dt} = n_t \nu_n e^{-E_t/kT} - n(N_t - n_t) v_n S_{nt} - n p_t v_n R_{nt} \qquad [3.33]$$

If $p \simeq 0$ and $n << n_t$, $n_t \simeq p_t$ and the solution to Eq. [3.33] is

$$n = n_t N_c v_n S_{nt} e^{-E_t/kT} \tau_r e^{-t/\tau_r} \qquad [3.34]$$

where

$$\tau_r = [(N_t - n_t) v_n S_{nt} + n_t v_n R_{nt}]^{-1} \qquad [3.35]$$

Eq. [3.34] is equivalent to Eq. [3.29] when recombination at the hole trap is negligible, and τ_r reduces to the free electron lifetime.

In the more specialized case where thermal freeing from the electron traps is negligible and those traps are saturated, the decay of n is given by

$$n = n_o e^{-(n_t v_n R_{nt})t} \qquad [3.36]$$

When the model discussed above applies, parameters of the electron trap are found as before. The recombination cross section at the hole trap is found by analyzing the decay of n according to Eq. [3.34] or Eq. [3.36].

RETRAPPING

When retrapping of thermally freed carriers is important, it is necessary to correct the rate equation for n_t. Specifically, the thermal

emission rate,

$$\left[\frac{dn_t}{dt}\right]_{thermal} = -n_t \nu_n e^{-E_t/kT} \qquad [3.37]$$

must be multiplied by the probability that the carrier will recombine. The transitions involved are shown in figure III-6. The recombination probability is given by[1]

$$R.P. = \frac{p_t R_{nt}}{p_t R_{nt} + (N_t - n_t) S_{nt}} \qquad [3.38]$$

But if $p_t \simeq n_t + n$, and $n_t >> n$, then $p_t \simeq n_t$ and

$$R.P. = \frac{n_t R_{nt}}{n_t (R_{nt} - S_{nt}) + N_t S_{nt}} \qquad [3.39]$$

The correct expression to substitute for the thermal emission rate is

$$\left[\frac{dn_t}{dt}\right]_{thermal} = \frac{-n_t^2 R_{nt} \nu_n e^{-E_t/kT}}{n_t (R_{nt} - S_{nt}) + N_t S_{nt}} \qquad [3.40]$$

When $n_t(R_{nt}-S_{nt}) >> N_t S_{nt}$, it must also be true that $R_{nt} >> S_{nt}$, so equation [3.40] reduces to [3.37]. For $N_t S_{nt} >> n_t(R_{nt}-S_{nt})$, the behavior is given by

$$\left[\frac{dn_t}{dt}\right]_{thermal} = \frac{-n_t^2 R_{nt} \nu_n e^{-E_t/kT}}{N_t S_{nt}} \qquad [3.41]$$

Under these conditions, when an electron trap fills from the conduction band and retrapping is allowed, the steady state value of n_t is

$$n_t = \left[\frac{T N_t}{N_c \nu_n R_{nt}}\right]^{1/2} e^{E_t/2kT} \qquad [3.42]$$

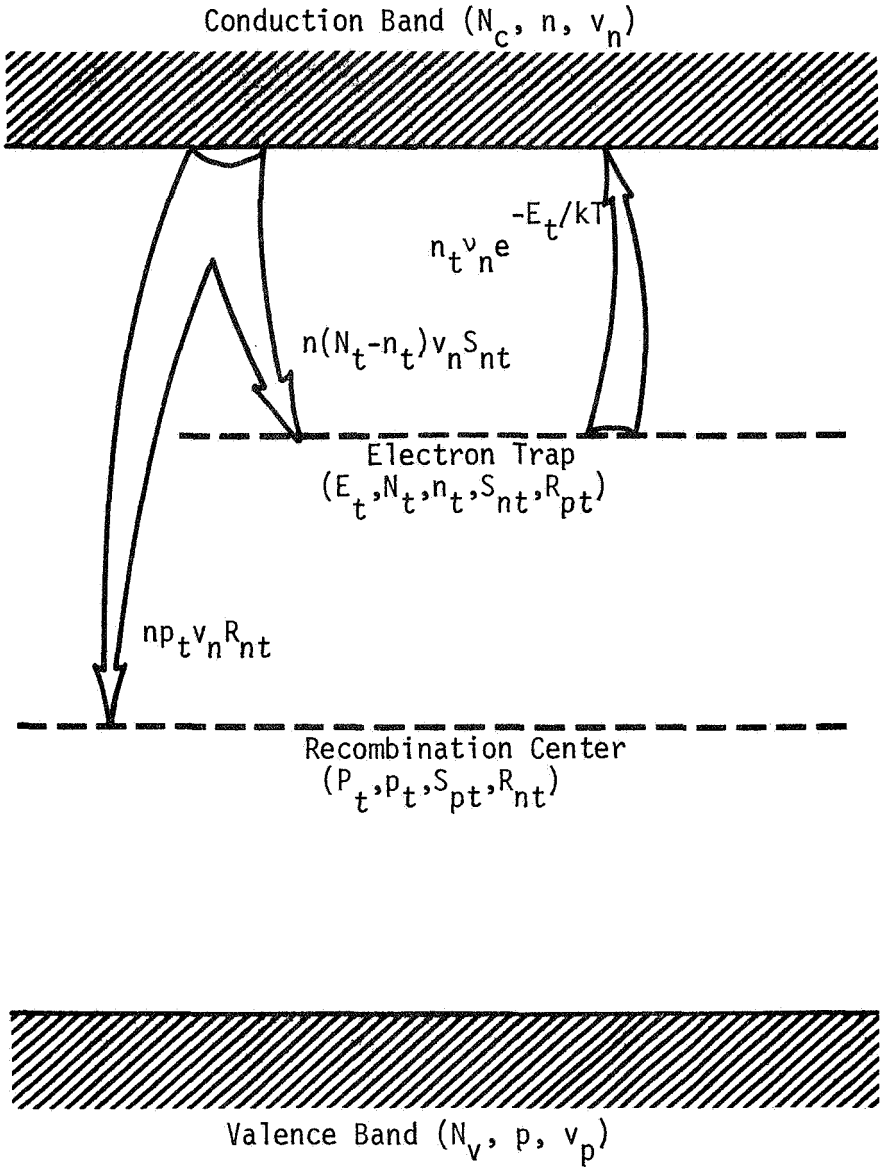

Figure III-6. Shown are the transitions involved when retrapping effects must be considered. The gross thermal emission rate from the electron trap is $n_t \nu_n \exp(-E_t/kT)$, whereas the net rate, corrected for retrapping is

$$(dn_t/dt)_{thermal} = \frac{-n_t^2 R_{nt} \nu_n \, e^{-E_t/kT}}{N_t S_{nt}} .$$

The decay of n_t follows the relation

$$n_t = \frac{n_t(\infty)}{1 + n_t(\infty)\left[\frac{N_c}{N_t}\right]v_n R_{nt} e^{-E_t/kT} t} \qquad [3.43]$$

The time required for n_t to decay to 1/2 $n_t(\infty)$ is therefore

$$\tau_{1/2} = \frac{N_t e^{E_t/kT}}{n_t(\infty) N_c v_n R_{nt}} \qquad [3.44]$$

The equilibrium value of n is given by Eq. [3.8], after correcting for retrapping and allowing for recombination, resulting in

$$n = \frac{n_t^2 R_{nt} N_c e^{-E_t/kT}}{N_t^2 S_{nt}} = \frac{T}{p_t v_n R_{nt}} \qquad [3.45]$$

When the free carrier lifetime is primarily determined by recombination, such that $p_t v_n R_{nt} >> N_t v_n S_{nt}$, Eqs. [3.42], [3.44], and [3.45] may be used to find R_{nt}, N_t, and p_t from measurements of n, n_t, and T. It is important to remember that p_t is the density of recombination centers, which means that it consists of the part of the total hole trap density which has captured a hole and is ready to capture an electron.

CHAPTER IV.

EXPERIMENTAL TECHNIQUES

The accuracy and sensitivity of the experiments described in Chapter V are determined primarily by the limits of the equipment used to make the measurements. This chapter lists the apparatus employed in the standard and photodielectric experiments and describes equipment limitations. Characteristics of the semiconductor samples are given first.

SEMICONDUCTOR SAMPLES

Except for the CdS:Al powdered sample, all samples used in the experimental work described here are single crystals. The CdS:Al was obtained from Texas Instruments in the form of a large ($\sim$ 1 cm^3) irregular single crystal chunk. The presence of aluminum was confirmed by neutron activation analysis performed in the University of Texas Nuclear Reactor Laboratory. The CdS:Al sample was prepared by cutting a wafer from the chunk with a diamond saw. Next, a circular shape was obtained using an ultrasonic grinder, and then the surfaces were lapped and polished to a smooth, glassy finish. When it was judged to be necessary, the sample was cleaned in boiling trichloroethylene and etched in dilute hydrochloric acid. Some physical characteristics of all of the samples are listed in Table IV-1.

The CdS:Ag was also obtained from Texas Instruments, but it was supplied in the form of a highly polished, irregularly shaped piece with parallel faces. The sample shape was not altered because it is roughly circular and it was desirable to preserve the excellently prepared surface. Since no excess material existed, no neutron activation analysis could be performed.

TABLE IV-1

Characteristics of Samples					
Parameter	CdS:Al	CdS:Al powder	CdS:Ag	CdTe	ZnTe
V, cm^3	0.143	1.245×10^{-2}	0.052	0.1335	0.0668
t, mm	1.93	0.18	1.5	1.8	1.7
A, cm^2	0.742	0.70	0.343	0.742	0.393
G	0.0532	0.0042	0.0266	0.0347	0.0367
$\rho(300^{\circ}K)$ ohm-cm	10^{10}	10^{10}	2×10^{10}	2×10^{5}	2.5
Conductivity Type	n	n	n	p	p

Both CdS samples were heat treated by placing them in separate evacuated quartz ampoules and keeping them at $\sim$ 500°C for several days, a sensitization technique reported by Woods[46]. It is believed that this process creates sulphur vacancies which donate electrons to compensate native acceptor levels. In both samples, no new levels were detected after the heat treatment, but definite improvements in sensitivity occurred, indicating that the treatment simply increased the density of a defect which had existed before the heating was performed.

The CdTe and ZnTe materials were both purchased from the A.D. Mackay Company in the form of large, irregular chunks of about 1 cm^3 volume. Attempts to cut slices from the chunks proved to be unsuccessful, so samples were obtained by cleaving off plates about 2 mm thick. In both cases, the cleaving produced irregularly shaped samples with uniform thicknesses and glassy faces, so no polishing or etching was performed. Both materials were classified as "ultra high purity" by the supplier.

The powder sample of CdS:Al was obtained by crushing a small amount of material left over from the process of shaping the CdS:Al single crystal sample. The resultant powder consisted of grains estimated to be about the size of grains of #400 lapping powder. The powder was wetted with trichloroethylene which acted as a temporary binder, while the material was transferred to a 1 cm diameter, 2 mm thick glass disc and tamped to encourage settling. The trichloroethylene was then completely evaporated by warming the glass disc, and a thin film of Krylon brand crystal clear spray coating was applied as the permanent binder. In the characteristics listed in Table IV-1, the contributions due to the glass slide have been subtracted out.

LIGHT SOURCES

The light used in the experiment described in the next chapter was obtained primarily from one of two monochromators. The first is a Gaertner monochromator utilizing a sodium chloride prism, with a useful range of 0.589μ to 12.0μ. The other is a Bausch and Lomb grating monochromator covering the range from 0.2μ to 0.75μ. Each has variable input and output slits which were used to control the intensity and bandwidth of the light.

Two white light sources were available as sources for the monochromators. For visible and near infrared wavelengths a 500 watt type DHN projection lamp was adapted to either instrument. The lamp voltage was adjusted with a variable transformer and it was operated at 115 VAC. Tests showed that about 10 minutes of warm-up was required before the lamp output stabilized, and thus a warm-up period was allowed. Forced air cooling was used to prevent over-heating. The lamp spectrum approximates the spectrum of a 2000°K black body when it is operated at 115 VAC.

Since the glass envelope of the projection lamp absorbs wavelengths above about 3μ, it was necessary to use a Perkin-Elmer globar to obtain the longer infrared wavelengths. When operated at 5.2 amps, it furnishes 200 watts in a spectrum approximating a 1400°K black body. The globar also requires about a 10 minute warm-up period before it stabilizes, and water cooling is required.

A third source of light used was a Spectra Physics 125 helium-neon laser operating at 0.6328μ. It was employed both in exciting the samples and in calibrating the wavelength settings of the monochromators. The maximum output obtainable from the laser is about 16 mw, and the

power level was controlled by inserting a pair of rotating polarizing filters into the beam.

LIGHT CALIBRATION

Light intensity measurements were made using an Eppley sixteen junction Ag-Bi thermopile monitored with a Hewlett-Packard 425 microvoltmeter. The thermopile was calibrated against an NBS standard source at both microwatt and milliwatt intensities by the manufacturer. Both quartz and barium fluoride windows were available.

To measure the amount of light reaching a sample, a silicon solar cell was placed in the position normally occupied by the sample, the light was turned on, and the solor cell current was noted. Next the cell was placed in front of the output slit of the monochromator and the input was adjusted until the cell gave the same current reading seen before. Then the thermopile was substituted for the solar cell, and the power level was obtained. Five readings were obtained, and the average value was taken to be the correct value. The individual readings tended to be within 2% of the average value, and from one day to the next, repeatability was excellent.

OPTICAL ABSORPTION MEASUREMENTS

For measuring optical absorption by the sample at room temperature, a special sample holder is attached to the monochromator. The special holder allows two masks with one small hole in each to be placed between the monochromatic light source and the detector. As the wavelength is varied, the detector output is recorded. Next, the sample is placed between the masks so that light passing through the two holes must also pass through the sample, and the detector output is again recorded. Point-by-

point division of the second value by the first gives the fraction of the light which is transmitted, T. The fraction absorbed, A, is related to T by

$$A = (1 - T)(1 - R) \qquad [4.1]$$

where R is the reflection coefficient. R depends on the index of refraction n[58]

$$R = \frac{(n - 1)^2 + k^2}{(n + 1)^2 + k^2} \qquad [4.2]$$

Here, k is the extinction coefficient, related to the absorption coefficient α by

$$k = \frac{\alpha\lambda}{4\pi} \qquad [4.3]$$

It may be shown[58] that k has a negligible effect on R, except for some cases of strong bandedge absorption.

The accuracy of the absorption technique is limited by the constant bandwidth-power output characteristic of the monochromator. To allow for enough light through the sample to be measured, the output slit must be opened to 0.5 to 1.0 mm, which results in an optical bandwidth of about 1%. This means that fine structure in absorption tends to be smoothed out.

PHOTOCONDUCTIVITY AND TSC MEASUREMENTS

All experiments requiring ohmic contacts to the samples were performed in a special evacuated sample holder, shown in Fig. IV-1. Light is applied to the sample by aiming the beam down the large polished stainless steel tube. The length and diameter of the tube, and the position of the sample in relation to the end of the tube, are designed to duplicate the optical system for illuminating samples in the microwave cavity, which is discussed in one of the following sections. Measurements revealed that

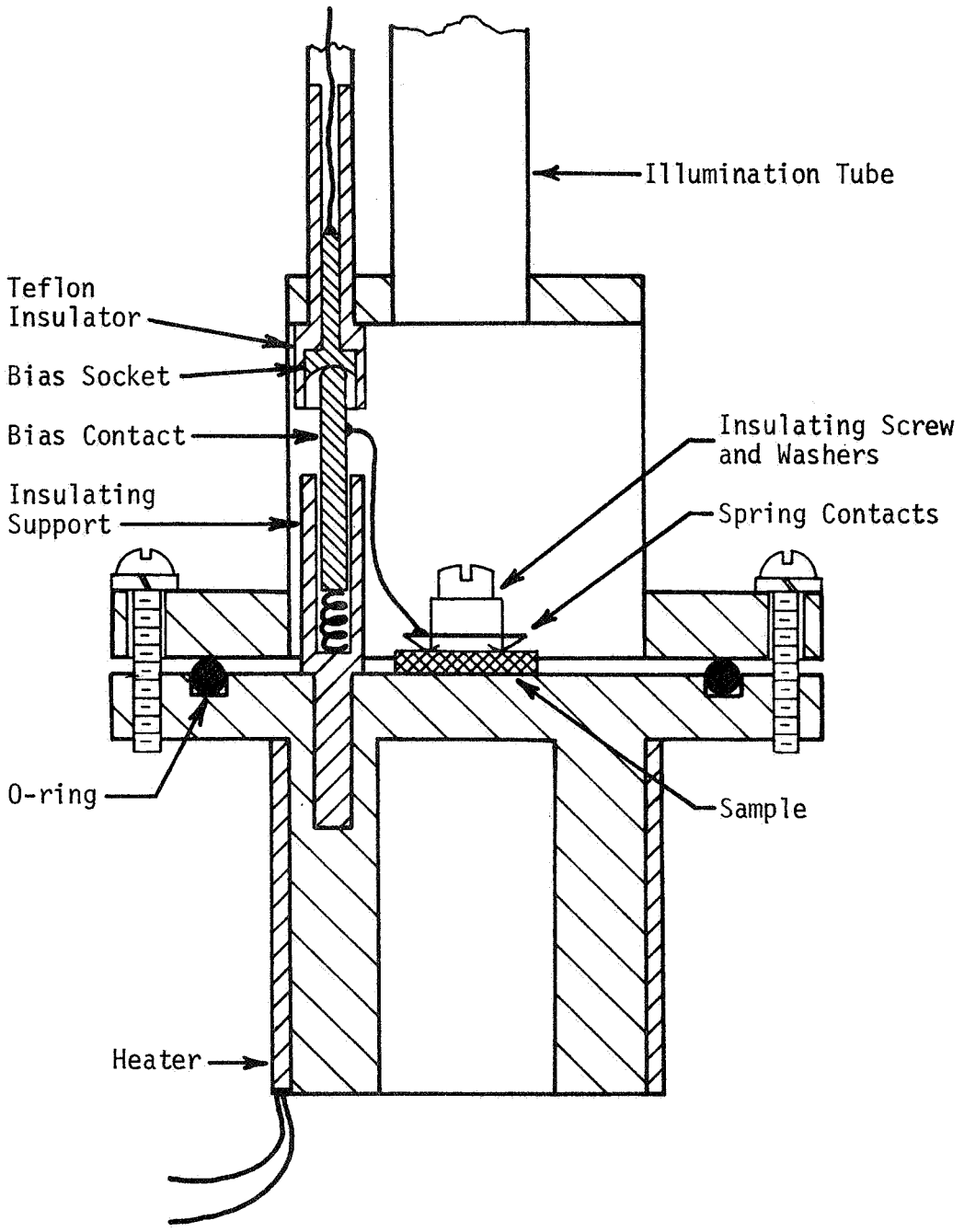

Figure IV-1. Evacuated Sample Holder.

no differences in transmission characteristics were discovered between the two systems.

Light is introduced into the stainless steel tube through a shutter-mirror-window assembly which is slipped over the protruding end of the tube and held securely in position with mechanical stops. The shutter is used in making decay measurements and for keeping unwanted light away from the sample. The silver first-surface mirror is rigidly mounted at 45° to convert the horizontal beam emerging from the light source to a vertical beam. A 2 mm thick barium fluoride window, with flat transmission characteristics from $\sim$ 0.2 μ to $\sim$ 12 μ is used to allow the sample holder to be evacuated; the vacuum port is also located in the shutter-mirror-window assembly, and all vacuum seals are made with O-rings.

The bottom half of the sample holder, to which the sample is mounted, is removable to allow for easy maintenance and rapid sample changes. The vacuum seal is preserved with an O-ring, and brass machine screws with heavy lock washers hold the two halves together and keep pressure on the seal. The sample rests on a pad of indium or other suitable contact metal, which is the cathode, and it is held in place by several indium plated brass spring fingers which form the other electrode. A spring loaded contact is connected to the fingers with a short flexible wire, and the bias circuit is completed when the spring contact engages the socket built into the roof of the sample holder.

When TSC experiments are performed, heat is provided by a single 50 VDC, 50 W Watlow silicone rubber heater clamped to the sample holder. Heater power is obtained from a Kepco power supply controlled by a clock driven variable resistor. Over a period of two years, the heater has

shown no sign of aging or degradation, and the heating scheme gives repeatable temperature vs. time profiles. The sample temperature is monitored with a chromel-alumel thermocouple inserted in a hole drilled from the outside of the sample holder to a position beneath the sample. During warming, frost formed on the holder melts within a two-second interval, indicating the temperature difference between any two points on the holder never exceeds about 1°K. The sample is cooled by completely submerging the holder assembly in liquid nitrogen or partially submerging it in liquid helium; the O-ring is not effective in sealing out liquid helium.

The sample is biased with either a 6V or 67V battery, and the current is measured with a Hewlett-Packard 425 picoammeter and plotted with a Moseley X-Y recorder whose vertical axis is driven by the output of the HP 425. The horizontal axis is driven either by the internal time base or the thermocouple voltage. All wiring is completely shielded by routing it in metal tubing and using Beldfoil shielded strain gauge cable for the flexible connections. The leakage resistance of the entire biasing network is $\sim 10^{13}$ ohms; the measurement limit of the HP 425 is $\sim 10^{-12}$ amps, and these two factors determine the sensitivity of the system.

THERMALLY STIMULATED CONDUCTIVITY

Thermally stimulated conductivity (TSC) experiments are performed by submerging the sample holder in the coolant while the sample is kept in the dark. When the temperature stabilizes, a known intensity, wavelength, and duration of light is focused on the sample. Finally, the coolant is removed, the clock driven heater is started, and the current is plotted against time or temperature. The heating rate β can be varied by adjusting the clock driven resistor; normally, the value $\beta \simeq 0.5$°K/sec was used.

The relations used in TSC analysis are well known[1,5]. It may be shown that when retrapping at a level is negligible, the trap energy E_t (measured from the band to which the carrier is emitted) is related to the temperature of the TSC peak, T_m, by

$$E_t = kT_m \ln\left[\frac{N_c S_t v k T_m^2}{\beta E_t}\right] \qquad [4.4]$$

Additional assumptions are that none of the physical constants, such as μ, N_c, S_t, τ_L, and v vary greatly with temperature in the region of the peak. Physically, the TSC maximum corresponds to the maximum rate of ejection of electrons from traps.

When retrapping does occur, the proper relation is[39]

$$E_t = kT_m \ln\left[\frac{N_c k T_m^2}{N_t \beta \tau_L E_t}\right] \qquad [4.5]$$

Only a small error is involved if the trap depth is equated to the depth of the Fermi level when the trap is half filled. This gives the simple relation[39]

$$E_t = kT_m \ln\left[\frac{N_c}{n_m}\right] \qquad [4.6]$$

where n_m is the free carrier density at $T = T_m$. Haering and Adams[5] have shown that the shape of a conductivity peak is virtually independent of the retrapping rate, with the shape following

$$-\ln\left[\frac{\sigma(T)}{\sigma_o}\right] = \frac{E_t}{kT} + \exp\left[\frac{E_t}{kT_m} - \frac{E_t}{kT}\right] \qquad [4.7]$$

Furthermore, at the maximum, the conductivity and temperature are related by a universal curve of the form

$$-\ell n\left[\frac{\sigma(T_m)}{\sigma_o}\right] = \frac{E_t}{kT_m} + 1 \qquad [4.8]$$

which follows from the preceding equation. Since T_m depends on the heating rate β, $\sigma(T_m)$ and T_m may be measured at two or more known heating rates and E_t may be found from

$$\ell n\left[\frac{T_m^2}{\beta}\right] = \frac{E_t}{kT_m} - \ell n[constants] \qquad [4.9]$$

Eq. [4.9] is obtained by rewriting either [4.4] or [4.5]. Clearly, the trap depth may be found by plotting $\ell n[T_m^2/\beta]$ vs. $(kT_m)^{-1}$.

Another way to find E_t is to analyze the initial rise of a TSC peak if it is not hidden by other peaks. Garlick and Gibson[17] show that the simple relation expected is

$$\frac{dn}{dt} = n_{to}\nu_n e^{-E_t/kT} \qquad [4.10]$$

where ν_n is the attempt to escape frequency. E_t is found without knowledge of $n_{to}\nu_n$ by analyzing a curve of ℓn n vs. 1/T.

PHOTODIELECTRIC MEASUREMENTS

The reason for the great sensitivity of the photodielectric technique is the superconducting microwave cavity used. A full size cutaway drawing of the cavity employed in this study is shown in Fig. IV-2. A layer of lead, the superconducting material, is electroplated onto the

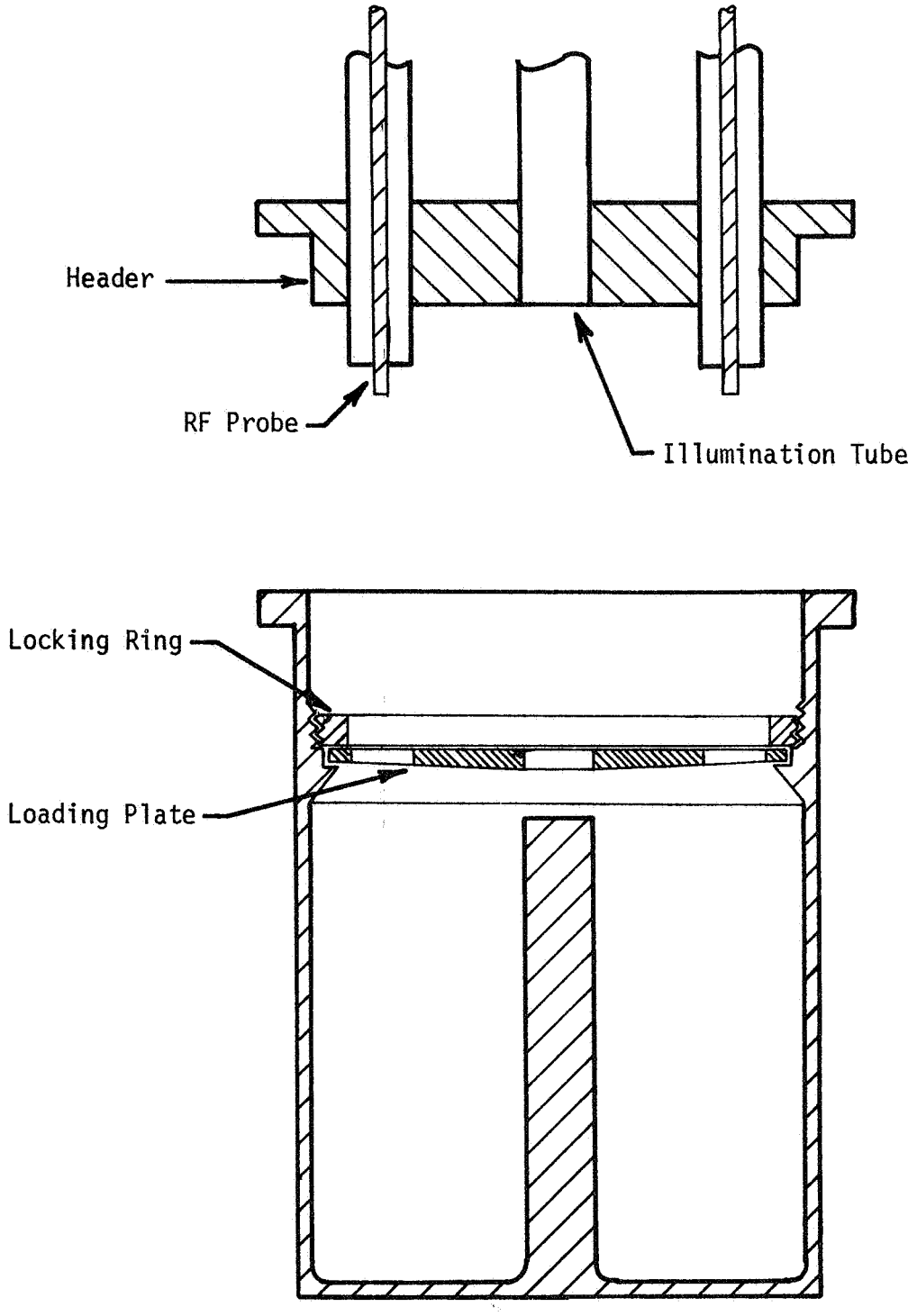

Figure IV-2. Superconducting Microwave Cavity.

cavity, loading plate and probe surfaces. The design of the cavity and the plating process are completely covered by Stone[26] and are not considered further here. The cavity unloaded resonant frequency is about 9 x 10^8 Hz; loaded, it is about 8.5 x 10^8 Hz.

The capacitive loading plate is tapered slightly and small holes are provided around its perimeter to allow helium gas bubbles to escape the cavity. A small hole is provided in the cavity wall above the loading plate to facilitate the entry of helium liquid into the cavity. A variety of small teflon collars is available for holding the semiconductor sample in place in the high field region at the end of the stub. Microwave energy is coupled into and out of the cavity with two capacitive probes. Coupling is varied by adjusting the length of the probe which extends into the cavity. Generally, the coupling is kept as light as possible, consistent with a useable output signal. In all of the experiments reported here, the cavity Q was limited not by the cavity or teflon collar, but by the sample; with the large samples used, the Q was between 2 x 10^4 and 9 x 10^5, depending on the sample. The unloaded cavity Q is much greater than 10^6, so the sample determines the cavity sensitivity.

The accuracy of photodielectric experiments is limited primarily by the sample-cavity system. A large lossy sample causes the Q to be poor, and as a result the cavity bandwidth is wide and the resonant frequency is not easily determined. The inaccuracy in the measurement due to this reason is $\sim$ 1 kHz or one part per million. For higher Q situations where the frequency can be read very accurately, the random generation of helium bubbles in the cavity produces noise which leads to $\sim$ 100 Hz frequency variations or errors of one part in 10^7.

A block diagram of the photodielectric measurement system is shown in Fig. IV-3. The cavity resonant frequency is measured by maximizing the signal transmitted by the cavity and then reading the oscillator frequency. The phase locked oscillator is stable within a few Hz over a period of several minutes, and the counter gives the frequency to nine significant figures. Power absorption measurements cannot be made with such a high degree of accuracy, however; the Hewlett-Packard microwave detector exhibits small output fluctuations of less than 1%, possibly caused by small temperature variations. Its output signal varies roughly as the 2/3 power of the input power level, and a calibration curve is required for converting the output signal into P_{abs}/P_o. Q measurements are made by pulsing the input signal to the cavity, observing the decay of the pulse with an oscilloscope, and analyzing the result according to the relation (see Stone [26]),

$$Q = \pi f \tau \qquad [4.11]$$

where τ is the time required for the signal to drop to 1/e.

The low temperature environment, which allows the phenomenon of superconductivity to be used to advantage, and which also provides a constant temperature bath for the sample, is obtained by submerging the cavity in liquid helium. The helium is placed in the inner dewar of a nested pair of vessels; the outer dewar is filled with liquid nitrogen, providing a low temperature background to minimize heating of the contents of the inner dewar by radiation from the outside. Both dewars are suspended inside a light-tight box to prevent light from entering the cavity through the bubble relief holes.

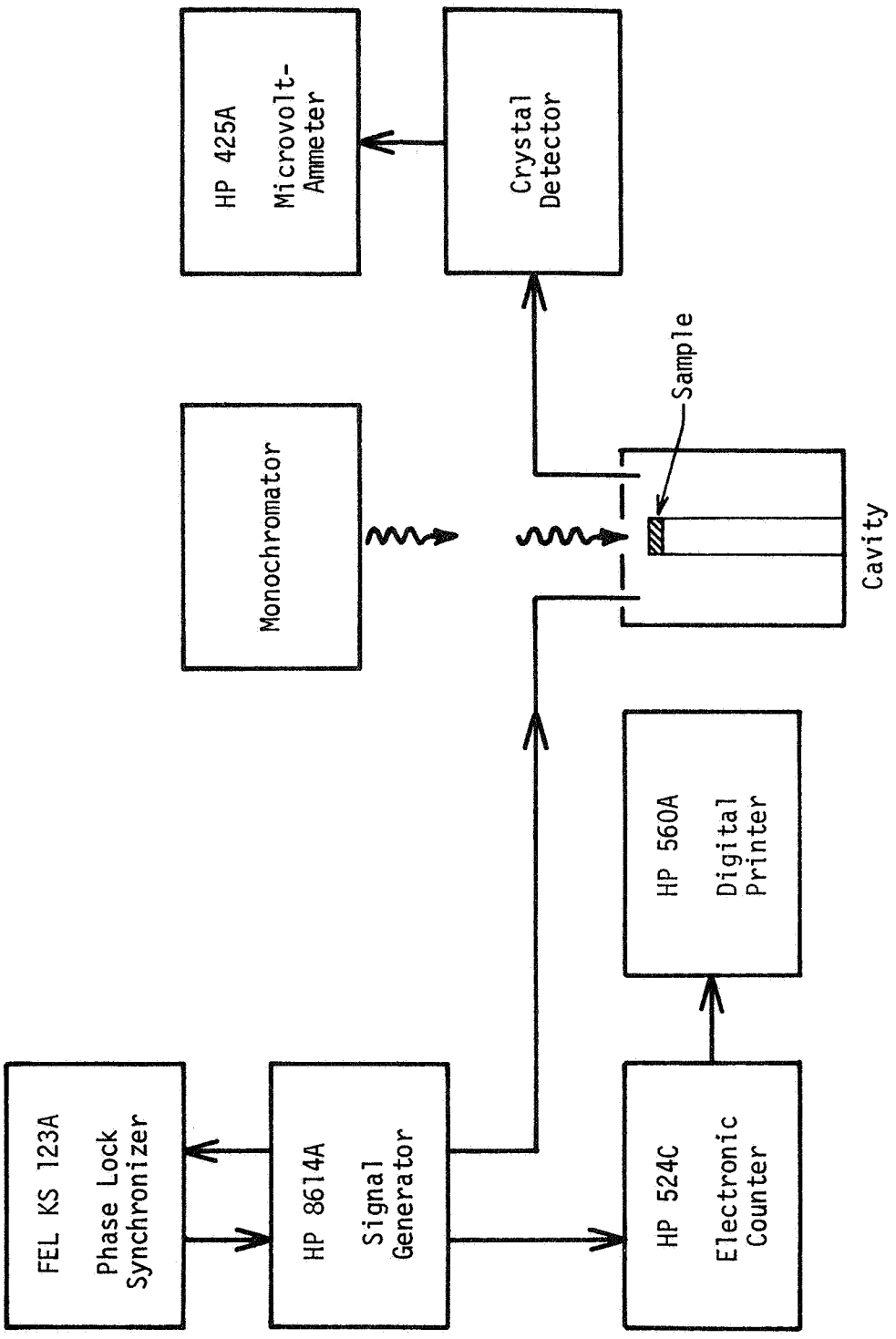

Figure IV-3. Block Diagram of Photodielectric Measurement System.

The inner dewar may be sealed, and temperatures down to about 2°K may be obtained by reducing the pressure over the helium. The temperature is controlled by varying the orifice between the inner dewar and a vacuum pump, and the temperature is monitored with a manostat connected to the inner dewar.

CHAPTER V.

EXPERIMENTAL RESULTS

INTRODUCTION

The results of photodielectric experiments on three different II-VI compounds, CdS, CdTe, and ZnTe, are presented here. One sample of CdS is aluminum doped and the other is silver doped; the tellurides are both high purity materials.

The CdS:Al was chosen because the sample exhibits both tap and storage effects and is very photosensitive. The CdS:Ag does not display tap or complete storage effects, but it is very sensitive to infrared quenching. Both CdS samples were heat treated in a vacuum at $\sim 500^{\circ}C$ to insure a large density of compensated acceptors or hole traps. No changes in the electron trap properties were observed as a result of the heating. The tellurides were chosen because their crystal structure and behavior differ markedly from those of CdS. Both samples are p-type and thus no heat treatment was performed.

Before performing photodielectric tests on the samples, each was subjected to several standard experiments which also yield values for trapping and recombination parameters, in order to obtain standards for comparison. In the following sections, the investigations of each material are presented, and results obtained with the photodielectric effect are compared with the results of the other tests whenever possible.

CdS:Al - STANDARD EXPERIMENTS

Four methods were first used to find discrete energy levels in the CdS:Al; absorption spectra, photoconductivity spectra, thermally stimulated conductivity, and decay curve analysis. The absorption spectrum

for the CdS:Al at 300°K is shown in Fig. V-1. The lack of any sharp details is primarily due to the thickness of the sample. There are two fairly well defined peaks in the curve at 6050 ± 50 Å and 5450 ± 50 Å, corresponding to transitions of 2.05 ± 0.02 eV and 2.275 ± 0.02 eV, respectively. Since the bandgap energy is 2.40 eV, the energy levels indicated must lie 0.35 ± 0.02 eV and 0.125 ± 0.02 eV below the conduction band. The curve also shows high absorption in the vicinity of 1.55 μ, corresponding to an 0.8 eV transition. This probably does not represent absorption by the expected compensated acceptor sites, which normally occurs near 1.0 μ[1]. Thus, a discrete level also exists about 0.8 eV below the conduction band.

The photoconductivity spectrum of the CdS:Al at 300°K is presented as Fig. V-2; its shape is similar to the absorption curve in the band-edge region, as would be expected. The photoconductivity peaks occur for λ = 5450 ± 50 Å and λ = 6100 ± 50 Å, corresponding to levels 0.125 ± 0.02 eV and 0.37 ± 0.02 eV below the conduction band. These two levels are clearly the same two seen in the absorption spectrum.

The sample shows photoconductivity at wavelengths between 1.5 μ and 9 μ, but the effects are small and no clear peaks are seen.

Thermally stimulated conductivity (TSC) experiments with the CdS:Al confirm the presence of a trap at about 0.35 eV, and also reveal a deeper trap near 0.74 eV. No peak is contributed by the level at 0.13 eV because all TSC tests were started at 77°K, and the peak temperature for a 0.13 eV trap should be near 60°K. Evidence for the shallow trap is seen in the decay of photoconductivity at 77°K following excitation of the crystal by bandgap light. A typical decay curve is shown in Fig. V-3. Using

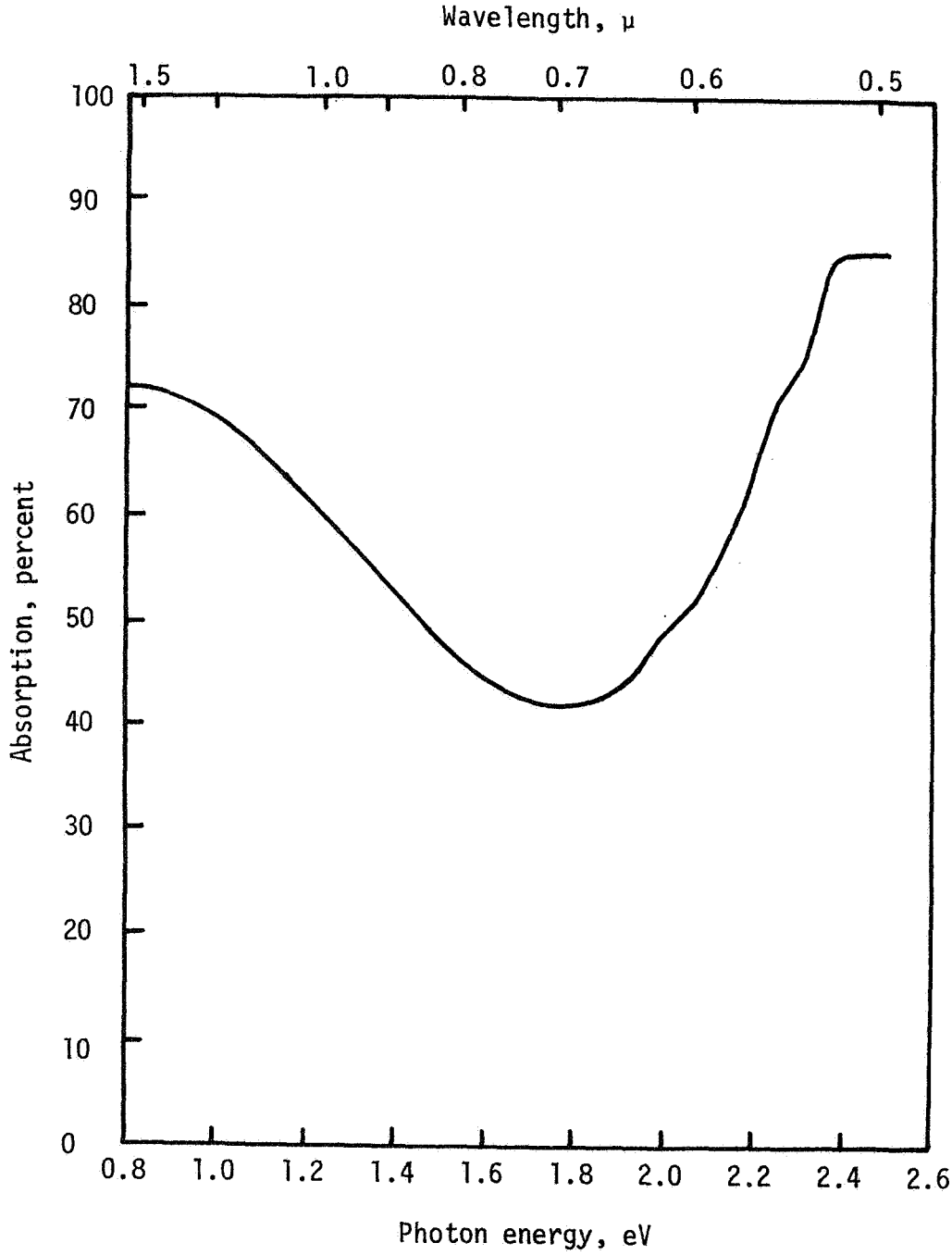

Figure V-1. Absorption Spectrum in CdS:Al at 300°K.

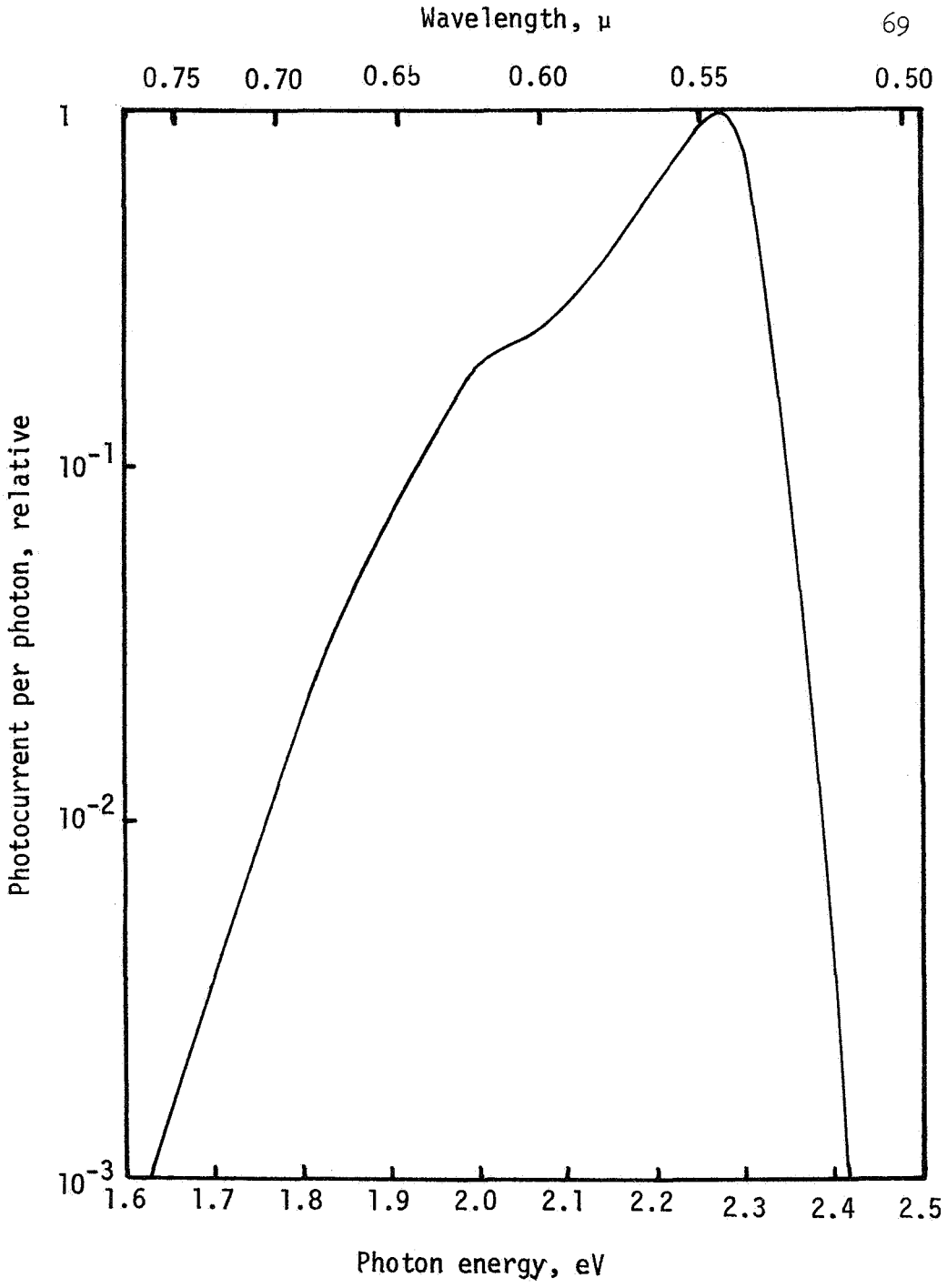

Figure V-2. Photoconductivity Spectrum for CdS:Al at 300°K.

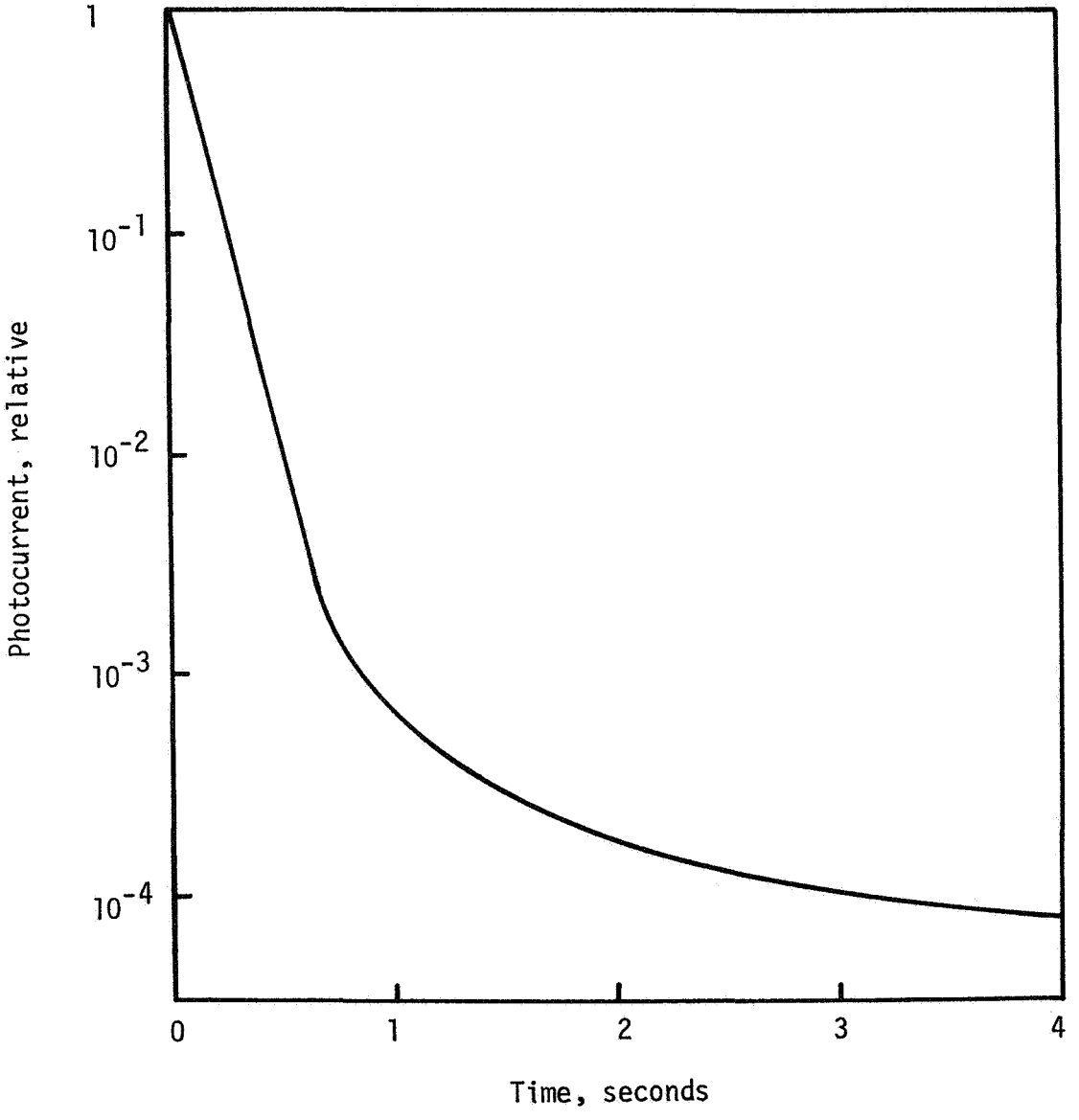

Figure V-3. The decay of the photocurrent in CdS:Al at 77°K is shown. The optical excitation is removed at t = 0.

Eq. [3.31] for E_t in terms of τ_d, the value E_t = 0.13 eV is found for τ_d = 0.23 seconds and $S_t = 10^{-14} cm^2$.

A series of TSC experiments was performed to determine the rates of filling of the two TSC traps. Fig. V-4 shows that the deeper trap is partially filled before the bandgap light is applied, due to incomplete emptying during the preceding TSC test. Furthermore, the 0.74 eV trap fills very slowly in comparison to the deeper traps. Both of these facts imply that the level has a small capture cross section S_t, which can be estimated to be about $10^{-18} cm^2$, using Eq. [3.16]. The trap at 0.35 eV fills more rapidly than the deeper trap, indicating a capture cross section of about $2 \times 10^{-16} cm^2$.

The third curve on Fig. V-4, labeled "0.13 eV trap" is actually a plot of the rise of photoconductivity at 77°K. It has already been shown that the variation of conductivity at that temperature is governed primarily by the 0.13 eV trap. At first, it appears that the trap saturates after about 300 seconds, but the leveling-out of the curve is actually a result of the lifetime becoming so short that the rate of recombination approaches the carrier generation rate. At temperatures below T_m (0.13 eV), the TSC peak temperature for the 0.13 eV level, the trap does not tend to return carriers to the conduction band as it does at 77°K, and hence it fills to a much greater density.

Fig. V-4 also shows that the 0.74 eV trap resumes filling immediately when the light is turned on, while no increase in the density of carriers at the 0.35 eV trap is seen until about 2×10^{14} photons have entered the crystal. Similarly, the 0.13 eV trap begins to fill after about 4×10^{15} photons have arrived. Therefore, the electrons prefer to

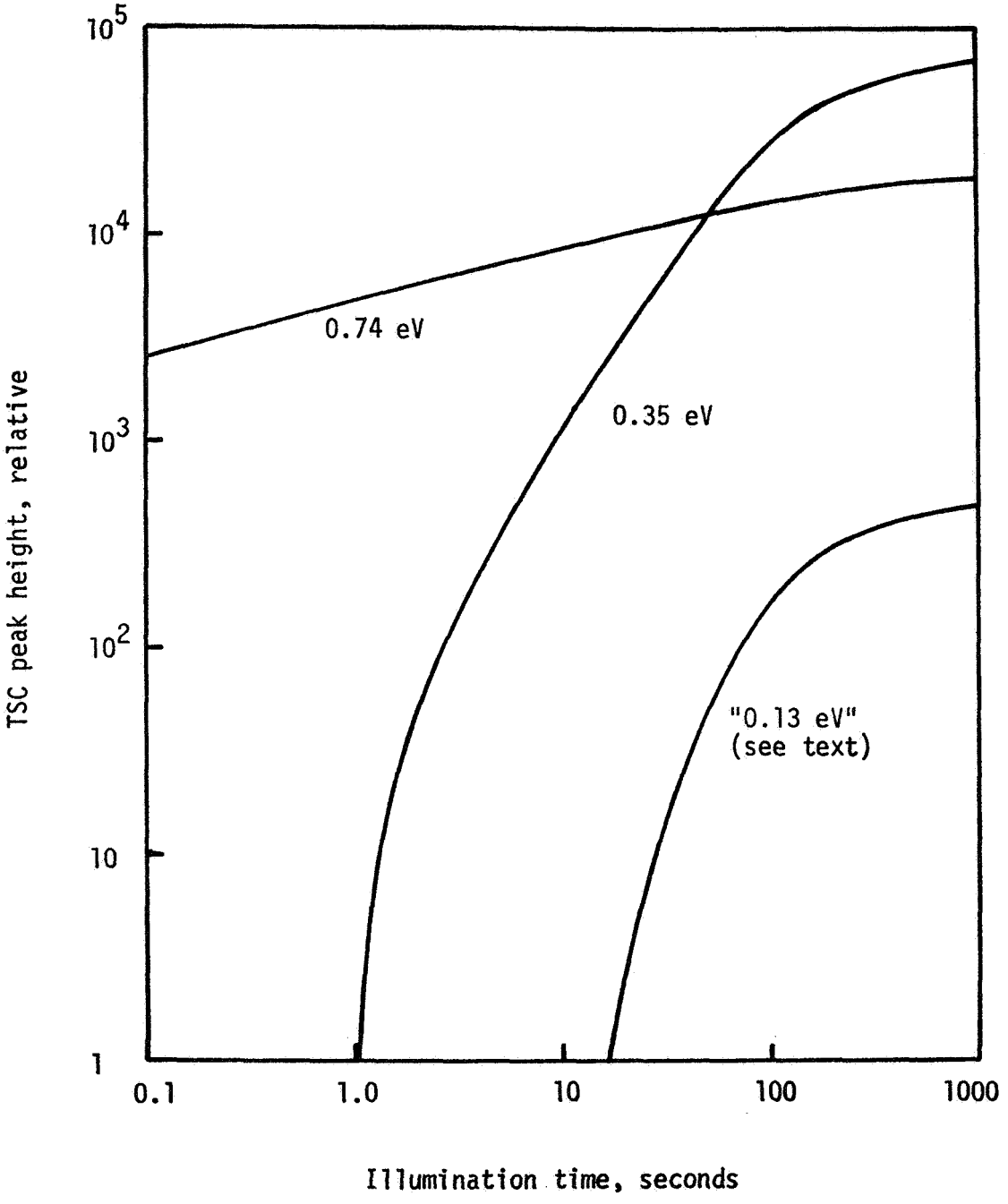

Figure V-4. Shown are the rates of filling of three electron traps in CdS:Al at $77^{o}K$ for constant bandedge illumination of 1.7×10^{14} photons/sec.

occupy the lowest energy states as long as the probability of finding a vacant site is high. As the number of empty sites at deeper traps is reduced by filling, electrons begin collecting at shallower levels. Since the volume of the sample is 0.143 cm^3, these figures may be used to roughly estimate the trap densities as follows: N_t (0.74) $\simeq 1.5 \times 10^{15}$, N_t (0.35) $> 3 \times 10^{16}$, and N_t (0.13 $> 4 \times 10^{16}$ cm^{-3}.

The CdS:Al is sensitive to sub-bandgap light at certain wavelengths. The result of a TSC spectrum shows that traps are filled if the light is sufficiently energetic to excite carriers from the valence band to the trap. Furtherfore, weak photoconductivity is seen throughout the wavelength range 9.0 $\mu > \lambda > 1.55$ μ, which corresponds to energies between 0.138 eV and 0.80 eV. Thus the infrared light excites carriers to the conduction band from the traps. The photoconductivity increases for $\lambda < 1.25$ μ; this near-infrared response is presumed to be brought about by exciting carriers to the conduction band from a compensated acceptor level near 1.2 eV above the valence band. No infrared quenching is seen at any wavelength. If any is occurring, it is masked by stimulation of conductivity at the same wavelength.

CdS:Al SINGLE CRYSTAL-PHOTODIELECTRIC EXPERIMENTS

When a photodielectric experiment is performed on the CdS:Al sample, both permanent and temporary frequency changes are produced, depending on the wavelength of the light used. The initial frequency change and change in absorbed power due to bandedge light are shown in Fig. V-5 and Fig. V-6. The variation fits the model from Chapter III assuming the existence of a single sensitizing center with fast hole trapping. The frequency change is linear and amounts to -480 kHz in 20 minutes for an

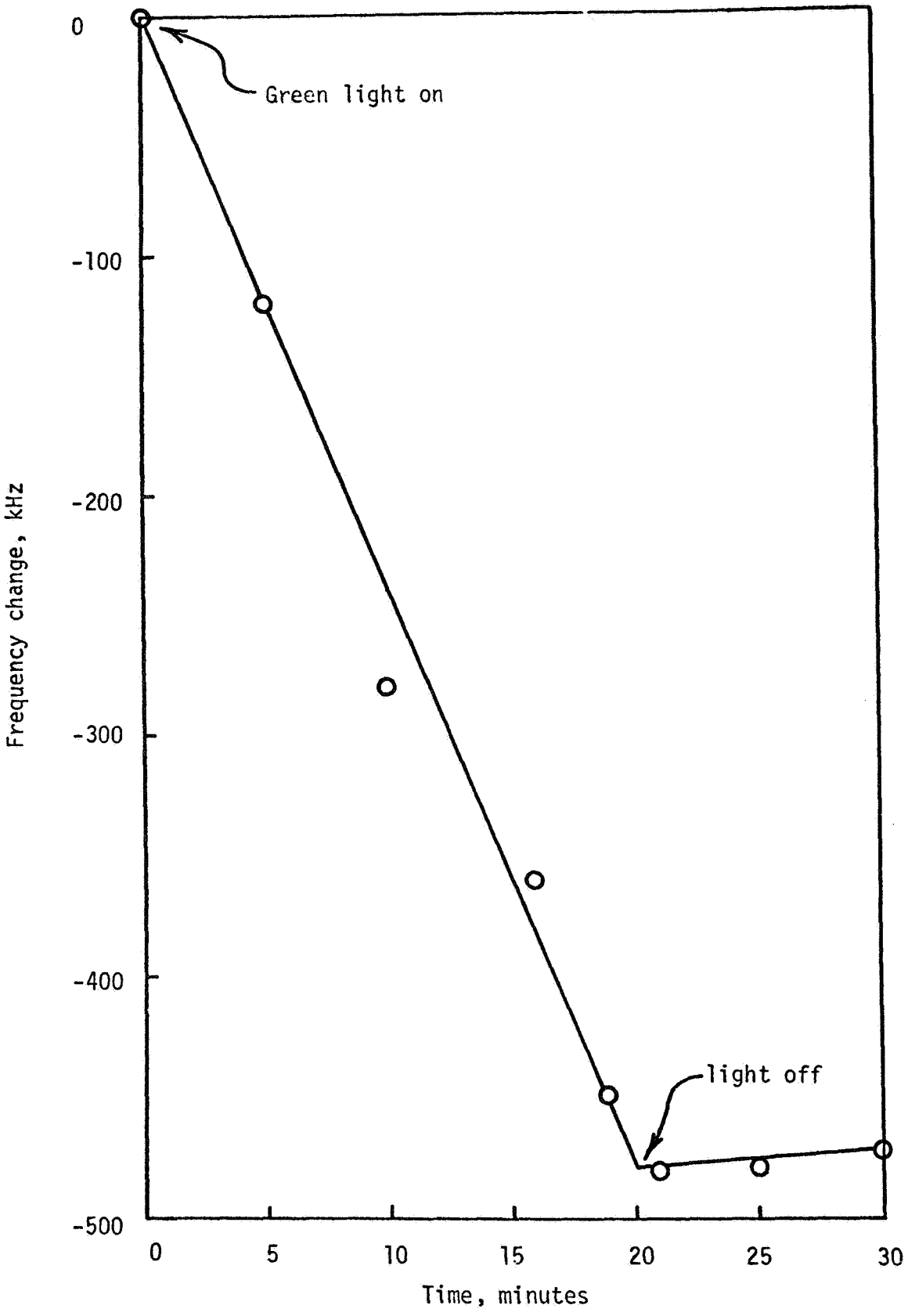

Figure V-5. Frequency change vs time for CdS:Al at 4.2°K with $\tau = 6.4 \times 10^{13}$ photons/cm^3-sec, $f = 8.5 \times 10^8$ Hz, and $G = 0.0532$.

Figure V-6. Power absorption vs time in CdS:Al at 4.2°K with $\tau = 6.4 \times 10^{13}$ photons/cm^3-sec. The solid curve represents the variation observed, the linearly rising dashed curve represents the contribution due to trapped carriers, and the dotted curve represents the contribution due to carriers in the shallowest trap.

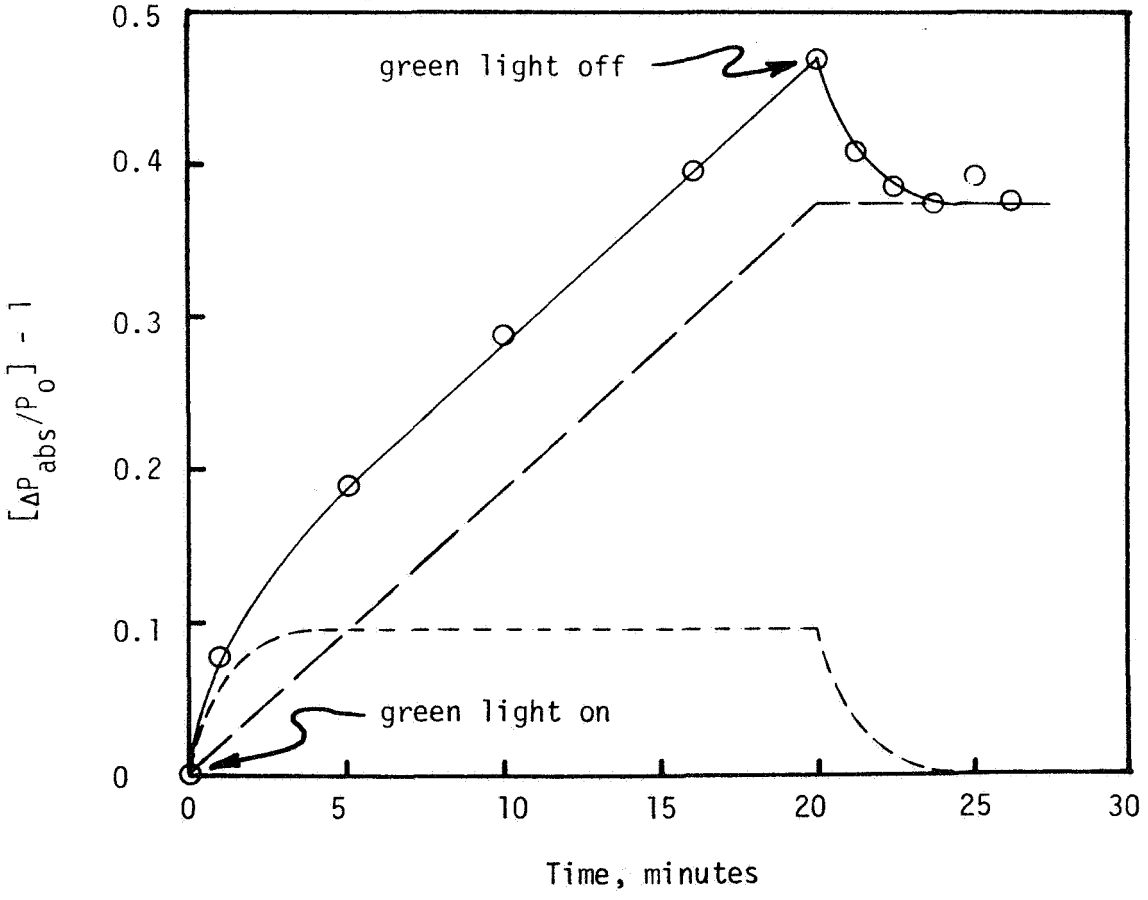

incident photon flux of 1.25×10^{13} photons/sec. The absorption coefficient for the light was measured to be 73.3%, and the sample volume is $0.143\ cm^3$. Assuming unity conversion efficiency, we find $\Delta n = 7.69 \times 10^{16} cm^{-3}$. With $f = 8.5 \times 10^8$ Hz, $G = 5.32 \times 10^{-2}$, and $\varepsilon_r^2 = 60$, Eqs. [2.31] and [2.16] give $E_t = 0.1315$ eV (see Table I-1 for calculated value of τ). Therefore, the shallowest of the three traps appears to capture the generated carriers. This implies that the 0.13 eV level has a relatively large capture cross section and that the density of sites is large. To measure S_t (0.13), a photodielectric experiment near 50°K is needed.

To estimate N_t (0.13), it is only necessary to find the maximum attainable frequency shift; this shift was found to be -3.15 MHz. Use of Eq. [2.31] once again indicates that a lower bound on N_t (0.13) is $6 \times 10^{17} cm^{-3}$. This requires two assumptions; first, the traps should be saturated. This condition is easily satisfied by using a very high light level and making the measurement after the frequency has decreased to its lowest value. The second assumption is that all of the frequency shift is due to the shallowest trap. It is easily seen that deeper levels make only a very small relative contribution to the frequency change. For example, if the level at 0.35 eV were filled to the same density as the shallower level, its contribution to Δf would only be 5% of the contribution of the 0.13 eV trap. The 0.74 eV trap would contribute $\sim 0.1\%$.

Fig. V-5 also shows that when the light is removed, the frequency shows a very slow upward drift. Observation for a longer period of time reveals a decay time of many hours. At 4.2°K the probability of escape from the 0.13 eV level to the conduction band by thermal excitation

is $\sim 10^{-100}$ sec^{-1}, so it is conceivable that carriers slowly tunnel out of the trap into a recombination center located nearby in the crystal.

EVIDENCE FOR VERY SHALLOW ELECTRON TRAP

The power absorption curve for CdS:Al exposed to band-edge light is given in Fig. V-6. It consists of a linearly varying component plus a transient component; the two components are shown in the figure by dotted lines. The linear component is expected to result from filling shallow traps. The other component would be attributable to excess free carriers if the rise and decay were instantaneous. The fact that rise and decay times of $\sim$ 60 seconds are observed indicates that a previously unsuspected, very shallow trap must exist.

An estimate of E_t for this very shallow trap is obtained by assuming any reasonable value of S_t. For example, if $S_t = 10^{-14}$ cm^2, E_t = 4.80 meV, and if $S_t = 10^{-18}$ cm^2, E_t = 8.13 meV, using Eq. [3.31]. From the decay time of 142 seconds at 4.0°K, $S_t \simeq 10^{-17}$ cm^2 and $E_t \simeq 7$ meV.

The density of carriers in the very shallow trap may be calculated from the power absorption curve. Fig. II-2 indicates that for $\tau = 10^{-15}$ sec, a carrier in a trap within about 20 meV of the conduction band has a relative contribution to power absorption B" of 10^{-15} sec from Eq. [2.30]. At a level at 0.1315 eV an electron has a contribution of $B" = 7.7 \times 10^{-21}$ sec if $\omega = 5.34 \times 10^9$, from Eq. [2.22]. Thus, the power absorption experiment is 7.7×10^{-6} times as sensitive to a carrier in the 0.13 eV trap compared to one in the shallowest trap. Fig. V-6 indicates that the carriers in the deeper trap have a total effect which is about 4 times larger. Therefore, during illumination the equilibrium density of carriers in the very shallow trap is

$$n_t(0.007) = \frac{7.7}{4} \times 10^{-6} \times n_t(0.13) \simeq 1.15 \times 10^{12} cm^{-3}$$

The density of conduction band electrons is related to this density by Eq. [3.32], $n = n_t(0.13) \times (\tau_L/\tau_d)$. The effects of free electrons are not visible in Fig. V-6 since τ_L/τ_d is probably less than 10^{-4} and the power absorption experiment is equally sensitive to free electrons and electrons in very shallow traps.

Since there is an appreciable density of electrons in the very shallow trap, it may seem unusual that apparently no trace of them was seen in Fig. V-5. The reason for this is explained by reference to Fig. II-1. The factors B'(0.007) and B'(0.13) are about the same magnitude, but $n_t(0.007)$ is quite a bit smaller than $n_t(0.13)$. The result is a failure to observe the small increase in frequency ($\sim$ 300 Hz) expected when the carriers from the shallower trap decay to the deeper trap. The effects of the 0.007 eV trap would probably be observable if stronger illumination were used to increase $n_t(0.007)$.

INFRARED RESPONSE OF THE SENSITIZING CENTER

Infrared light at various wavelengths was applied to the sample, resulting in two different types of effects. Light with $\lambda \simeq 0.95$ μ has the same effect as band edge light; irreversible increases in both ε_r' and ε_r'' are observed. This behavior can be explained as excitation of electrons from the compensated acceptor sites 1.28 eV above the valence band to the conduction band, followed by decay into a shallow trap. The rate of frequency decrease is 1.17 kHz/sec for a photon flux of nearly 3×10^{14} photons/sec. The applicable absorption coefficient is obtained from Fig. V-1, and Eq. [2.31] then yields $E \simeq .13$ eV. Thus, the 0.95 μ light effectively excites electrons from the deep sensitizing center to the 0.13 eV trap.

The electrons prefer to decay into the shallow trap rather than return to the sensitizing center because the capture cross section of the latter is usually very small (normally $\sim 10^{-21} cm^2$)[8].

The density of deep sensitizing centers can be estimated by noting the amount of time that passes before the sample no longer responds to 0.95 μ light at a given photon flux. In the CdS:Al, with a volume of 0.143 cm^3, α = 65.5%, and T = 2.8 x 10^{14} photons/second, the frequency begins to level off after about two minutes of irradiation, indicating a density of about $10^{17} cm^{-3}$ of the compensated sensitizing centers.

The power absorption data must be used to confirm that the effect discussed above does not occur because of saturation of the traps. In that case, the electrons would begin collecting in shallower traps or the conduction band, and the power absorption curve would break upward. (This phenomenon was illustrated in Reference 27). In the case of the 0.95 μ light, however, the power absorption curve levels off, indicating that the process of excitation of electrons has ceased, and hence the deep level has been exhausted.

INFRARED RESPONSE INVOLVING A DEEP ELECTRON TRAP

From TSC data, reported in Table V-1, there is a deep electron trap at 0.74 eV below the conduction band. Photodielectric measurements of the defect reveal some interesting behavior. A temporary increase in ε_r' is caused by wavelengths longer than about 1 μ, with a sizeable peak at 1.6 μ. At the peak, a frequency change of 165 kHz results from irradiating the sample with 5.8 x 10^{14} photons per second. The rise and decay times for the effect are about one minute, indicating that the level at 0.007 eV is also involved. The photon energy at 1.6 μ is 0.775 eV,

so the photosensitivity at that wavelength indicates it must be a result of exciting carriers from the electron trap at 0.775 eV to the conduction band, followed by circulation through the 0.007 eV level.* After spending about a minute in the shallowest state, the electron returns to the deep level. Relating Δf to Δn_t by Eq. [2.31] indicates both levels have densities greater than $5 \times 10^{14} cm^{-3}$.

The fact that 1.6 μ light caused no permanent frequency change means that no carriers were permanently added to the 0.13 eV level. The traps at 0.13 eV were not saturated, because a subsequent application of band edge light permanently lowered the frequency as before. The only explanation consistent with the other data is that carriers removed from the level at 0.775 eV are quickly replaced by electrons initially in the 0.13 eV level. For this to be the case these two levels would have to be related. Two of the most common possibilities would be for the shallow level to be an excited state of the deeper one, or for the two sites to exist at a complex imperfection such as a donor-vacancy pair.

For the model given above, the irradiation is assumed to excite an electron to the conduction band, followed by rapid decay to either the 0.13 eV or 0.007 eV trap. Meanwhile, a carrier from the 0.13 eV level drops to the 0.775 eV level. Therefore, the net effect is an increase in the density $n_t(0.007)$ and a decrease in $n_t(0.13)$, which would be expected to lead to a small reduction in resonant frequency. When the light is removed, the excess density in the shallow levels decays into the deeper levels in about 60 seconds, returning the frequency to the initial value. The total maximum frequency excursion is expected to have a contribution due to an excess density of carriers in each of the traps, but the components cannot be separated because of the rapid decay times involved.

The properties of the traps observed with the four standard tests, absorption, photoconductivity, TSC, and decay curve analysis, are listed in Table V-1. Likewise, data derived from the contactless photodielectric experiments is given. A comparison of the numerical values gives excellent agreement, especially if the dilation of the energy gap and increase in trap energy with decreasing temperature are taken into account[77].

CdS:Al POWDER SAMPLE - PHOTODIELECTRIC RESULTS

A photodielectric experiment was performed on the powdered sample of CdS:Al, and the resulting Δf and ΔP curves are shown in Figs. V-7 and V-8. These should be compared with the corresponding curves for the single crystal sample, Figs. V-5 and V-6. For strongly absorbed light, the response of the powder sample matches the response of the single crystal sample of CdS:Al. Like the single crystal, the polycrystalline sample operates as a light integrator at 4.2°K, and exhibits no observable infrared quenching.

The two samples may be quantitatively compared by finding the value $\Delta f/\Delta t$ for a given level of light and then dividing by the sample G factor to normalize the result. For the single crystal, $\Delta f/\Delta t = 4.00 \times 10^2$ Hz/sec and G = 0.0532, so $\Delta f/G\Delta t = 7.66 \times 10^3$ Hz/sec. For the polycrystalline sample under identical illumination, $\Delta f/\Delta t$ = 31.7 Hz/sec and $G = 4.2 \times 10^{-3}$, so $\Delta f/G\Delta t = 7.54 \times 10^3$ Hz/sec. The power absorption may also be compared by calculating $\Delta P/G\Delta t$. For the single crystal, $\Delta P/\Delta t = 3.9 \times 10^{-4}$ sec^{-1}, so $\Delta P/G\Delta t = 7.4 \times 10^{-3} sec^{-1}$. The powder sample has $\Delta P/\Delta t = 4.32 \times 10^{-5} sec^{-1}$, so $\Delta P/G\Delta t = 1.0 \times 10^{-2} sec^{-1}$. The slow decay Δf also proceeds at nearly the same rate in the two samples. For both samples the slow upward drift initially corresponds to $\Delta f/G\Delta t \simeq 350$ H

TABLE V-1

Trapping and Recombination Parameters of CdS:Al				
Level*	Method	T, ^{o}K	S_{nt}, cm^2	N_t, cm^{-3}
0.007	PD	4.2	10^{-17}	$>5x10^{14}$
0.125	Abs PC	300		
0.13	Decay	77	10^{-14}	$>4x10^{16}$
0.1315	PD	4.2	large	$>6x10^{17}$
0.35	TSC Abs	300	$2x10^{-16}$	$>3x10^{16}$
0.37	PC	300		
0.74	TSC		$\sim 10^{-18}$	$>1.5x10^{15}$
0.775	PD	4.2		$>5x10^{14}$
1.3	PD	4.2	small	$\sim 10^{17}$

* Measured from the conduction band in eV.

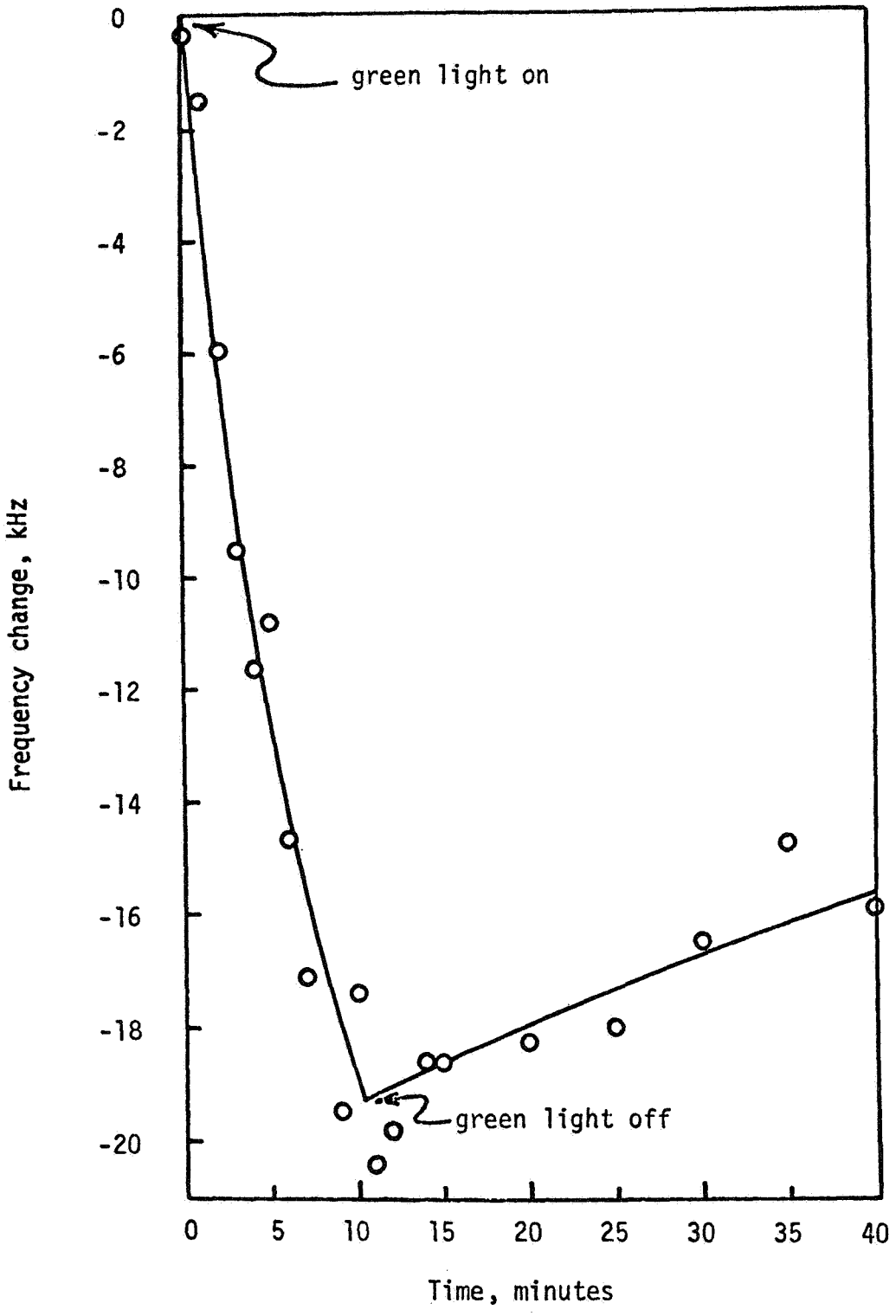

Figure V-7. Frequency change vs time for CdS:Al powder sample at 4.2°K with $\tau = 6.4 \times 10^{13}$ photons/cm^3-sec, $f = 8.5 \times 10^8$, and $G = 0.0042$.

Figure V-8. Variation of absorbed power in CdS:Al powder sample at 4.2°K with $\Upsilon = 6.4 \times 10^{13}$ photons/cm^3-sec.

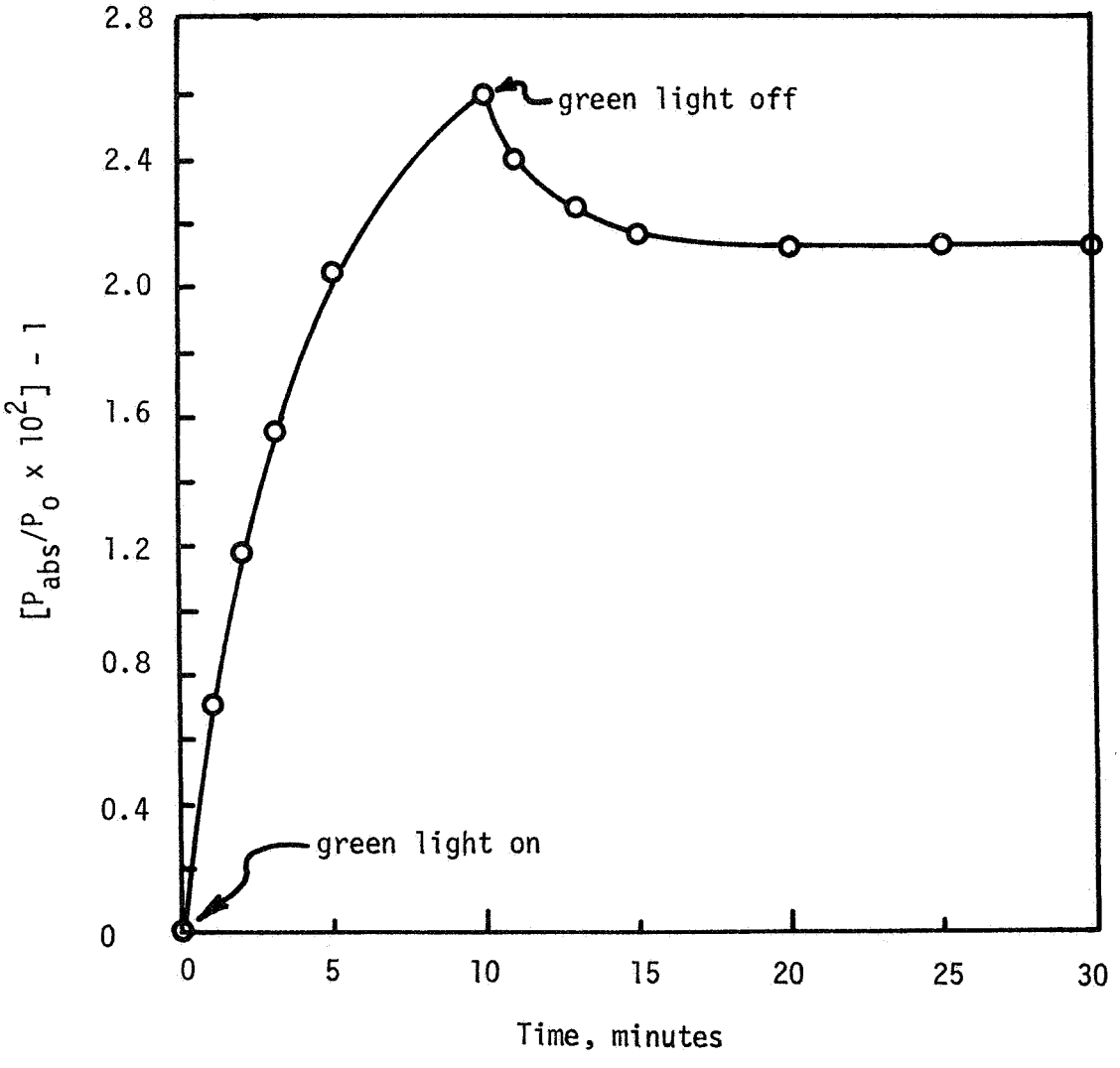

Similarly, no differences are observed between the two samples with infrared stimulation applied.

It is, therefore, evident that the two samples behave similarly in every respect and all of the analysis previously applied to the single crystal of CdS:Al also applies to the polycrystalline sample. This conclusion was expected since the light used was strongly absorbed in the bulk rather than at the surface. Furthermore, if the distance a free carrier drifts during one-half cycle of the rf field is estimated as

$$d = \mu E_e / f \qquad [5.1]$$

where the mobility $\mu \simeq 10$ cm^2/volt sec[14], the frequency $f \simeq 10^9$ Hz, and the electric field E_e is estimated at 100 V/cm, then $d \simeq 10^{-6}$ cm = 100 Å, which is obviously very small compared to the average size of a CdS grain in the powder sample (estimated to be 10^{-2} to 10^{-3} cm on a side). This implies that the average carrier in a CdS grain does not tend to encounter the grain surface, and bulk effects are still observed.

CdS:Ag - STANDARD EXPERIMENTS

The CdS:Ag is analyzed with the same techniques used in testing the CdS:Al. The absorption spectrum is shown here as Fig. V-9. A correction for reflection has been made by multiplying by (1-R) = .848, where R is the calculated reflection coefficient. The result shows that the absorption edge at room temperature is at 0.525 (2.36 eV) while the bandgap is generally given as 2.40 eV. Very small peaks appear at 0.595 μ (2.08 eV, or 0.32 eV below the conduction band) and 0.64 μ(1.94 eV, or $E_g - E_T = 0.46$ eV, where E_g is the bandgap energy and E_T is the photon energy). A very large peak occurs at 1.0 μ(E_T = 1.24 eV, $E_g - E_T$ = 1.16 eV). In the infrared, there are peaks at 2.6 μ(E_T = 0.477 eV), 3.2 μ (E_T = 0.387 eV), and about 3.9 μ(E_T = 0.318 eV).

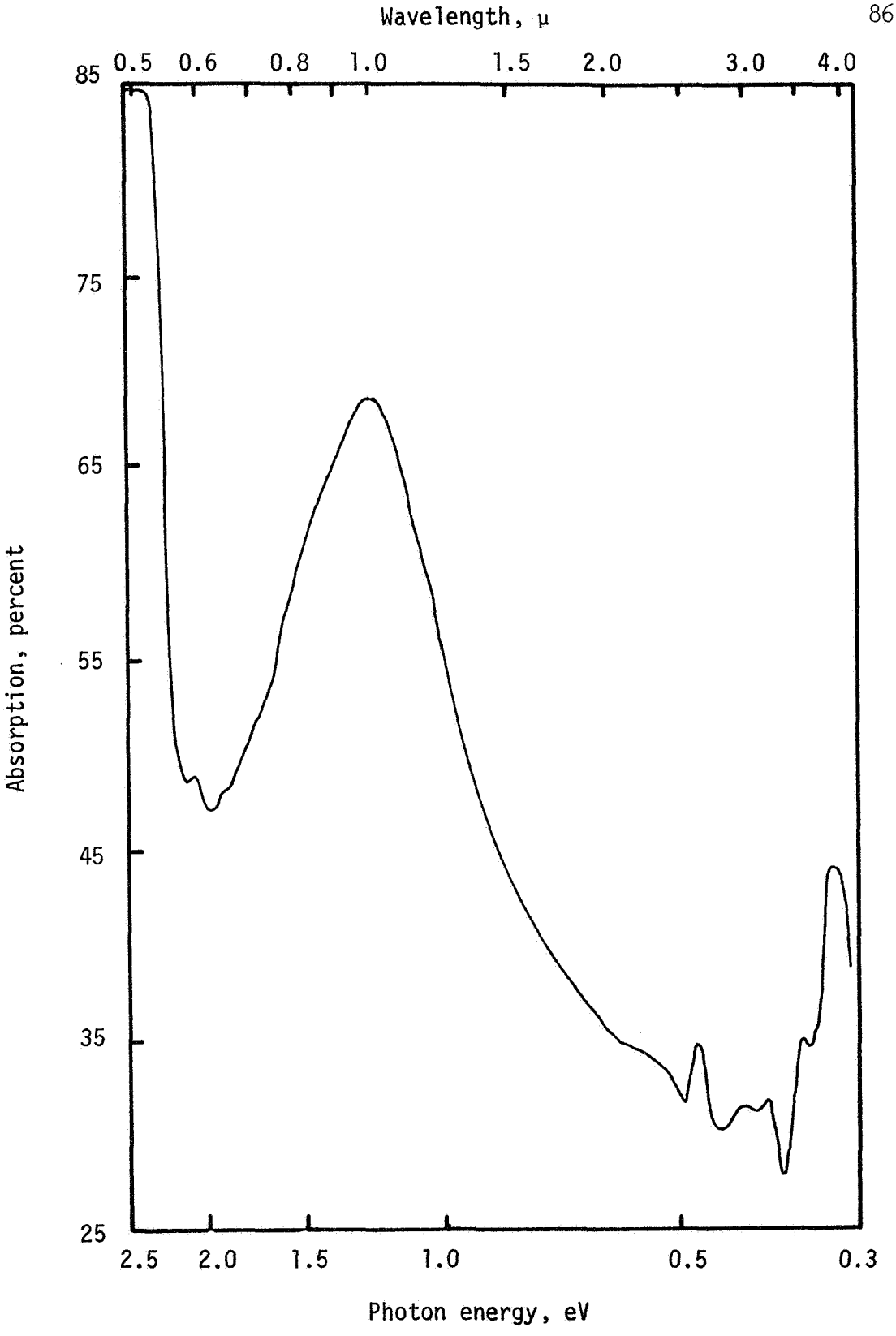

Figure V-9. Absorption spectrum in CdS:Ag at 300°K.

The absorption measurements imply the energy level scheme shown in Fig. V-10. The data is consistent with the presence of three electronic states located 0.47, 0.39, and 0.32 eV below the conduction band. Except for the 0.39 eV level, transitions are seen both to the level in question from the valence band, and from the level to the conduction band; the unseen transition from the valence band to the 0.39 eV level could easily be hidden in the data. The large amount of detail in the infrared portion of the spectrum could contain peaks other than those listed above. It is probable that a quasi-continuum of states exists between 0.5 eV and 0.2 eV.

The large peak seen at 1 μ appears to be abnormally wide, and it could easily result from two complementary transitions. If the sample is compensated, which is usually the case, the compensated acceptor sites normally seen in CdS near 1.0 eV above the valence band are partially filled with electrons. In this case, the data indicates that the level is $\sim$ 1.24 eV from one of the bands, which would place it very close to the center of the gap. It is likely that part of the 1 μ light excites electrons to that level from the valence band, while the remainder of the light excites electrons from the level to the conduction band. Thus, with two possible transitions of slightly different energies available, the absorption shows a high, wide peak.

The room temperature photoconductivity spectrum of the CdS:Ag for light in the visible region is given in Fig. V-11. There is little detail except for the large peak at 0.545 μ(E_T = 2.275 eV, $E_g - E_T$ = 0.125 eV). It is tempting to interpret the peak as a shallow trap, but this cannot be done with complete confidence. In the wavelength region near 0.545μ

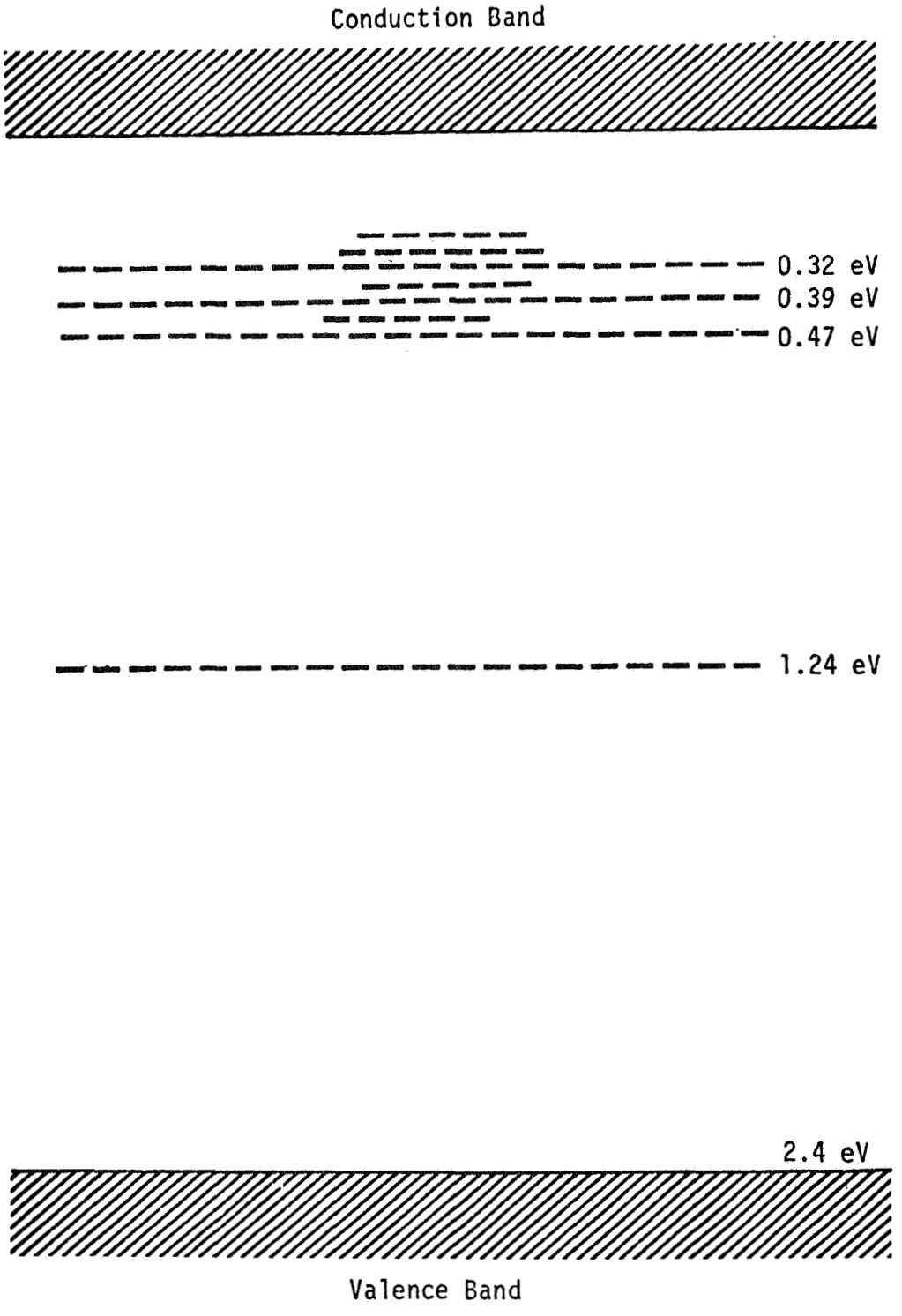

Figure V-10. Energy band diagram for CdS:Ag at 300°K. Energies are measured relative to the conduction band.

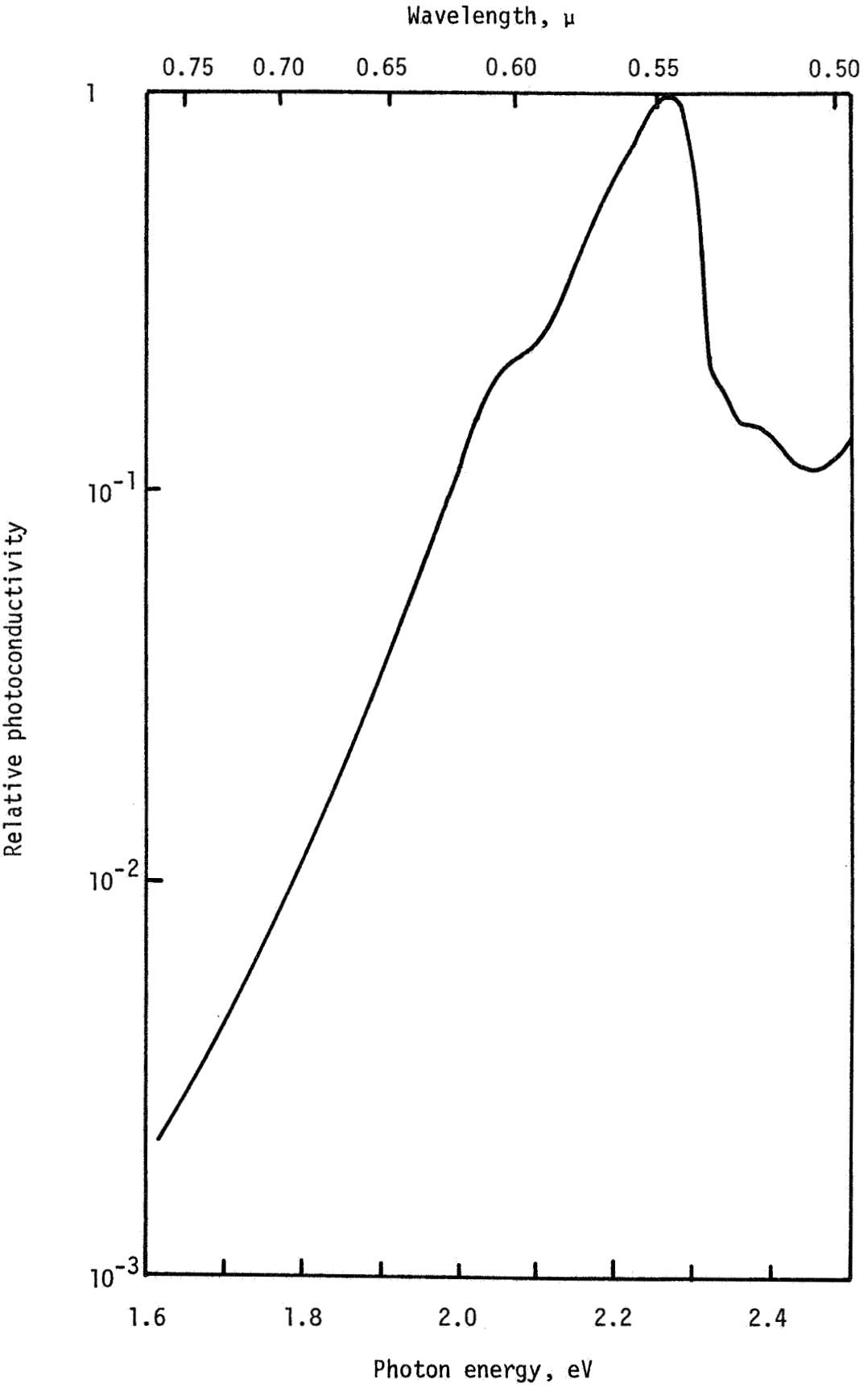

Figure V-11. Photoconductivity spectrum for CdS:Ag at 300°K.

absorption rapidly increases as wavelength decreases. As the region of absorption becomes limited to the front surface of the sample, the free carrier lifetime is expected to drop sharply due to the large number of recombination centers at the surface. Thus a peak is expected at the wavelength where the best combination of absorption and lifetime exists. Whether the 0.545 μ peak results from the absorption vs. lifetime effect or from the existence of a discrete level is uncertain.

The photoconductivity spectrum also contains a bulge from 0.60 μ to 0.615 μ. This indicates a transition of ∿ 2.07 eV, and, therefore, the bulge probably results from exciting electrons from the valence band to the 0.32 eV trap. The conductivity increase occurs because of thermal generation of the excess trapped carriers into the conduction band or from the free holes in the valence band.

Efforts to obtain infrared photoconductivity spectra in CdS:Al are not very successful because the sample exhibits a quenching effect which interferes with the excitation process. Tests at 300°K, 77°K, and 4.2°K all tend to show the same results: excitation occurs for ∿ 7 μ > λ > ∿ 2.6 μ(∿ 0.17 eV to ∿ 0.47 eV) and two peaks appear at λ ≃ 3.5 μ (∿ 0.35 eV) and 2.5 μ(∿ 0.47 eV). The data tends to confirm the existence of a distribution of states within 0.47 eV of the conduction band, with appreciable concentration at 0.35 eV and 0.47 eV.

More details about the traps are learned from observing photoconductivity decay. At room temperature the decay has a rapidly varying component with $\tau < 1$ second and a slower component with $\tau \simeq 30$ seconds. Using Eq. [3.16] allows only an estimate of E_t to be made, since S_t is not known. The slower decay is governed by a level at 0.7 ± 0.1 eV.

Consistent results are obtained if the rapid decay is due to the 0.47 eV trap with a capture cross section of $1.4 \times 10^{-18} cm^2$; the 0.35 eV level could cause the decay if its capture cross section were $\sim 10^{-20} cm^2$, but this is not considered to be reasonable. A check on these values is obtained using TSC data.

TSC tests on CdS:Ag reveal three major peaks at 337°K, 210°K, and 125°K. Use of Eqs. [4.2] and [3.16] and the decay data given above indicates that the deepest discrete level is at 0.82 eV with $S_t = 2 \times 10^{-15}$ cm^2.

Decay tests at 77°K show short and long period decays, with the longer time being about 120 seconds. The short term decay is probably influenced by excess carriers and shallow traps and cannot be measured accurately. Assuming the 120 second decay goes with the TSC peak at 125°K, Eq. [4.2] can be used to calculate $E_t \simeq 0.16$ eV. Eq. [3.16] then indicates that $S_t(0.16) \simeq 10^{-16} cm^2$, but the small uncertainty in E_t causes a large uncertainty in S_t.

Light at 7 μ causes a small increase in the CdS:Ag conductivity at 77°K, with a decay time of about 120 seconds. Light at 3.5 μ causes a larger conductivity increase with about the same response time. The 120 second decay time for both wavelengths means that the photogenerated carriers circulate between the conduction band and the 0.16 eV.trap at 77°K. A small conductivity increase for 7 μ light results, since the carriers must be excited from the 0.16 eV trap. The density of trapped carriers there is always small because carriers are able to escape thermally from the trap. A larger effect occurs with 3.5 μ light because the excitation

frees carriers from the 0.35 eV trap, which tends to be highly populated because of the lack of enough thermal energy to empty it.

Light at 1 μ also leads to an increase in the sample conductivity when the shallow traps are empty. Both the rise and decay times of the effect are essentially instantaneous. The 1 μ light is expected to free both holes and electrons from the compensated acceptor center, and therefore it creates an excess density of carriers in both bands. A rapid decay is seen when the infrared is removed because the two excess densities rapidly recombine. The small size of the effect is also a result of the fast recombination rate.

A series of TSC experiments shows that the traps fill in the expected order, with deeper levels filling first. The 0.82 eV level tends to fill in the dark at room temperature, so the 0.35 eV level quickly starts capturing carriers when illumination is first applied. (The 0.47 eV level was never detected in a TSC experiment, which implies either a low trap density or a small capture cross section). The light, absorbed at the rate $7 \times 10^{14} cm^{-3} sec^{-1}$, fills the 0.35 eV level to $\sim$ 10% of the saturated density of the trap in about 30 seconds, which implies the density of traps at that level is about $2 \times 10^{17} cm^{-3}$. In the same amount of time, the shallower level at 0.16 eV fills to $\sim$ 5%, so its density is estimated to be about $4 \times 10^{17} cm^{-3}$. If any recombination takes place due to a long free hole lifetime, these estimates must be reduced.

Infrared light in the wavelength interval $3.0\ \mu > \lambda > 0.9\ \mu$ quenches the photoconductivity in CdS:Ag at room temperature; the most efficient wavelength is 1.175 μ which corresponds to a transition from the valence band to a level 1.1 eV above it. The mechanism for quenching

at other wavelengths is not known, but it may involve an optical transition to an excited state of the sensitizing center, followed by thermal emission to the filled band. At 77°K the quenching efficiency of 1 μ light is at least 20 times higher than at other wavelengths. A sequence of TSC experiments shows that 1 μ light applied for a sufficient length of time empties virtually all of the electron traps below 0.50 eV; the density in the 0.82 eV trap is unchanged.

The variation of the sample current at 4.2°K during bandedge and infrared illumination and during decay is shown in Fig. V-12. The free carrier density varies only by a factor of four between the most unexcited and most highly excited situations. The density of carriers at the lowest point corresponds to $1.65 \times 10^{7} cm^{-3}$. The response time during decay is about 3 minutes, and a TSC peak can be observed at 9°K, indicating $E_t \simeq 0.007$ eV with $S_t \simeq 10^{-16} cm^2$.

CdS:Ag - PHOTODIELECTRIC RESULTS

The behavior of the CdS:Ag in a photodielectric experiment is shown in Figs. V-13 and V-14. No change in the frequency appears until about 7×10^{15} photons per cm^3 are absorbed in the crystal. This represents the filling of deep traps which contribute relatively little to the frequency change. Figs. V-13 and V-14 are representative of the effects seen after the filling of the deep traps is accomplished.

The frequency change observed corresponds to an incident photon flux of 1.7×10^{13} photons per second on a 0.052 cm^3 sample with G = 0.0266. At this light level the frequency changes about 33 kHz in 22 minutes, following a non-exponential curve. The rate of decrease drops shorply after about 6 minutes of excitation, and appears to assume a constant value by

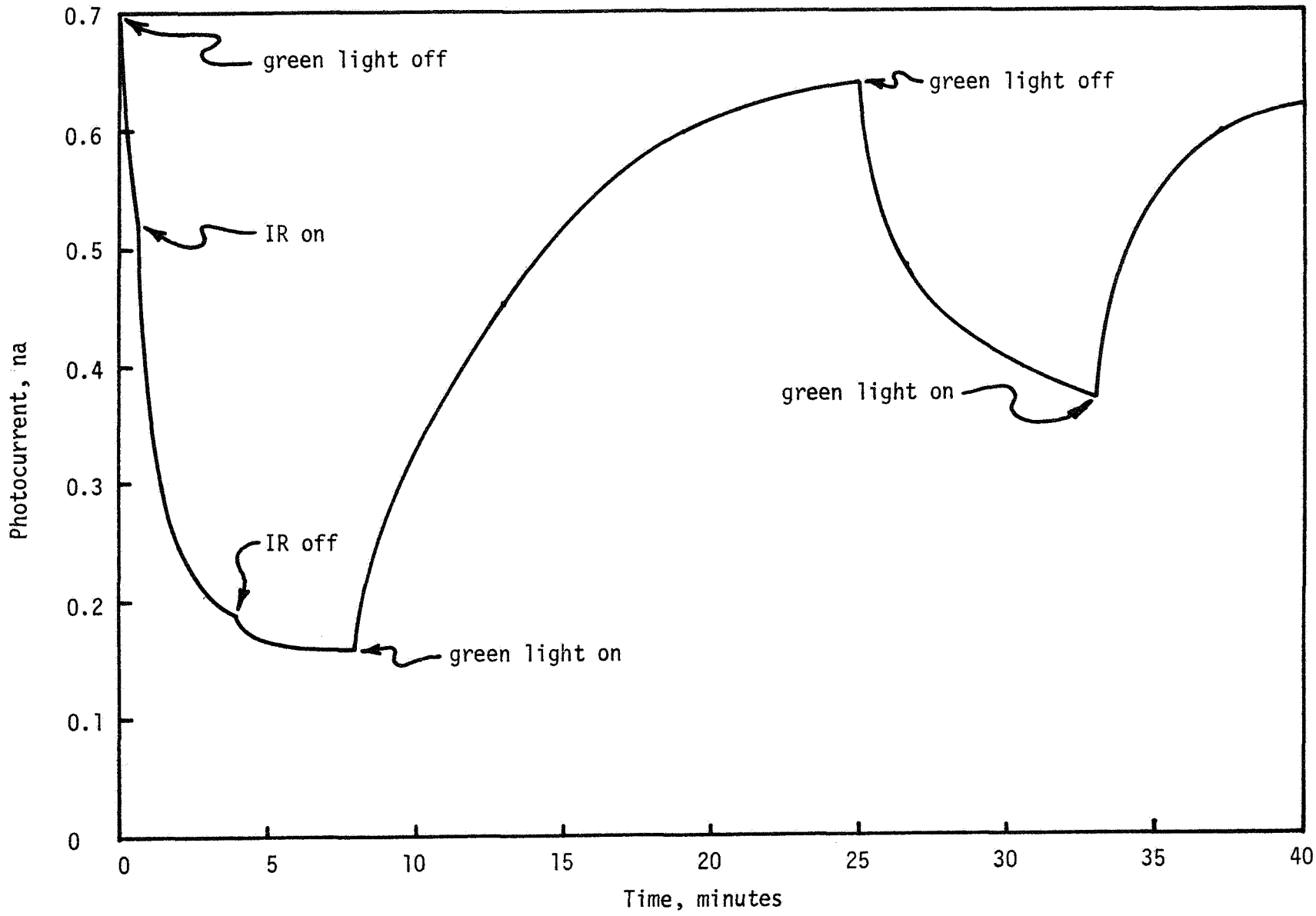

Figure V-12. Photoconductivity and quenching in CdS:Ag at 4.2°K.

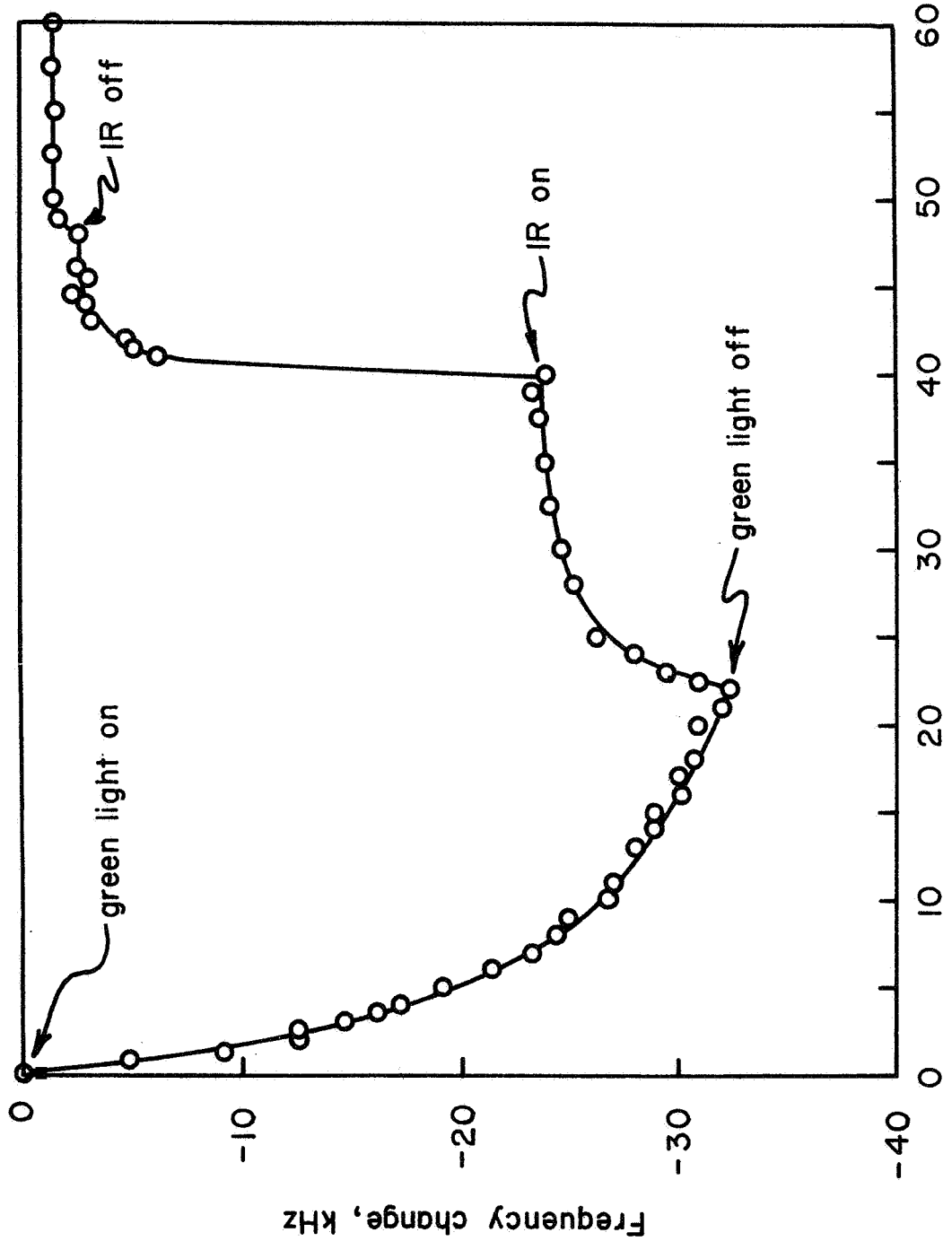

FIGURE V-13. Photodielectric frequency variation in CdS:Ag at 4.2°K.

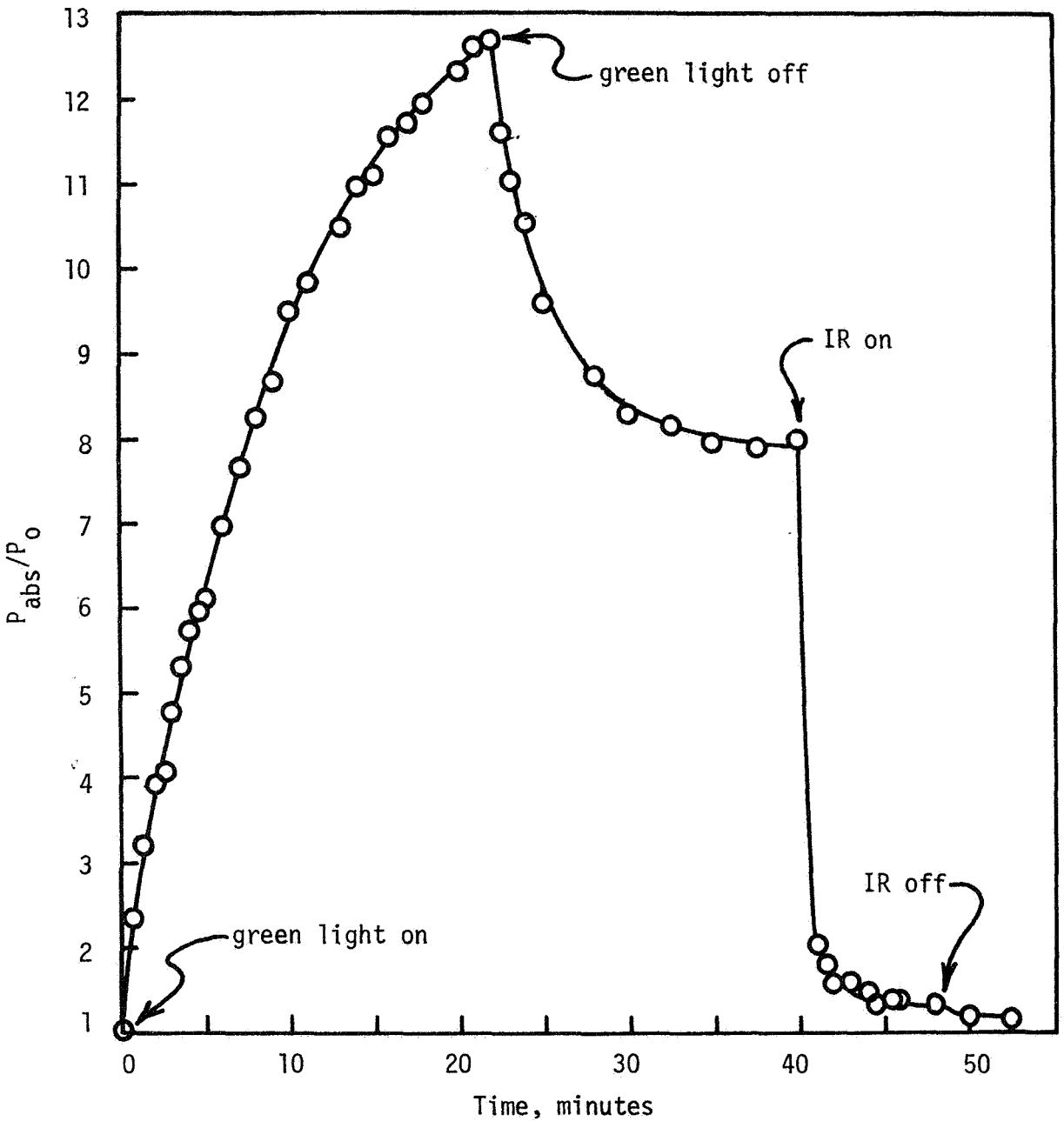

Figure V-14. The photodielectric power absorption variation in CdS:Ag at 4.2°K.

the 20 minute mark. Simultaneous power absorption measurements reveal a rapid increase in ΔP which begins to level off after about 10 minutes have elapsed. At the 20 minute mark the rate of change of ΔP is at a relatively low and constant value. When the band edge light is removed, both Δf and ΔP show a partial recovery with a response time of about 3 minutes.

Analysis of the traps is made somewhat difficult by the participation of several traps at the same time. The overall behavior indicates that the model having a single sensitizing center with slow hole trapping should be used. The depth of the shallow trap is easily obtained from the decay curve when the band edge light is removed, but the depth of the other traps cannot be found without knowledge of the density of carriers in each one. Since the energies of the deeper traps may easily be found by other methods such as TSC, this analysis will concentrate on making accurate calculations of S_t and n_t, given E_t.

TSC measurements reveal traps at 0.32 eV, 0.16 eV and 7.0 meV in the sample of CdS:Ag. Data from Kulp, et al.[77] suggests the levels shift to 0.35, 0.17, and 0.007 eV at 4.2°K. The presence of the level at 0.007 eV is confirmed by studying the decline of Δf. The decay time observed is 168 seconds; Eq. [3.16] gives $E_t = 7.68 \pm 0.8$meV for any reasonable value of S_t assumed. Since the frequency increase amounts to 9 kHz, Eq. [2.31] reveals that the density n_t (0.007) is $1.34 \times 10^{14} cm^{-3}$.

The Δf curve can be approximated by three regions where Δf vs. time is linear, as shown in Fig. V-15. In the initial region, the frequency drops at a rate of -117 Hz/sec. Next come slopes of -37.3 Hz/sec and -8.09 Hz/sec. Therefore, the model to be used has three levels

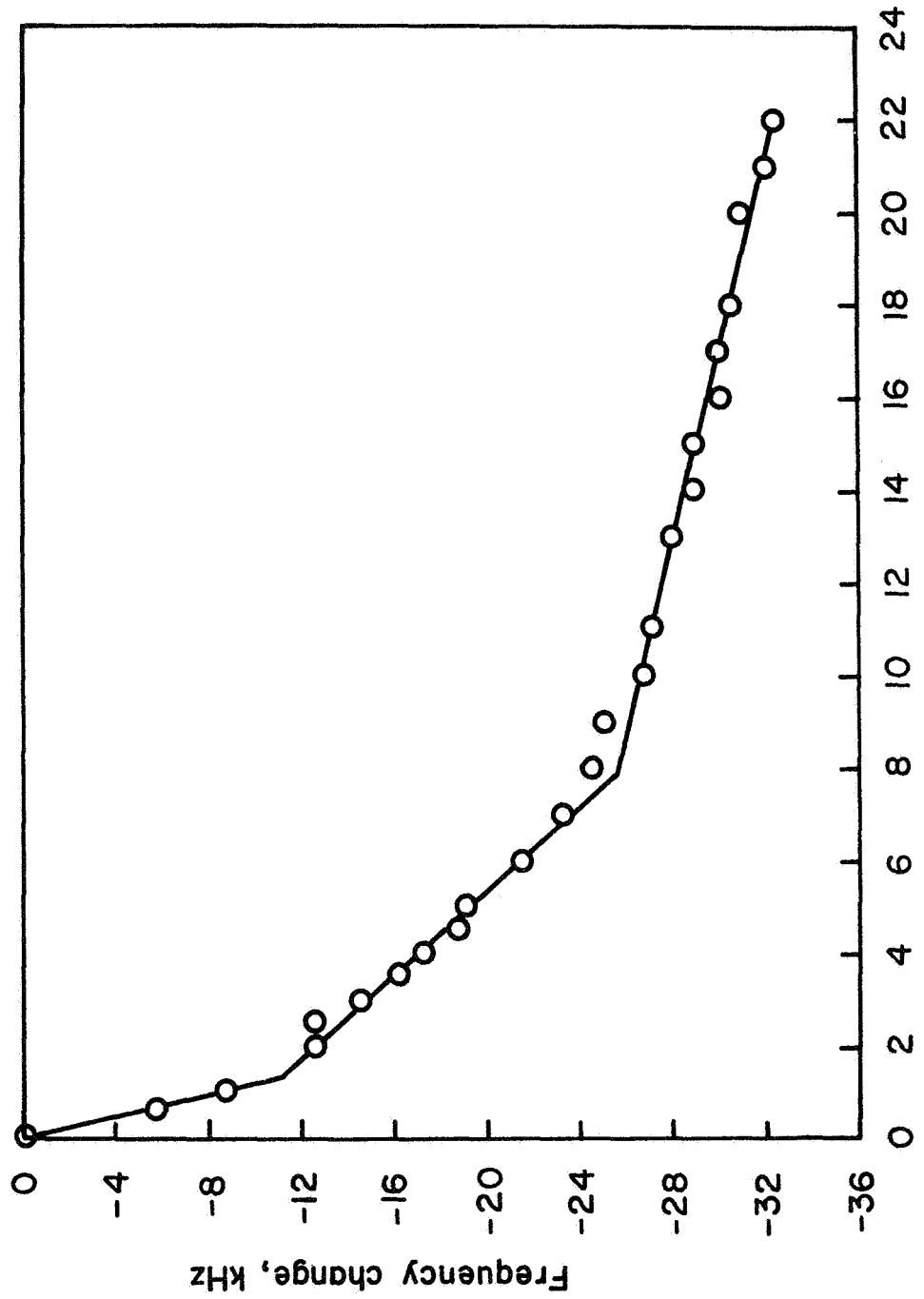

FIGURE V-15. Linearized initial frequency variation in CdS:Ag at 4.2°K.

contributing frequency variations of -8.09, -29.21, and -87.8 Hz/sec when the absorbed light flux is 2.33×10^{14} photons/cm^3 sec. The value of B'(0.35) is too low to allow the 0.35 eV level to account for any but the lowest slope. Similarly, the 0.17 eV level cannot account for the highest slope. Application of Eq. [2.31] then indicates that the three traps have net capture rates of 1.23×10^{12}, 1.98×10^{13}, and $4.27 \times 10^{13} cm^{-3} sec^{-1}$, in order of increasing E_t. The sum of the three rates accounts for only 27% of the electron-hole pair generation rate. This implies that the free hole lifetime is sufficient to cause recombination of the remainder of the electrons, and therefore that infrared quenching should be observable.

The linearized frequency change curve also allows the capture cross sections and densities of the traps to be found. The response time of 168 seconds for the 0.007 eV trap at 4.2°K gives $S_t(0.007) = 1.61 \times 10^{-16}$, while the density of carriers there at saturation is 1.34×10^4. Equating this density to N_t (0.007), taking 1.23×10^{12} for the initial value of $dn_t(0.007)/dt$, and using Eq. [3.2] with $n_t \to 0$ yields the density of free carriers $n \simeq 2.26 \times 10^7 cm^{-3}$. The fact that dn_t (0.007)/dt is fairly constant during the period when $n_t(0.007)$ is a small fraction of $N_t(0.007)$ indicates that n does not change by a large factor.

The filling of the 0.17 eV trap proceeds for $\sim$ 480 seconds and accounts for a net frequency drop of -13.8 kHz when it is saturated, so Eq. [2.31] gives N_t (0.17) $\simeq 9.4 \times 10^{15} cm^{-3}$. Similarly, saturation of the 0.35 eV trap causes a Δf of -44 kHz, indicating $N_t(0.35) \simeq 2.62 \times 10^{17} cm^{-3}$. Application of Eq. [3.2] then yields S_t (0.17) = 3.82×10^{-17} cm^2 and $S_t(0.35) = 2.86 \times 10^{-18} cm^2$. The excess free electron lifetime is $\sim 10^{-7}$ seconds.

INFRARED EFFECTS

Figs. V-13 and V-14 show that the CdS:Ag is very sensitive to quenching radiation. The absorbed flux of 1 μ light is 4.5×10^{15} photons/cm^3-sec, and 60 seconds worth is sufficient to remove 85% of $\sim 10^{17} cm^{-3}$ trapped electrons. This indicates that about half of the holes freed by the infrared light eventually recombine with a trapped electron rather than being recaptured at a hole trap. The capture cross section of the hole traps for holes is therefore about the same as the capture cross section of filled electron traps for holes, and the time required for the frequency change depends mainly on the infrared photon absorption rate. The 1 μ light eventually removes at least 95% of the trapped electrons.

When the 1 μ light is turned off, a small additional frequency increase occurs, with a fast response time. This transient component occurs because a small part of the infrared light frees electrons from the compensated acceptor sites, and they give rise to a small negative Δf by spending a small amount of time in the shallow traps before recombination with the free holes. Removal of the 1 μ light allows the excess free holes to remove these electrons, and the frequency rises as a result. This phenomenon cannot be explained by the transferring of electrons from the valence band to the acceptor sites because B' for electrons at that level is $\sim 10^{-30}$. To achieve the frequency change observed would require the impossible condition of more excitation events than absorbed photons. When the traps are empty, the effect is observed immediately following the application of the long wavelength light. The proposed model requires

only 5×10^{14} electrons/cm^3 to be freed from the deep level, which can be accomplished in less than a second.

The application of longer infrared wavelengths to the CdS:Ag leads to small values of Δf and ΔP which correspond to excitation from the electron traps. The spectrum obtained appears in Fig. V-16. The frequency change occurs rapidly following the introduction and removal of light. The infrared is preceded by bandgap light to fill the electron traps. An increase in frequency occurs at $\sim$ 7.0 μ due to the partial emptying of the trap at 0.17 eV. All other wavelengths cause the frequency to decrease, but an increase at 3.5 μ is superimposed over the general decrease.

The behavior seen in Fig. V-16 is explained by assuming the infrared light at each wavelength excites electrons from a certain trap to theconduction band. The electron may then decay into any unfilled trap, including the one it left initially. Carriers in very shallow traps eventually relocate in deeper levels if empty sites exist. An increase in frequency results when an electron is removed from a trap, and a decrease occurs upon retrapping; the size of Δf depends on B'. The probability that a free carrier will be trapped at a level depends on $S_t(N_t - n_t)$ for that level. Thus the amount and sign of Δf involves a comparison of the $B'S_t(N_t - n_t)$ products of the traps and $B'\Delta n_t$ at the initial level.

The increase in f seen at 7 μ occurs because the product $B'\Delta n_t$ for the 0.17 eV level exceeds $B'\Delta n_t$ for the 0.007 eV trap. The near-saturation of the shallowest trap allows this situation to occur. The remainder of the electrons ejected from the 0.17 eV trap remain in the conduction band as excess electrons, and are retrapped at the deeper level

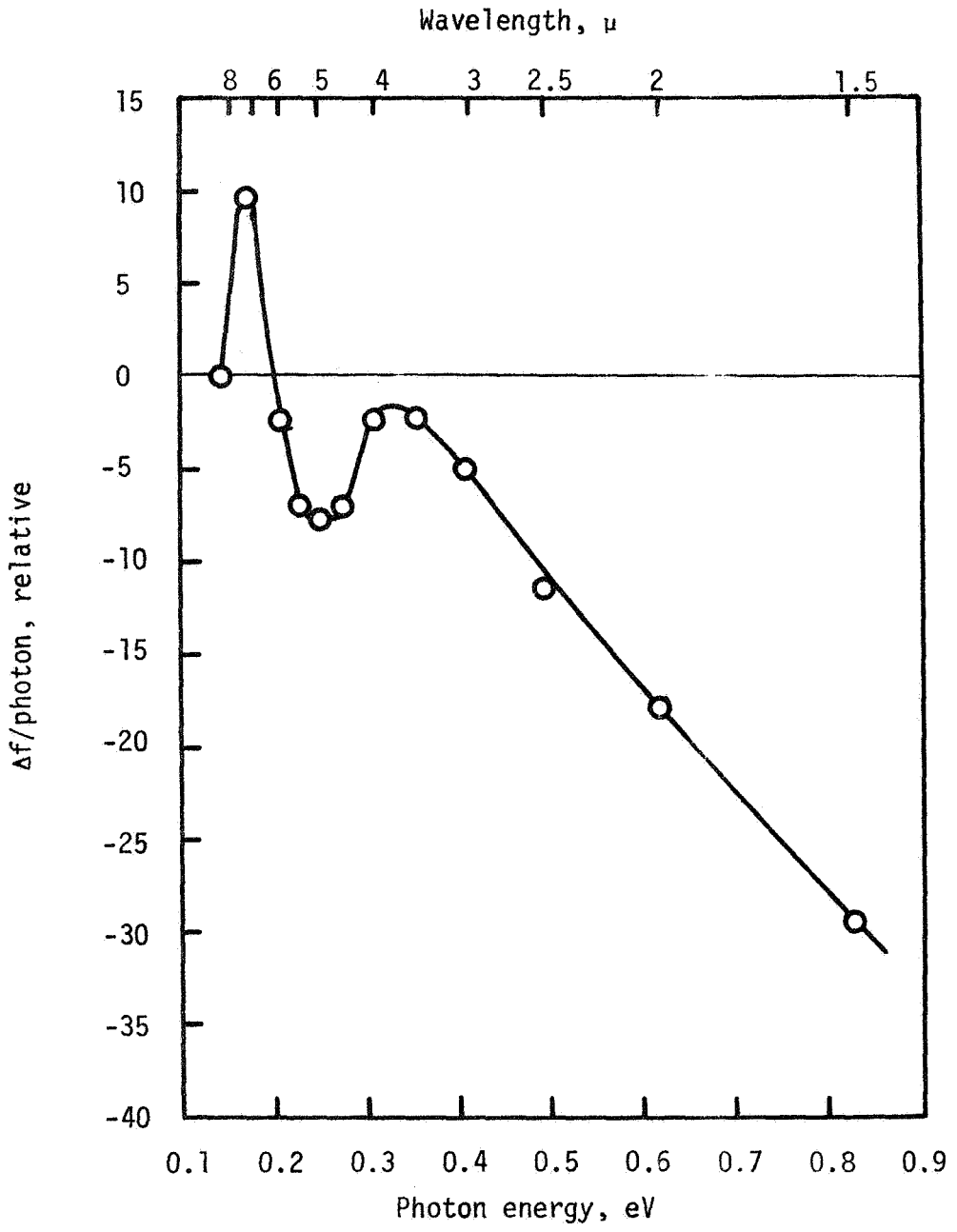

FIGURE V-16. The relative frequency change vs photon energy infrared wavelengths in CdS:Ag at 4.2°K.

when the light is removed. No permanent component of Δf is seen because the traps are all nearly saturated.

The general increase in Δf with decreasing λ for $\lambda < 3\ \mu$ results from exciting electrons from a low density distribution of states. The average time these electrons spend in the shallow level is relatively long possibly due to a small capture cross section characterizing the distribution. As the energy of the deep trap increases, its value of B' increases, and thus a more negative Δf occurs, showing the increasing relative importance of the shallow trap. The peak seen at 3.5 μ is present becuase of the large density of traps at 0.35 eV. More excitation transitions are possible there than for adjacent energies, but the value $\Delta n_t(0.007)$ is still limited to a low value due to saturation of that level. However, $B'(0.007) >> B'(0.35)$ and the net effect is near cancellation of Δf due to carriers leaving the deep level by Δf due to excess carrners in the shallow level.

The results of the standard and photodielectric experiments performed on the CdS:Ag are listed in Table V-2.

HIGH PURITY CdTe SINGLE CRYSTAL - STANDARD EXPERIMENTS

The CdTe single crystal sample is a thick plate cleaved from a single crystal chunk. Four standard experiments were performed on the sample: optical absorption, photoconductivity spectra, decay analysis, and TSC. The absorption measurements did not produce any conclusive data, probably because of the large sample thickness ($\sim$ 2 mm), and thus those experiments are not included here.

The results of a 77°K photoconductivity spectrum of the CdTe sample, which is p-type down to that temperature, is given in Fig. V-17.

TABLE V-2

Trapping and Recombination Parameters of CdS:Ag				
Level †	Method	T, ^{o}K	S_{nt}, cm^2	N_t, cm^{-3}
0.007	TSC	9	10^{-16}	
0.0076	PD	4.2	1.61×10^{-16}	$>1.34 \times 10^{14}$
0.16	TSC+Decay	125	$\sim 10^{-16}$	$< 4 \times 10^{17}$
0.17	PD	4.2	3.82×10^{-17}	9.4×10^{15}
0.32	Abs PC	300 300		
0.35	Quench TSC PD	300 210 4.2	2.86×10^{-18}	2×10^{17} 2.62×10^{17}
0.387	Abs	300		
0.47	Abs Quench Decay	300 300 300	1.4×10^{-18}	small
$\sim$0.7	Decay	300		
0.82	TSC	337	2×10^{-15}	
$\sim$1.24*	PD	4.2		
1.16*	Abs	300		
1.1*	Quench	300		

† Energies measured in eV from the conduction band, except (*), measured from the valence band.

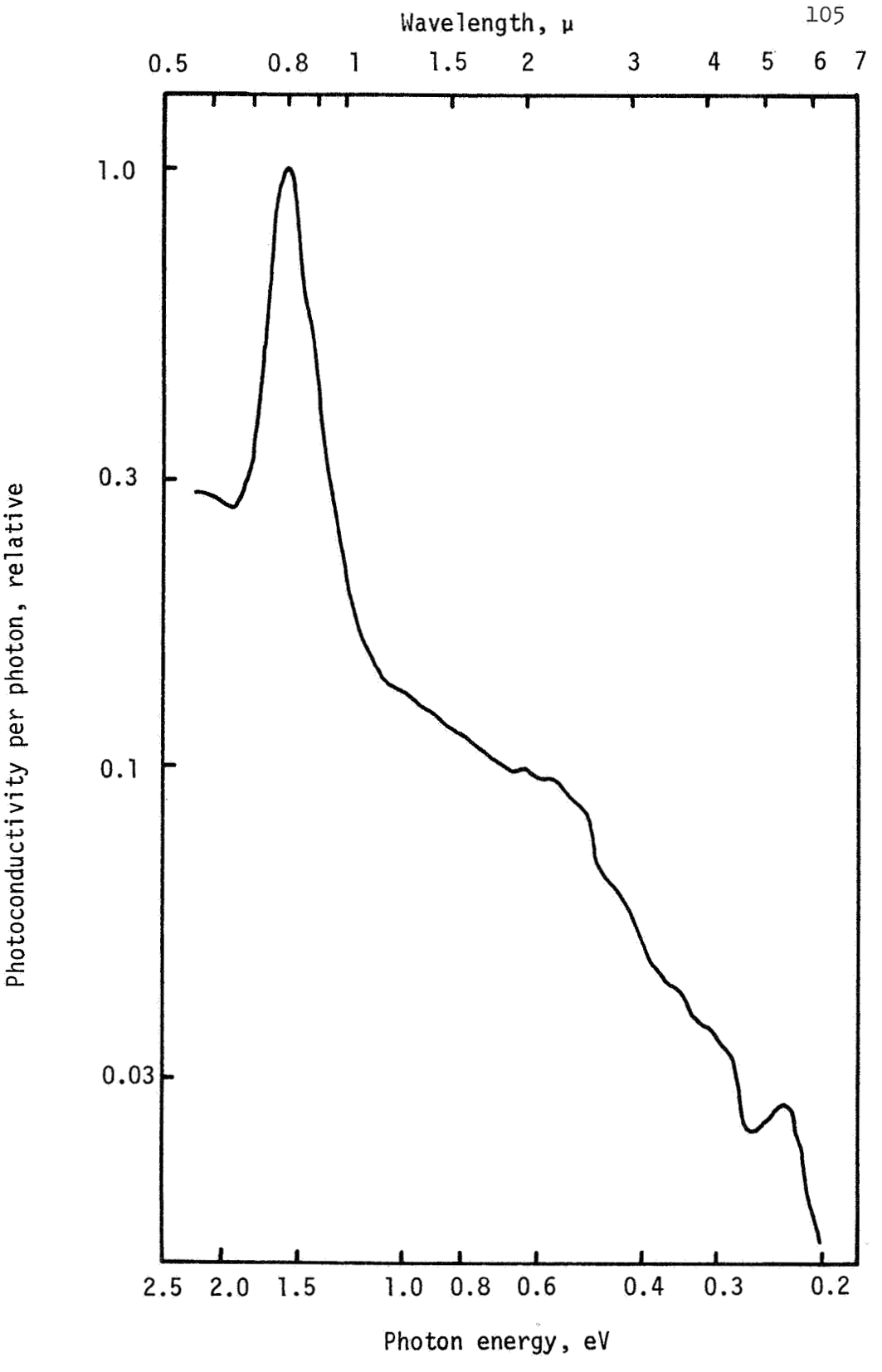

Figure V-17. The relative photoconductivity spectrum in CdTe at 77°K.

The large peak at 0.8 μ represents the band-to-band transition, corresponding to the low temperature bandgap of 1.59 eV according to Marple and Segall[66]. Another obvious transition occurs with λ = 5.4 μ, corresponding to an energy increase of 0.23 eV. No other reports of this level have been found in the literature, and it is assumed to be a hole trap 0.23 eV above the valence band. Another peak apparently exists around λ = 2.25 μ, with E ≃ 0.55 eV. This may result from the doubly ionized acceptor at a cadmium vacancy, reported by DeNobel[68] at 0.60 ± 0.5 eV.

At 4.2°K the sample is an insulator with $\rho > 10^{12}$ Ω-cm. This value can be lowered to $\sim 10^{10}$ Ω-cm by relatively strong bandgap light with $\Upsilon \simeq 10^{14}$ cm^{-3}sec^{-1}. The rise and decay of the photoconductivity occur immediately upon changing the illumination, and the rapid decay exceeds the dynamic response of the instruments. The free hole density varies linearly with Υ, which indicates that τ_L is constant and the optical free hole generation dominates the behavior. The calculated lifetime is 2×10^{-8} seconds for $\Delta P = 1.5 \times 10^{6}$ cm^{-3} and $\Upsilon = 7.5 \times 10^{13}$ cm^{-3}sec^{-1}.

The results of TSC experiments given in Figure V-18 show that two traps with very small densities exist in the CdTe. The first peak at 25°K has E_t = 0.045 ± 0.015 eV, and it probably corresponds to the hold trap at 0.05 eV seen by Lorenz and Segall[80] in pure CdTe and attributed to Cd vacancies. The second peak occurs at 60°K and causes the current to decay in about 7 seconds at 77°K. Use of Eqs. [3.16] and [4.1] indicates that the level is 0.124 eV above the valence band with $S_t \simeq 10^{-18}$. The densities of carriers in the traps after high illumination, as estimated from the area under the TSC peaks, are both less than 10^{15} cm^{-3}, with P_t (0.05) by about 10.

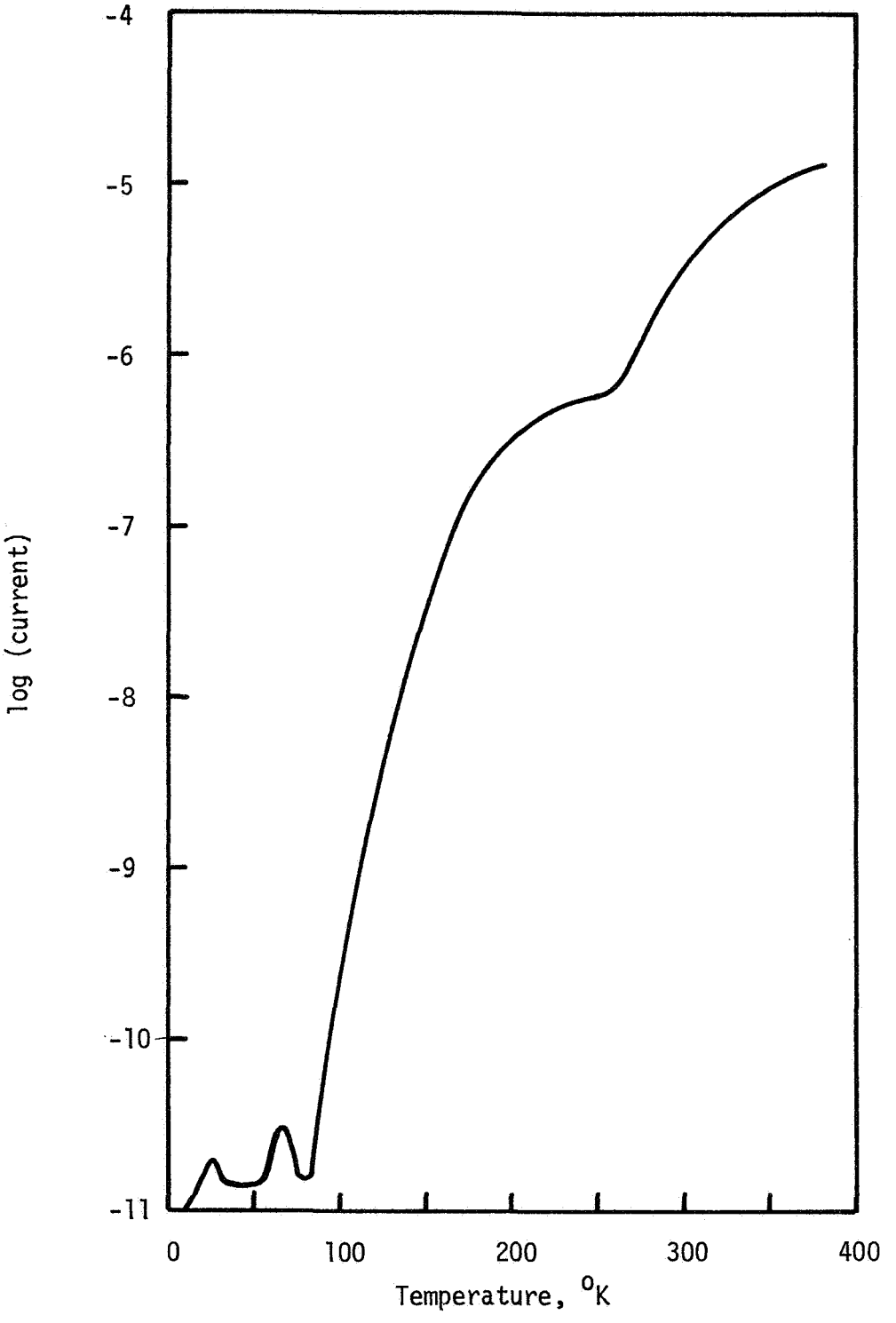

Figure V-18. Thermally stimulated conductivity in CdTe. A hole trap at 0.045 eV appears at 25°K, and another at 0.124 eV appears at 60°K. The current variation between 80°K and 250°K reveals an acceptor level at 0.105 eV, while an acceptor at 0.23 eV is indicated by the behavior above 250°K.

At temperatures above 80°K, p rises exponentially over five orders of magnitude with a slope indicative of an acceptor level at ∿ 0.105 eV, and for T > 250°K, the slope increases to show another acceptor at 0.23 eV. The latter is also seen in photoconductivity spectra, as was mentioned previously. A change in photosensitivity occurs for temperatures between 4.2°K and 2°K, and analysis using Eq. [3.8] modified for holes for the dependence of p on T gives E_t = 0.003 eV. Also, the magnitude of the second term of Eq. [3.8] is about 1/7 of the first term at 4.2°K, which indicates that $p_t S_{pt} \simeq 6 \times 10^{-6} cm^{-1}$ when $T = 7.5 \times 10^{13}$.

HIGH PURITY CdTe - PHOTODIELECTRIC EXPERIMENTS

Typical photodielectric behavior of the CdTe sample is shown in Figs. V-19 and V-20. The curve of Δf has the same shape as the photoconductivity variation in the same sample at 4.2°K. The only differences are that the Δf plot does not return to the initial value when the light is removed, but rather retains a permanent shift of ∿ 19 kHz. This offset occurs after the first illumination cycle and represents the permanent filling of traps. The other difference is that the signal seen for the photodielectric effect is about four orders of magnitude above the noise level of the equipment, while the photoconductivity signal is only about ten times greater than the measurement limit when approaching the onset of space charge limited biasing. Photodielectric data allows the calculation of the model to be completed.

The shape of Fig. V-19 is easily explained by trapping in the 0.003 eV level seen in the low temperature conductivity tests. It is assumed that light creates free carriers and the electrons immediately proceed to recombination centers near the middle of the band. Although

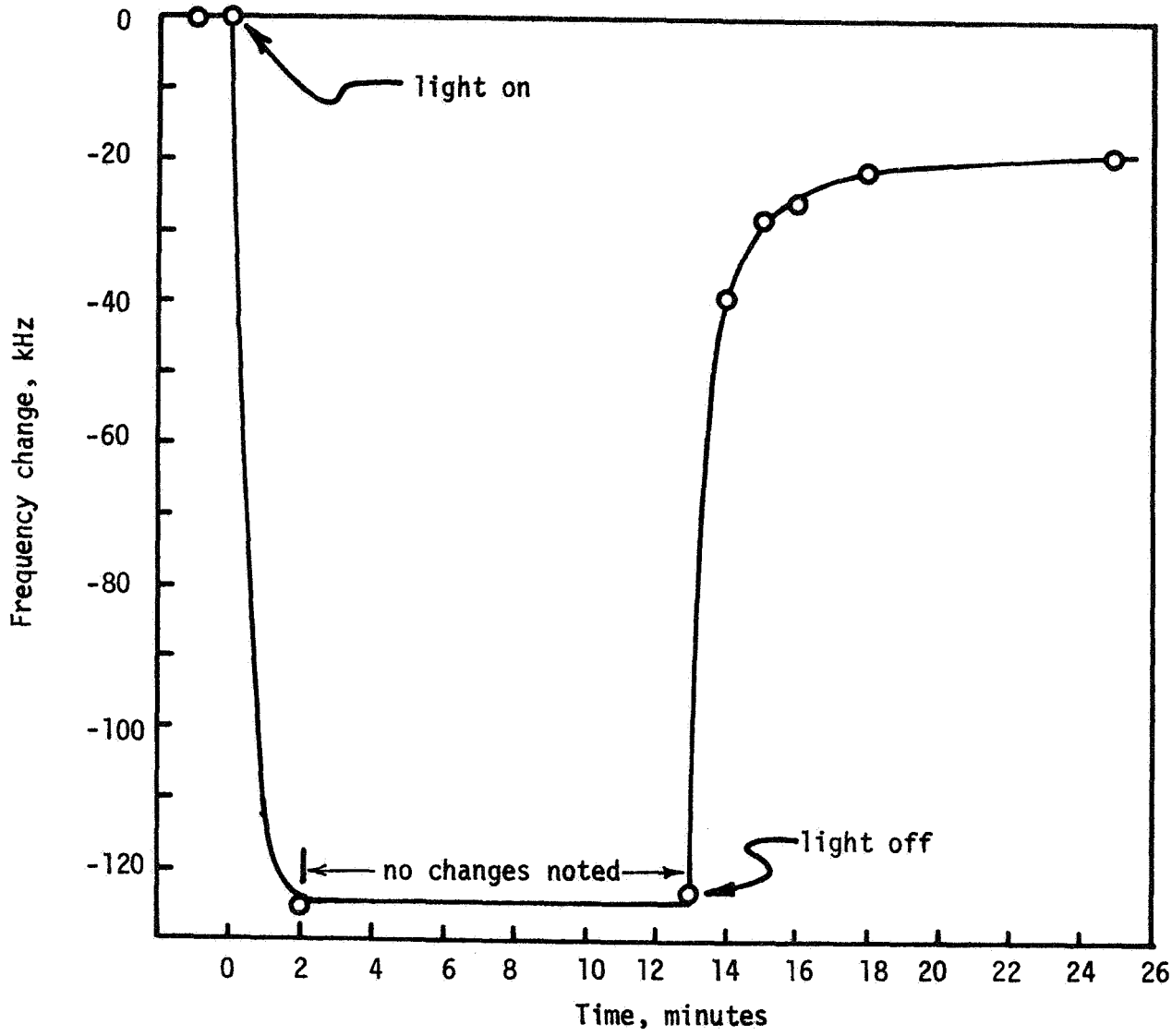

FIGURE V-19. Photodielectric frequency change in CdTe at 4.2°K due to 7.5×10^{13} photons/cm^3-sec at 0.8 μ.

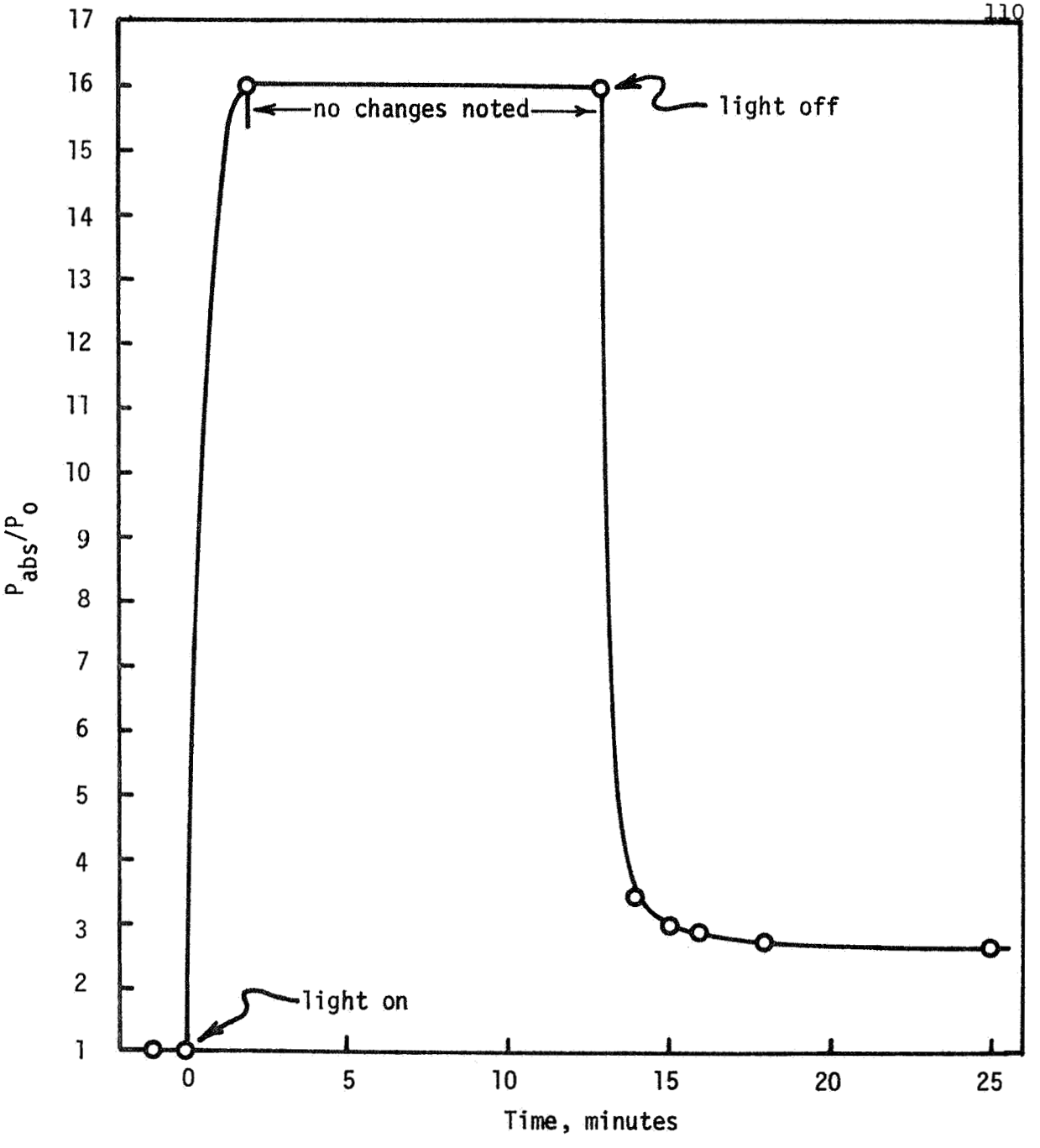

FIGURE V-20. Photodielectric power absorption variation in CdTe at 4.2°K due to 7.5×10^{13} photons/cm^3-sec at 0.8 μ.

these levels were not actually observed in these experiments, their presence is expected because of the occurrence of p-type conductivity and because other experimenters[37] have reported them as luminescence killer centers in p-type material. Free holes are either trapped at the shallow hole trap or proceed to the killer centers and recombine. Thus the recombination centers account for the small value of conductivity. A few holes are permanently trapped; the levels detected with TSC experiments contribute the offset frequency of 19 kHz seen in Fig. V-19.

The large temporary frequency change, due to holes in the 3 meV trap, represent a density of trapped carriers of $3.9 \times 10^{11} cm^{-3}$. This result comes from Eq. [2.31] with $B'(0.003) = 4 \times 10^{-23}$. Since the photoconductivity gives $p = 1.5 \times 10^{6} cm^{-3}$ and $p_t S_{pt} = 6 \times 10^{-6} cm^{-1}$ under the same conditions, the hole capture cross section $S_{pt}(0.003)$ is $1.55 \times 10^{-17} cm^{2}$. the density of hole traps, $P_t(0.003)$ is found to be $2 \times 10^{18} cm^{-3}$, again using Eq. [3.8].

The value of S_{pt} may be checked using the photodielectric decay when the light is removed. The response time given by Eq. [3.31] appears to be $\sim$ 30 seconds, which implies $S_{pt}(0.003) \simeq 2 \times 10^{-17} cm^{2}$. The response time actually represents the emptying of the trap here; the photoconductivity response time should be the same. After the holes are thermally ejected from the trap, they recombine at a killer center instead of returning to the trap, so the frequency change is reversible.

The preference by holes for recombination implies that $N_k R_{pk} >> P_t S_{pt} \simeq 10$ cm, where the k subscript refers to the killer centers. Since the hole trap has only a minor effect on the carriers, the killer centers may be treated with the single electron trap model discussed in Chapter

III. Use of Eq. [3.11] then gives $R_{pk} = 2.78 \times 10^{-16} cm^2$, only an order of magnitude larger than S_{pt}. It is likely, therefore, that $N_k > 2 \times 10^{18} cm^{-3}$. The lack of data on the specific variation of the free electron concentration precludes calculating N_k and E_k. This estimated value of N_k is too large if appreciable recombination also occurs at P_t.

The power absorption data does not shed additional light on the analysis because B"(0.003) ≈ B"(free hole). Since $p << p_t(0.003)$, the power absorption curve is expected to be similar to the frequency change plot, and a comparison of Figs. V-19 and V-20 shows that that is the case.

The permanent frequency offset of 19 kHz is attributed to trapping at the 0.05 eV and 0.124 eV hole traps, which were the only two traps observed by TSC methods. It has been noted that $p_t(0.124)$ tends to be about ten times $p_t(0.05)$; on the other hand, B'(0.05) ≈ 16 B'(0.124). Thus, lacking better information, it is assumed that each of the traps contributes an 8.5 kHz frequency shift to the photodielectric experiment after long periods of illumination. This indicates that $p_t(0.05) \approx 1.3 \times 10^{14} cm^{-3}$ and $p_t(0.124) \approx 2.1 \times 10^{15} cm^{-3}$. The fact that both traps fill within two minutes for $T = 7.5 \times 10^{13}$ absorbed photons/cm^3-sec is obvious from Figs. V-18 and V-20. Thus, the 0.124 eV trap captures at least 10% of the photogenerated holes before it saturates, indicating its capture cross section is comparable to the cross section of other levels.

The relative photodielectric sensitivity of the CdTe to different wavelengths is shown in Fig. V-21; the power absorption curve has a similar shape. The independent variable is the photon energy of the light used. Only one positive piece of data is obtained from the curve - the bandgap at 4.2°K is 1.6 eV. The sensitivity remains quite high for λ <

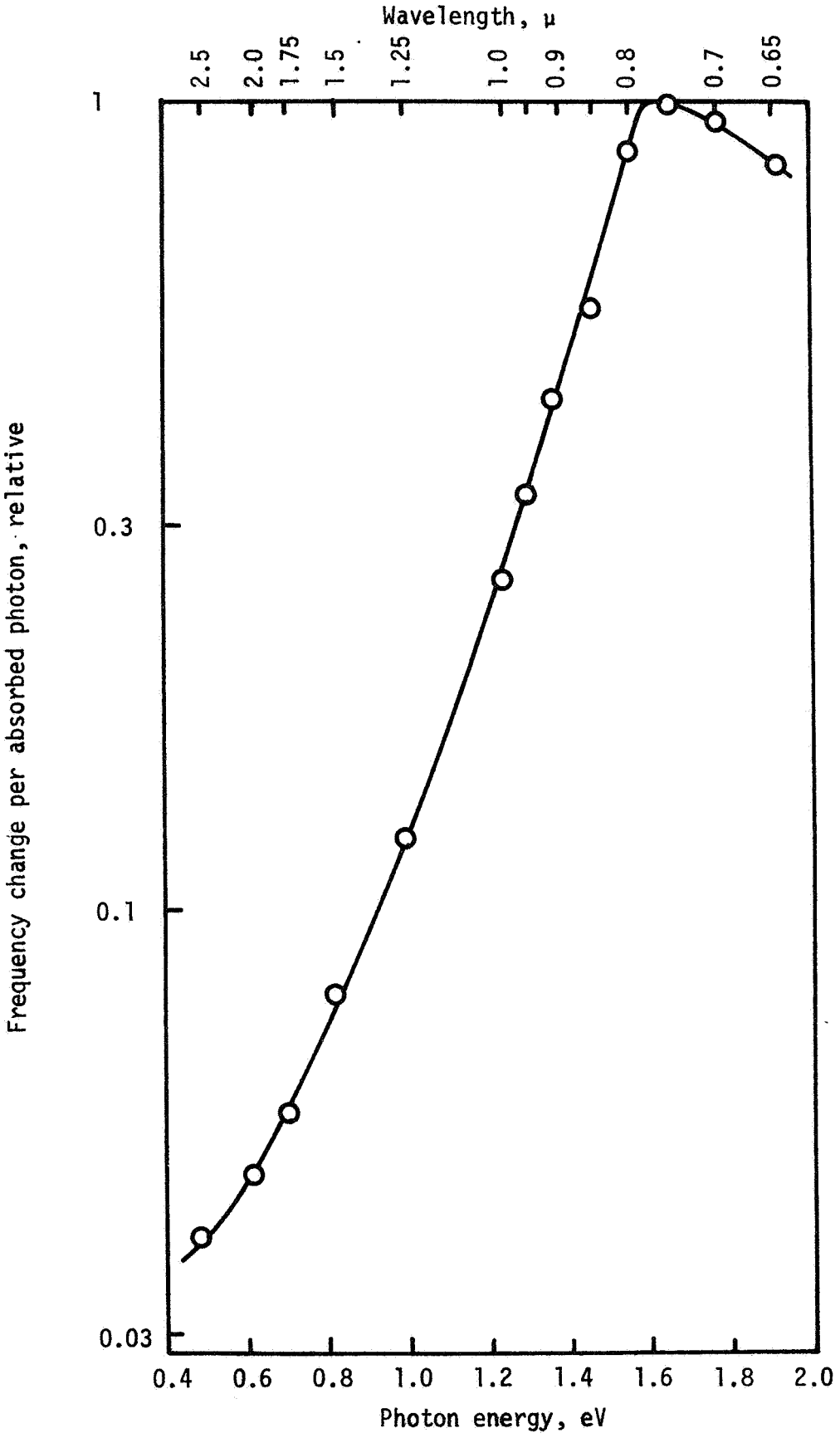

FIGURE V-21. Absorption spectrum for CdTe at 4.2°K, obtained using the photodielectric technique.

0.775 μ, but it falls rapidly for longer wavelengths. No sub-bandgap transitions are observed, which would be the expected result due to the rapid recombination and small trap densities seen in the crystal.

The dependence of the reversible portion of the frequency change on light intensity is shown in Fig. V-22. The power absorption curve once again has the same shape. It is seen that Δf, and therefore the density of carriers in the shallow trap, closely follow the relation $p_t \propto \sqrt{T}$. According to the analysis of Chapter II, this behavior is seen in the model of a single electron trap and also when strong retrapping effects are observed. The second model may be tested quickly by calculating p_t/R_{pt} from Eq. [3.42], using the known values of E_t, p_t, T, N_v, and v_p. The result is $P_t/R_{pt} \simeq 10^{22} cm^{-5}$, which is not a reasonable answer. The largest likely value of R_{pt} is $\sim 10^{-14} cm^2$, which would make $P_t = 10^8 cm^{-3}$, giving the impossible result that $p_t > P_t$.

Thus, it is concluded that at the levels of light employed, the 3 meV level behaves as if it were the only discrete level in the forbidden band. Physically, this could occur when the other hold traps are saturated and no longer active in influencing the sample characteristics. Also, the killer center must be highly populated in order to make recombination between free electrons and trapped holes more likely when the light is increased.

The trapping and recombination parameters observed in CdTe by the different techniques are summarized in Table V-3.

CdTe:Ag SINGLE CRYSTAL

A portion of the high purity CdTe was doped with silver in an attempt to achieve high sensitivity in the near infrared. Silver

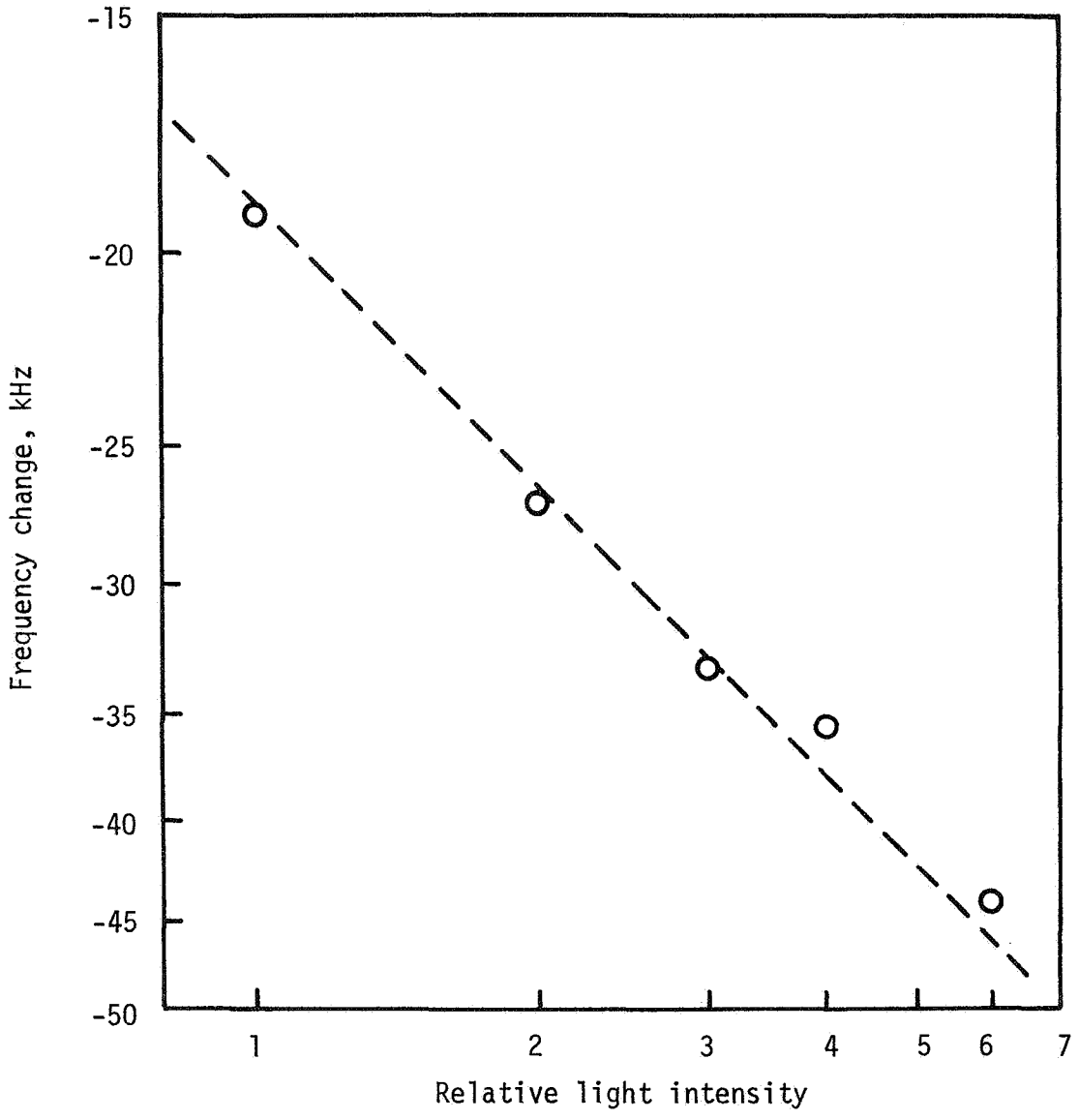

Figure V-22. Dependence of the photodielectric frequency change on the light intensity in high purity CdTe at 4.2°K. Unit light intensity is 7.5×10^{13} photons/cm^3-sec at 0.6 μ. The scales are both logarithmic, and the dotted line represents the relationship $\Delta f \propto \sqrt{T}$.

TABLE V-3

Trapping and Recombination Parameters of CdTe				
Level †	Method	T, ^{o}K	S_{pt}, cm^2	P_t, cm^{-3}
0.003	PD PC	4.2 4.2	1.55×10^{-17}	2×10^{18}
0.045±0.15	TSC	25		$< 10^{15}$
0.05	PD	4.2		$> 1.3 \times 10^{14}$
0.105	TSC	∿80	acceptor	
0.124	TSC+Decay PD	∿60 4.2	$\sim 10^{-18}$ **	$< 10^{15}$ $\sim 2 \times 10^{15}$
0.23	PC TSC	77 >250	acceptor	
0.55	PC	77		
1.6	PD	4.2	bandgap	
killer center	PD	4.2	2.78×10^{-16}	$\sim 2 \times 10^{18}$

† Measured from the valence band in eV.

** Comparable to cross sections of other levels.

generally places an acceptor level 0.3 - 0.33 eV above the valence band at 300°K[38]. It was found that at low temperatures the level is ∿ 0.37 eV from the valence band and it completely dominates the sample behavior. The levels seen in the high purity material were not seen and no levels other than the silver level are detected. The low temperature photosensitivity of the sample is very poor and the response time is less than 0.1 sec, too fast to be measured. The current cannot be measured accurately at the lower temperatures due to the small size of p, but it may be estimated that the free carrier lifetime is about a nanosecond, assuming a single hole trap model.

Since the sample possesses only a deep acceptor level, very low mobility[65], and poor sensitivity, each of which indicates the photodielectric response would be exceedingly small, no photodielectric experiments were attempted.

HIGH PURITY ZnTe - STANDARD EXPERIMENTS

Of the six common II-VI photoconducting compounds, ZnTe is generally regarded as the least sensitive[38]. The sample discussed here proved to be quite insensitive to most of the experiments performed on it, because of a very high density of acceptors which cause it to be high conductivity p-type at 300°K and 77°K, and a very good insulator below 35°K. The sample does not produce peaks in a TSC test, but rather shows an exponential increase of conductivity with temperature. At high temperatures, the slope reveals an acceptor level at 0.142 eV, which has been observed by Aven and Segall[10] and attributed to the second ionization of a zinc vacancy. They have also reported that the first ionization of the vacancy requires 0.048 eV, and a slope with approximately

0.05 eV activation energy was indeed observed at low temperatures. The expected energy is somewhat uncertain, however; Crowder and Hammer[82] show that the depth exhibits a decrease in effective ionization energy with increasing concentration, with E = 0.075 eV at infinite dilution. The room temperature resistivity of the high purity ZnTe is 2.5 Ω-cm, which suggests that the density of zinc vacancies causing acceptor levels is about 10^{18} cm^{-3}. Considering the large density of ionized acceptors at temperatures down to 77°K, as well as the absence of trapping effects, it is no surprise that the ZnTe is not highly photosensitive.

Photoconductivity spectra in the sample at various temperatures reveal only the band edge peak and a broad peak near 2 μ. The latter apparently corresponds to a 0.6 eV transition involving one of the bands; no other reference to a level at this depth has been noted. It could represent excitation from a third acceptor level or the freeing of a compensating hole or trapped electron from a deep donor or "killer" center.

The optical absorption curve for the ZnTe is given in Fig. V-23. Evidence for the 0.14 eV acceptor appears at 5950 Å, where the excitation of an electron from the acceptor level to the conduction band is the expected mechanism. The broad peak around 2 μ, noted previously in the photoconductivity spectrum, is also seen in the absorption curve. No trace of the 0.048 eV acceptor is observed, due to the onset of bandgap excitation in the region where absorption by the shallow acceptor should be seen.

At 4.2°K, the sample is an insulator with $p > 10^{12}$ Ω-cm. Photon fluxes of 10^{14} to 10^{15} photons/cm^3-sec at visible and near infrared wavelengths produce no observable photoconductivity in the material,

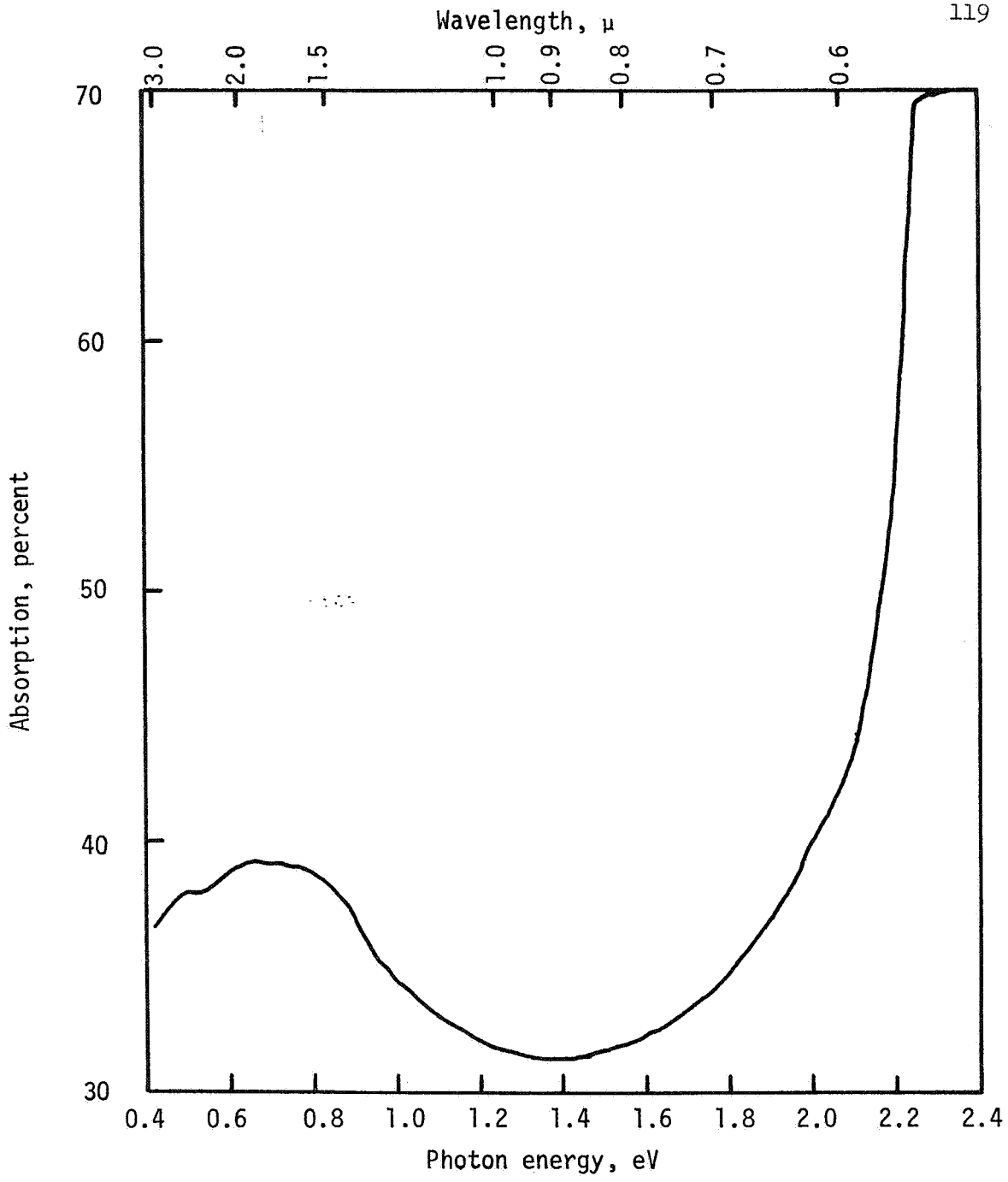

Figure V-23. Room temperature absorption spectrum of high-purity ZnTe single crystal.

where the measurement equipment detection limit corresponds to an excess density of about 10^5 free carriers per cm^3. This implies the lifetime is less than a nonosecond. A flux of $\sim 5 \times 10^{17}$ photons/cm^3-sec from an HeNe laser also produces no noticable increase in current. To get any photoconductivity response at 4.2°K, it is necessary to apply copious quantities of light; excitation with an estimated 1 to 10 watts of white light from a projection lamp (photon flux $\simeq 10^{19} - 10^{20}$photons/cm^3-sec) causes the excess carrier density to rise to about $10^7 cm^{-3}$. These numbers can only be taken as crude approximations, however, because the amount of the white light actually absorbed by the sample is uncertain, and problems are always encountered in making ohmic contact to ZnTe at very low temperatures. The rise and decay of the excess current density generated by the strong white light occurs faster than the response time of the measurement equipment.

ZINC TELLURIDE-PHOTODIELECTRIC EXPERIMENTS

The results of photodielectric experiments on the ZnTe are quite unusual and difficult to explain. Operating with a minimum detectable frequency change of about 100 Hz in a high Q cavity resonant at 873 MHz, no frequency shifts were observed at any visible or infrared wavelengths at photon fluxes of $10^{14} - 10^{15} cm^{-3} sec^{-1}$. The He-Ne laser, delivering $\sim 2 \times 10^{17}$ absorbed photons/cm^3-sec at 6328 Å, does produce a frequency change; at 4.2°K $\Delta f = +44.7$ kHz, and this increases to +68.5 kHz at 2.75°K, as shown in Figure 24. The sign of the frequency change has been emphasized because the frequency decreases in all of the other II-VI compounds studied. The size of the frequency increase in ZnTe is plotted in Figure V-25 against the relative light power, and it is noted

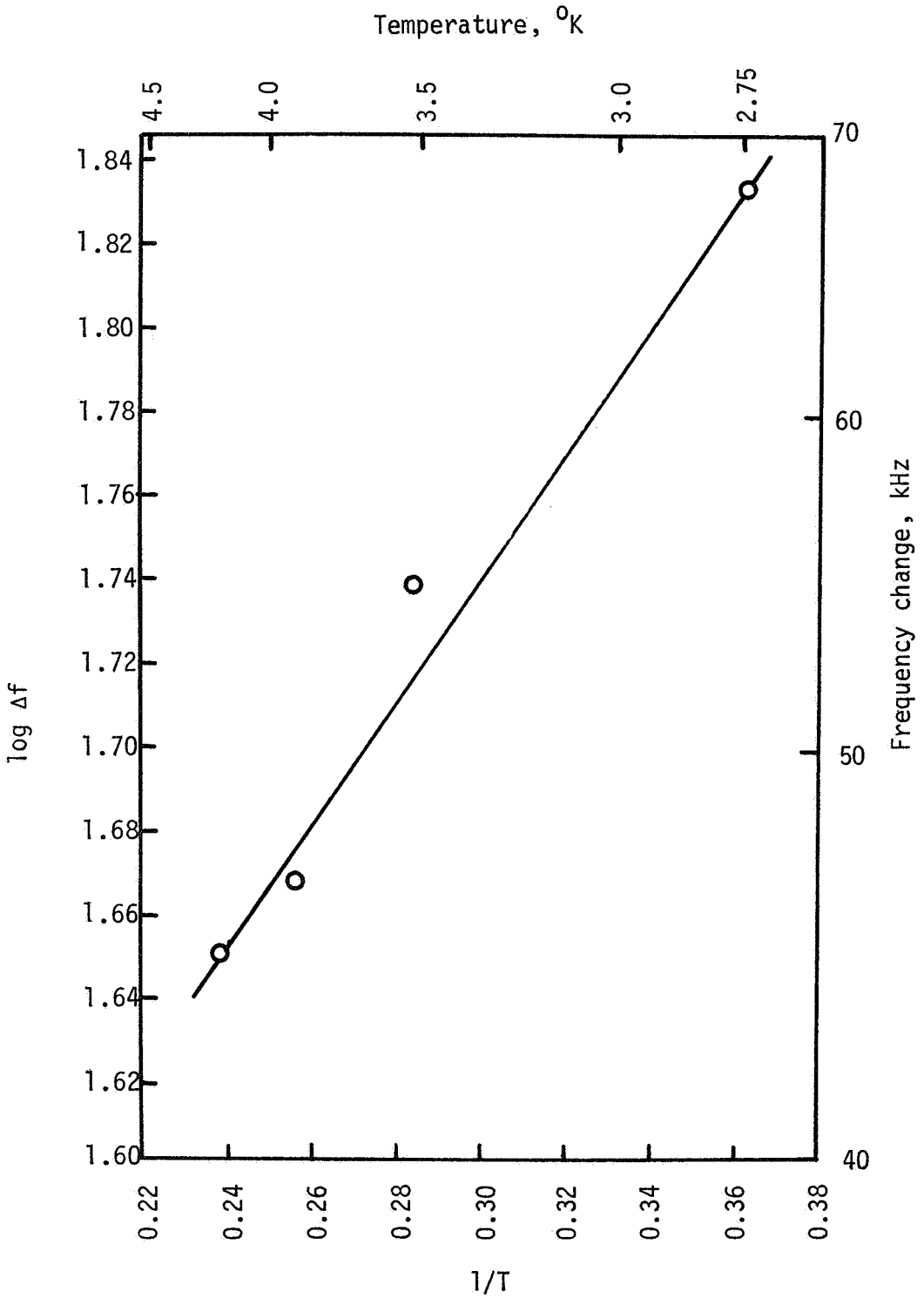

Figure V-24. Variation of Δf vs T, plotted as log Δf vs 1/T, showing the shallow hole trap in ZnTe.

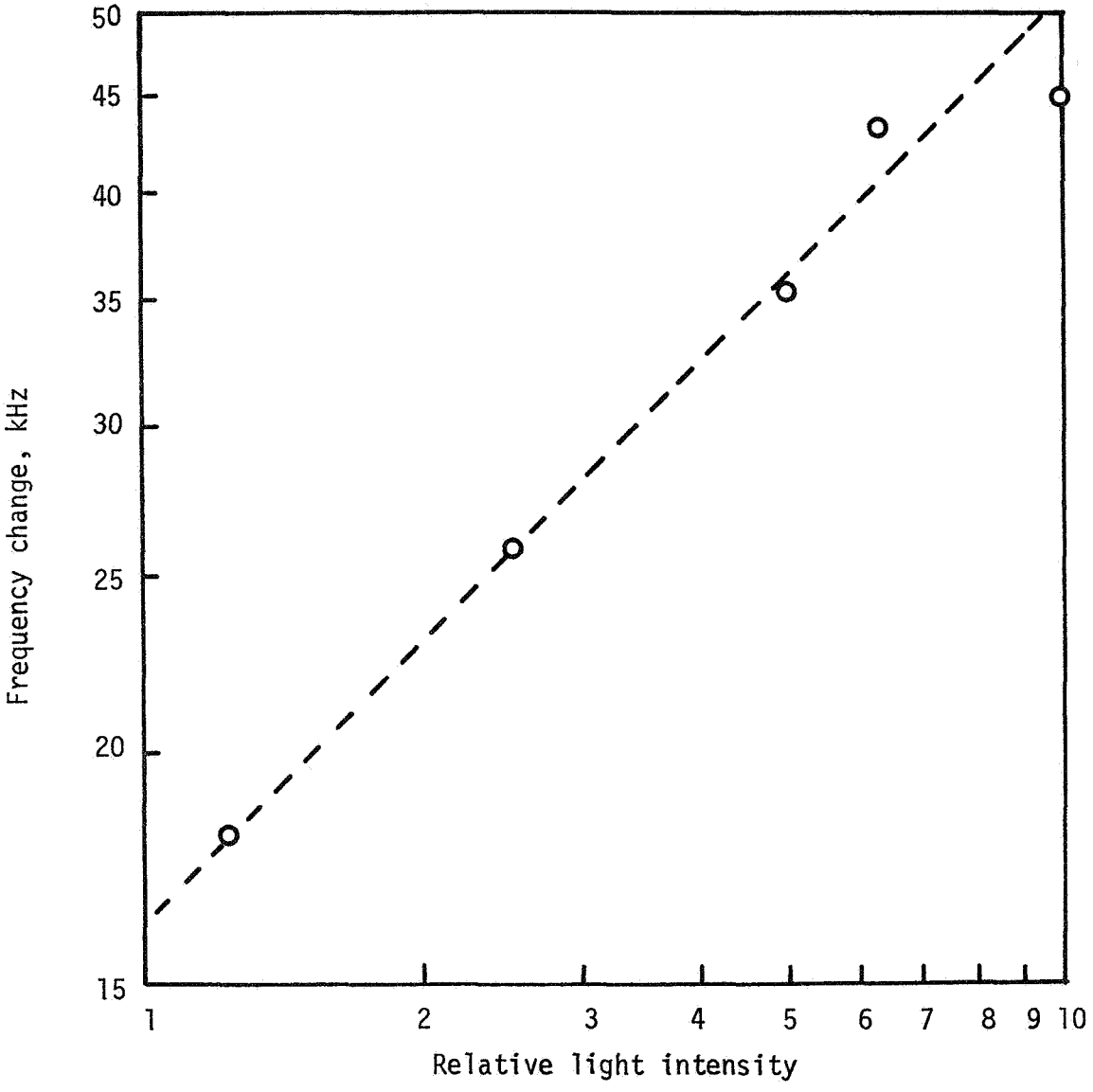

Figure V-25. Dependence of the photodielectric frequency change on the light intensity in high-purity ZnTe at 4.2°K. Unit light intensity is 2×10^{16} photons/cm^3-sec at 6328 Å. Both scales are logarithmic, and the dotted line represents the relation $\Delta f \propto \sqrt{T}$.

that the relation $\Delta f \propto \sqrt{T}$ holds over most of the range of light intensity. The frequency change is completely reversible, with an unmeasurably short response time. No rf power absorption changes are seen at any light level.

Applying Eq. [2.31] with $\Delta f = 4.47 \times 10^{4}$ Hz, $f = 8.73 \times 10^{8}$ Hz, $G = 3.67 \times 10^{-2}$, and $\varepsilon_r^2 = 102$ gives $B'\Delta p_t = -7.55 \times 10^{-12}$ $sec^2 cm^{-3}$. The fact that the frequency increases during excitation means either free carriers or lightly bound carriers with $\omega_o < \omega$ produce the dielectric change. The value of B' for either type is given by Eq. [2.29], with $\omega << 1/\tau$, so that $B' = -\tau^2$. If the value of τ is 7.5×10^{-13} sec, then $B' \simeq -5.6 \times 10^{-25}$ sec^2 and Δp or $\Delta p_t \simeq 1.35 \times 10^{13}$ cm^{-3}.

To decide whether free or trapped carriers are responsible for the positive frequency change, the following facts are gathered from the data which has been presented. 1) In photoconductivity measurements at $4.2^{o}K$, the free carrier density appeared to be less than 10^{5} cm^{-3}. 2) The variation of Δf with T as seen in figure V-24 could be caused by a trap 0.29 meV above the valence band. 3) The variation $\Delta f \propto \sqrt{T}$ is seen in figure V-25. 4) The excitation is produced by 1.96 eV photons, while the bandgap is 2.4 eV. 5) Absorption data (figure V-23) reveals an allowed transition to a level 0.4 to 0.8 eV from one of the bands.

The first point appears to rule out the free carrier explanation since the frequency change results from about 10^{13} holes/cm^3, while $\Delta p < 10^{5}$ cm^{-3}. The fact that the contacts are non-ohmic, however, causes us to question the validity of the Δp measurement and to seek other evidence for the model. The second point indicates that a hole trap with an ionization energy of 0.29 meV exists. Equations [2.21] and [2.16] reveal that B' for this trap is negative, so that carriers trapped there could produce a positive frequency change.

The $\Delta f \propto \sqrt{T}$ variation could be explained using a model with a single hole trap or with a trap where retrapping effects are important. Rose[9] shows that this variation could also result from free carriers when there are electron traps, hole traps, and recombination centers in the forbidden band*. The density of trapped carriers also varies as $\sqrt{T}$ in Rose's model, and the condition $p_t >> p$ is required. Thus either free or trapped carrier effects could give rise to the $\Delta f \propto \sqrt{T}$ variation, but it appears more likely that the effect is caused by the trapped carriers.

Since points 4) and 5) do not shed additional light on the free vs trapped carrier question, we are forced to accept the trapped carrier model, primarily on the basis of the first two points, although the possibility of a free carrier effect can not be positively eliminated.

A simple model to explain the data must have a hole trap 0.29 meV from the valence band. Since it is populated by 1.96 eV photons, another discrete level must exist about 1.96 eV above the valence band. A consistent model results if we assume the smaller peak in figure V-23 represents a level about 0.5 eV from the conduction band, or about 1.9 eV from the valence band. Assume that the laser light excites an electron from the valence band to that level, which acts as an electron trap or recombination center. The free hole left behind may then either be trapped at the shallow level or recombine at the deep level.

* The model requires $p + p_t \simeq N_r$, the density of recombination centers. The model is referred to as the "transition range" model by Rose because it covers the transition between the two situations $p + p_t >> N_r$ and $p + p_t << N_r$. The notation of Rose is altered here to treat holes rather than electrons as the majority carrier.

The great height and width of the 2μ peak in the absorption experiment suggests that the density of the deep level is large. The small values of p and p_t observed at strong light levels suggests that the recombination center also has a large capture cross section for holes. The fact that $p_t >> p$, although the trap is shallow means that it also has a large capture cross section, and thus the $\sqrt{T}$ dependence of Δp suggests that the carrier density is subject to retrapping effects. The application of Eq. [3.42] yields $P_t(2.9 \times 10^{-4})/R_{pt}(1.8) = 1.8 \times 10^{31}$ cm^{-5}. We expect that $P_t(2.9 \times 10^{-4}) >> 10^{13}$ cm^{-3}, in which case $R_{pt}(1.8) >> 10^{-18}$ cm^2.

The product $P_t S_{pt}$ is estimated to be 10^5 cm, using Eq. [3.45] with p taken to be 10^5 cm^{-3}. This value for the product requires P_t or S_{pt} to have a value about 10 times larger than values normally encountered. Furthermore, if it is assumed that $n_t = p_t$, the value of R_{pt} obtained with $p = 10^5$ cm^{-3} is about 10^{-9} cm^2, which is considered unreasonable large. There are several possible reasons for the occurrence of these unlikely results. The shallow level may somehow be related to the recombination center so that the necessity of the hole entering the valence band before reaching the recombination center is eliminated. The existence of another level, invisible to the photodielectric and standard experiments, could also invalidate the model and results given here. It is felt, however, that the most likely source of error is the lack of good contacts to the photoconductor at low temperatures. If the true bias field in the ZnTe is significantly lower than the applied field, then the calculated value of p is less than the true value by the same amount, causing the calculated value of R_{pt} to be too large. Unfortunately, the behavior of p cannot be separated out of the photodielectric data because both free carriers and holes at the shallow trap have the same value of B' and no variations in

P_{abs} are seen.

A summary of the trapping and recombination parameters observed in the ZnTe sample is given in Table V-4.

TABLE V-4

Trapping and Recombination Parameters of ZnTe				
Level †	Method	T, ^{o}K	S_{pt}, cm^2	P_t, cm^{-3}
$2.9x10^{-4}$	PD	4.2		
0.05	TSC		acceptor	
0.142	TSC Abs	>200 300	acceptor	
1.8	PC Abs PD	300 300 4.2	$>10^{-18}$	large

† Measured from the valence band in eV.

CHAPTER VI.

RESULTS AND CONCLUSIONS

In the preceding chapter, results from both standard and photodielectric experiments on four different II-VI samples were presented. The behavior of the CdS:Al was analyzed independently with the photodielectric technique, and values for most of the parameters of the impurity levels were obtained. The other samples were analyzed by using photodielectric data together with the data of the standard experiments. In the following sections, the results are discussed, comparing the different methods of obtaining parameter values. Suggestions for the application of photodielectric measurement techniques are given, and recommendations for further study are made.

ENERGY LEVELS

Four energy levels were found in the CdS:Al using only photodielectric data, and as Table V-1 shows, the values tend to agree with the values obtained in other ways. The photodielectric technique did not reveal the 0.35 eV trap in CdS:Al, probably because that level has a minimal effect on low temperature energy transport. The standard experiments failed to show the levels 0.007 and 1.3 eV below the conduction band, but this may be a result of not using the proper temperatures and wavelengths in the study.

The 0.13 eV level may be the same as the trap at 0.16 eV below the conduction band reported by Bradberry and Spear[75] and attributed to singly ionized sulphur vacancies; levels near 0.14 eV are often reported in CdS[78]. It was found by relating Δf to E_t with Eq. [2.31] after assuming a proportionality between Δn and $\int T\, dt$. The degree of confidence

in the value of E_t obtained in this manner depends on the confidence in calculating Δn, which in turn is related to the light flux and absorption coefficient, two quantities which are difficult to measure. In other samples not displaying the simple behavior of CdS:Al, calculation of E_t by way of Eq. [2.31] might involve some rather shaky assumptions.

A method judged to be better for calculating energies from photodielectric data involves photodielectric decay. The 0.007 eV levels seen in both CdS samples were found from decay measurements. Levels near that depth have been reported by Itakura and Toyada[74] and Pedrotti and Reynolds[44] in undoped CdS, but the origin of the levels is not clear. The decay method is so insensitive to errors in the value of S_t that values of E_t accurate to within about 25% may be found by assuming any reasonable value of S_t; this was demonstrated in both cases. The shallow traps in the tellurides were also discovered using photodielectric decay data. No published reports of them have been found.

Energies of levels may also be found by relating peak wavelengths for photodielectric behavior to the ionization energy of a level. The 0.17 eV trap in CdS:Ag, probably due to sulphur vacancies as discussed previously, was observed in this way, as was the 0.35 eV level. A level near 0.4 is expected in CdS:Ag[45], but there are also many reports of levels near 0.35 eV in materials not intentionally doped with silver[40,78]. The depth of the sensitizing center and the 0.775 eV level (both seen by many other observers[78]) in CdS:Al and the bandgap of CdTe were derived from analysis of the photodielectric spectral response, and the bandgap of CdS undoubtedly could have been determined if that had been the goal of the experiments. Similarly, the fact that the ZnTe is sensitive to the

sub-bandgap light from a He-Ne laser gives some idea of the location of the killer center in that material. The depth of the sensitizing center in CdS:Ag was found by equating the energy of the level to the energy of the photons which were the best for quenching.

Whenever a measurable parameter varies with T, such as n in Eq. [3.15], or τ_d in [3.16], the preferred method of determining E_t is to make measurements at several different temperatures. This allows the temperature invariant parameters to be removed from the equation. For example, [3.15] is replaced by [3.17] if two different measurement temperatures are used; [3.17] does not depend on N_t. The two different temperatures must be close enough together to insure that the same energy level determines the characteristics of the sample at both temperatures. Often, this may be the only easy way to determine E_t, as in the case of the shallow level in ZnTe.

CAPTURE AND RECOMBINATION CROSS SECTIONS

The cross sections can be calculated from photodielectric data if a model is assumed for the energy level scheme. Admittedly, any model must be a simplified approximation of the actual case, but it is usually possible to choose a model after determining how the carrier densities vary with light and how they interact with each other. Often several simple approximations must be combined to explain the complicated behavior of a sample; this is necessary for all of the samples described in Chapter V because they all display several levels.

Once the model is chosen, the cross sections are found using the trapping and recombination equations developed by Shockley and Read[56] and Hall[57] and extended here in Chapter III. The most accurate values of S_t

and R_t are likely to come from equations not involving the Boltzmann factor, such as [3.7] and [3.11]. This is true because small changes in the value of E_t lead to large changes in $e^{-E_t/kT}$ and, therefore, a small error in E_t gives a large error in S_t or R_t.

When the equation involving the cross section contains the Boltzmann factor, as Eq. [3.16] does, it is desirable to measure the observable quantity at two different temperatures. For example, the value of S_t (0.007) in the CdS:Al is found by measuring τ_d in Eq. [3.31] at two temperatures and finding E_t (0.007). This value is then used in Eq. [3.31] to evaluate S_t.

If the proper model is not obvious, a preliminary calculation of S_t and N_t using an assumed model may indicate whether the model assumed is the proper choice. In CdTe, the model involving retrapping effects was shown to be not applicable when a calculation using Eq. [3.42] yielded the impossible result that $p_t > P_t$.

FREE AND TRAPPED CARRIER DENSITIES

Carrier densities as a function of time may be directly observed using photodielectric techniques. Frequently, however, several effects occur simultaneously and must be separated; the filling of three electron traps in CdS:Ag is resolved from frequency change data, and the effects of free carriers and carriers in the 7 meV trap in CdS:Al are separated using power absorption information. It is necessary to remember that B' and B" are, in general, rapidly varying functions of ionization energy, and effects of moderately shallow levels tend to be weighted more heavily than effects of deep centers. In some ways this is a desirable feature; for example, in CdTe the effects of $\sim 10^{11}$ cm^{-3} weakly bound holes clearly

appear over the effects of $\sim 10^{14}$ cm^{-3} holes in deeper traps. Obviously, the same behavior tends to make the photodielectric effect insensitive to carriers in deeper traps. Power absorption data is somewhat less valuable than frequency change data in determining the time variation of carrier densities because there is a wide range of energies at which B" does not vary with E_t. This fact prevents the separation of free hole effects from trapped hole effects in CdTe, for example.

TRAP DENSITIES

The calculation of trap densities is a problem similar to the calculation of capture and recombination cross sections because the proper equations often involve the Boltzmann factor. In some cases, it is possible to find an imperfection density by making two measurements at different temperatures as described above.

Densities of levels are also estimated by saturating the levels, measuring the concentration of trapped carriers, and then equating the two densities. Any errors in this method are likely to be small, caused by the failure to achieve the complete saturation that is assumed. Another method of estimating trap densities is to measure or assume the filling rate for a trap at a constant light level, measure the time required for the trap to saturate, and multiply the rate by the elapsed time. There is much room for error in finding the filling rate and in the assumption that this rate remains constant until the time saturation is accomplished. Since the photodielectric response is proportional to the density of trapped carriers, the filling rate is often evident. Obviously, the saturation methods of finding two trap densities do not work if the trap empties through recombination or thermal freeing, and partial emptying causes the density estimate to be too large.

MOBILITY

No mobility values were calculated in this study; instead, mobilities were assumed in order to calculate other parameters. It does appear possible, however, to use photodielectric techniques to find the order of magnitude of carrier mobilities. The mobility of a carrier is related to the momentum relaxation time by the simple relation[49]

$$\mu = e\tau/m^* \qquad [6.1]$$

Photodielectric behavior depends very strongly on the value of τ. Equations [2.21] and [2.22] show the dependence of B' and B" on τ.

Assume the simple case of $\omega << 1/\tau$ so that for a free carrier $B' = -\tau^2$ (see Eq. [2.39]). Let a photosensitive sample be subjected to a photodielectric experiment and then a photoconductivity experiment, using identical temperatures and illumination. The frequency change due to excess free carriers is given by [2.31].

$$\Delta f = \frac{fG}{\varepsilon_r^2} \frac{e^2}{m^* \varepsilon_o} \Delta n \tau^2 \qquad [6.2]$$

The current change due to excess free carriers is given by

$$\Delta I = \frac{VAe\mu}{\ell} \Delta n \qquad [6.3]$$

where I is current, V is the bias voltage, A is the effective ohmic contact area, and ℓ is the effective thickness of the sample. Eliminating Δn and τ from [6.1] through [6.3] yields

$$\mu = \frac{\Delta f}{\Delta I} \frac{VA}{\ell} \frac{\varepsilon_o \varepsilon_r^2 e}{m^* f G} \qquad [6.4]$$

A sample calculation may be performed by using data from CdS:Ag tests. Since no free carrier component of Δf was observed, we may set an upper bound of $\sim 10^4$ Hz for Δf. At 4.2°K the photocurrent for the conditions of light used in the photodielectric test is $\sim 6 \times 10^{-9}$ amps. Other values are V = 6 volts, $A/\ell \simeq 0.1$ cm, $\varepsilon_r^2 \simeq 60$, $m^* = 0.2$ m, $f \simeq 10^9$ Hz, and $G \simeq 5 \times 10^{-2}$. The result is $\mu < 100$ cm^2/volt-sec, which does not disagree with the value of 10 cm^2/volt-sec used.

THERMALLY STIMULATED DIELECTRIC CONSTANT CHANGES

The preceding discussion has described the many ways in which trapping and recombination parameters are found from the data of a photodielectric experiment. In reality, a "photodielectric experiment" is many different experiments which are similar in some ways to the standard experiments described in Chapter I. For example, the photodielectric spectrum obtained for the CdS:Ag is roughly analogous to a photoconductivity spectrum. One standard technique currently without a photodielectric counterpart is the thermally stimulated conductivity experiment.

Hartwig[83] has considered the question of performing a photodielectric experiment while warming the sample, in order to observe the emptying of traps and ionization of donors and acceptors. Such a proposed experiment is theoretically feasible and offers the same advantages over TSC tests that photodielectric methods have over photoconductivity experiments. The equations applicable to the analysis are the same as those presented in Chapters II and IV.

The model used to describe the movement of electrons during a TSC experiment assumes that an electron in a shallow trap (small B", large B') is excited thermally to the conduction band (large B", small B') where

it remains for a time τ_L and then enters the valence band (small B", small B') by recombining. Similar behavior occurs for holes. It is a good approximation in this simple case to write

$$f = f_o - An_t \qquad [6.5]$$

$$P_{abs} = P_o + Bn_t + Cn \qquad [6.6]$$

where A, B, and C are collections of constants. It is frequently true that the third term in Eq. [6.6] is greater than the second term. Thus, since a TSC peak corresponds to a peak in n or dn_t/dt, it also corresponds to a peak in P_{abs} or df/dt.

In performing the proposed experiment, the frequency and power absorbed are plotted as a function of time while the sample is heated at several different constant heating rates. A plot of $\ell n(T_m/\beta)$ vs. $1/T_m$ for various values of β, the heating rate, then gives E_t according to Eq. [4.9]. This value then may be used in [4.1] to find S_t or in [4.2] to find $N_t\tau_L$.

Use of [2.31] gives a value for the initial density of trapped carriers, and the curve of Δf vs. t is then converted into a plot of Δn_t vs. t by properly relabeling the vertical axis. Once $n_t(T)$ and E_t are known, Eqs. [2.16] and [2.32] are used to find n(T), which has the same shape as $P_{abs}(T)$ when the effects due to trapped carriers are subtracted from $P_{abs}(T)$. When $n(T_m)$ and $dn_t(T_m)/dt$ are known, the lifetime found by using

$$\tau_L = \frac{n(T_m)}{\beta[dn_t/dT]} \qquad [6.7]$$

Preliminary calculations based on simple models indicate the proposed photodielectric experiment should compare favorably with the standard TSC

method in determining properties of traps within $\sim$ 0.3 eV of the conduction band.

SUMMARY

It has been shown that photodielectric techniques, when applied to a sample in a high Q superconducting microwave cavity, offer many advantages over standard experiments for analyzing low temperature trapping and recombination in II-VI compounds. The high Q of a superconducting cavity is necessary to insure that the sample maintains control of the cavity frequency and power absorption, while the liquid helium bath provides constant temperature, inert surroundings. The cavity perturbation technique is extremely sensitive to small material property changes. It has been demonstrated that in some cases (CdTe, ZnTe) the photodielectric experiment is clearly more sensitive than photoconductivity tests on the same material.

There are many advantages of photodielectric techniques besides the inherent sensitivity. The need to make ohmic contacts to the sample is not present; the witchcraft associated with making ohmic contact to some materials is forgotten, and powder samples may be tested. At high frequencies used, space charge limitations vanish.

In the actual analysis of properties, the photodielectric measurement directly gives the density of trapped carriers, which normally must be inferred when standard tests are employed. Trap densities are plotted as the traps fill and saturate or reach equilibrium. This extra information simplifies the problem of selecting a model to describe the behavior seen, and allows parameters to be calculated with fewer assumptions and more accurate results. The parameters which have been calculated include the ionization energy of the level, its density and the

density of carriers there, and the capture and recombination cross sections. A rough measurement of mobility also appears to be possible.

Like the other techniques evaluated, the photodielectric method has drawbacks. The temperature range available is very limited, the technique tends to be insensitive to deep levels and to levels which have small effects on energy transport in the crystal, and trap energies cannot always be calculated accurately. The best procedure to follow in analyzing material properties is to apply as many measurement methods as possible, so that the "extra" data may be used to check for consistency. Photodielectric data is best used in calculating cross sections and densities, given the energy of the level found by some other method.

BIBLIOGRAPHY

1. Bube, R. H., Photoconductivity in Solids, New York, Wiley and Sons, 1960.

2. Tubota, H., "Electrical Properties of $A^{II}B^{VI}$ Compounds, CdSe and ZnTe," Japan J. Appl. Phys. 2, 259 (1963).

3. Segall, B., M. R. Lorenz, and R. E. Halsted, "Electrical Properties of n-type CdTe," Phys. Rev. 129, 2471 (1963).

4. Bube, R. H., W. M. Grove, and R. K. Murchison, "Photoconductivity Decay in Imperfect Crystals," J. Appl. Phys. 38, 3515 (1967).

5. Haering, R. R., and E. N. Adams, "Theory and Application of Thermally Stimulated Currents in Photoconductors," Phys. Rev. 117, 415 (1960).

6. Bube, R. H., G. A. Dussel, C. Ho, and L. D. Miller, "Determination of Electron Trapping Parameters," J. Appl. Phys. 37, 21 (1966).

7. Lambe, J. J., C. C. Klick, and D. L. Dexter, "Nature of Edge Emission in CdS," Phys. Rev. 103, 1715 (1956).

8. Hemila, S. O., and R. H. Bube, "Optical Quenching of Photoconductivity in CdS and ZnS Crystals," J. Appl. Phys. 38, 5258 (1967).

9. Rose, A., Concepts in Photoconductivity and Allied Problems, Interscience Publishers, New York, 1963.

10. Aven, M., and B. Segall, "Carrier Mobility and Shallow Impurity States in ZnSe and ZnTe," Phys. Rev. 130, 81 (1963).

11. Shiozawa, L. R., et al., "Research on II-VI Compound Semiconductors," ASTIA AD 281718.

12. Lambe, J., "Recombination Processes in CdS," Phys. Rev. 98, 985 (1955).

13. Lambe, J., "CdS with Silver Activator," Phys. Rev. 100, 1586 (1955).

14. Kulp, B. A., K. A. Gale, and R. G. Schulze, "Impurity Conductivity of Single Crystal CdS," Phys. Rev. 140, 252 (1965).

15. Blount, G. H., A. C. Sanderson, and R. H. Bube, "Effects of Annealing on the Photoelectronic Properties of ZnS Crystals," J. Appl. Phys. 38, 4409 (1967).

16. Halsted, R. E., "Radiative Recombination in the Band Edge Region," Physics and Chemistry of II-VI Compounds, Wiley and Sons, New York, 1967.

17. Garlick, G. F. J., and A. F. Gibson, "Electron Trap Mechanism of Luminescence in Sulfide and Silicate Phosphors," Proc. Phys. Soc. London 60A, 574 (1948).

18. Broser, I., "Energy Transfer Processes," Physics and Chemistry of II-VI Compounds, Wiley and Sons, New York, 1967.

19. Segall, B., "Optical Absorption Edge in CdTe: Theoretical," Phys. Rev. 150, 734 (1966).

20. Marple, D. T. F., "Optical Absorption Edge in CdTe: Experimental," Phys. Rev. 150, 728 (1966).

21. Halperin, A., and G. F. J. Garlick, "The Absorption Spectrum of Excited Crystals of Cadmium Sulfide," Proc. Phys. Soc. London 68B, 758 (1955).

22. Bube, R. H., "Electronic Transitions in the Luminescence of Zinc Sulfide Phosphors," Phys. Rev. 90, 70 (1953).

23. Hartwig, W. H., "Use of the Photodielectric Response of Semiconductors to Detect Visible and Infrared Radiation," Air Force Contract Report 19(604)5717, 1961.

24. Genz, R. H., Frequency Dependence of Reentrant Coaxial Cavities upon Physical Properties of a Terminating Disc, Masters Thesis, The University of Texas at Austin, 1961.

25. Arndt, G. D., Photodielectric Effect of Bulk Semiconductors in Resonant Cavities, Ph.D. Dissertation, The University of Texas at Austin, 1965.

26. Stone, J. L., and W. H. Hartwig, "A Unique Laser Detector Utilizing the Photodielectric Effect in Cooled Semiconductors," Technical Report No. 39, Laboratories for Electronics and Related Science Research, The University of Texas at Austin, 1967.

27. Hinds, J. J., and W. H. Hartwig, "The Photodielectric Effect in Cadmium Sulfide," NASA Research Report on Digital Transducer Principles, Volume VI, The University of Texas at Austin, 1968.

28. Baker, G. L., and W. H. Hartwig, "Calculation of Free Carrier Photodielectric Parameters," NASA Technical Report, Electronics Research Center, The University of Texas at Austin, 1969.

29. Hartwig, W. H., and J. J. Hinds, "Use of Superconducting Cavities to Resolve Carrier Trapping Effects in CdS," J. Appl. Phys. 40, 2020 (1969).

30. Stone, J. L., W. H. Hartwig, and G. L. Baker, "Automatic Tuning of a Superconducting Cavity Using Optical Feedback," J. Appl. Phys. 40, 2015 (1969).

31. Kallmann, H., B. Kramer, and A. Perlmutter, "Infrared Stimulation and Quenching of Photoconductivity in Luminescent Powders," Phys. Rev. 99, 391 (1955).

32. Kallmann, H., B. Kramer, and P. Mark, "De-Excitation of ZnS and ZnCdS Phosphors by Electric Fields," Phys. Rev. 109, 721 (1958).

33. Broser, I., P. Brumm, and C. Reuber, "Der Photodielektrische Effekt in CdS-Einkristallen," Zeitschrift fur Physik 179, 367 (1964).

34. Garlick, G. F. J., and A. F. Gibson, "Electronic Traps and Dielectric Changes in Phosphorescent Solids," Proc. Roy. Soc. A188, 485 (1947).

35. Garlick, G. F. J., "Absorption, Emission, and Storage of Energy in Phosphors," Brit. J. Appl. Phys., Supp. 4, S 85 (1955).

36. Neuberger, M., "Cadmium Sulfide," ASTIA AD 810354.

37. Moorehead, F. F., "Electroluminescence," Physics and Chemistry of II-VI Compounds, Wiley and Sons, New York, 1967.

38. Devlin, S. S., "Transport Properties," Physics and Chemistry of II-VI Compounds, Wiley and Sons, New York, 1967.

39. Bube, R. H., "Photoconductivity," Physics and Chemistry of II-VI Compounds, Wiley and Sons, New York, 1967.

40. Kulp, B. A., "Defects in Cadmium Sulfide Crystals," J. Appl. Phys. 36, 553 (1965).

41. Litton, C. W., and D. C. Reynolds, "Edge Emission in CdS Crystals that Show Mechanically Excited Emission," Phys. Rev. 125, 516 (1962).

42. Litton, C. W., and D. C. Reynolds, "Double Carrier Injection and Negative Resistance in CdS," Phys. Rev. 133, A536 (1964).

43. Eastman, P. C., and D. E. Brodie, "CdS Films with Adjustable Carrier Density in any Given Sample," Proc. IEEE 53, 512 (1965).

44. Pedrotti, L. S., and D. C. Reynolds, "Energy Model for Edge Emission in CdS," Phys. Rev. 120, 1664 (1960).

45. Lambe, J., and C. C. Klick, "Model for Luminescence and Photoconductivity in the Sulfides," Phys. Rev. 98, 909 (1955).

46. Woods, J., "Changes in Conductivity Resulting from Breakdown in CdS Single Crystals," Proc. Phys. Soc. London 69, 975 (1956).

47. Roth, W. L., "Crystallography," Physics and Chemistry of II-VI Compounds, Wiley and Sons, New York, 1967.

48. Lorenz, M. R., and R. E. Halsted, "High-Purity CdTe by Sealed-Ingot Zone Refining," J. Electrochem. Soc. 110, 343 (1963).

49. Wang, S., Solid State Electronics, McGraw-Hill, New York, 1966.

50. Levine, S. N., Quantum Physics of Electronics, MacMillan, New York, 1965.

51. Kittel, C., Introduction to Solid State Physics, Wiley and Sons, New York, 1953.

52. Dresselhaus, G., A. F. Kip, and C. Kittel, "Cyclotron Resonance of Electrons and Holes in Silicon and Germanium," Phys. Rev. 98, 368 (1955).

53. Dekker, A. J., Solid State Physics, Prentice-Hall, Englewood Cliffs, New Jersey, 1965.

54. Nozieres, P., and D. Pines, "Electron Interaction in Solids. Collective Approach to the Dielectric Constant," Phys. Rev. 109, 762 (1958).

55. Dresselhaus, G., A. F. Kip, and C. Kittel, "Plasma Resonance in Crystals: Observations and Theory," Phys. Rev. 100, 618 (1955).

56. Shockley, W., and W. T. Read, "Statistics of the Recombinations of Holes and Electrons," Phys. Rev. 87, 835 (1952).

57. Hall, R. N., "Electron-Hole Recombination in Germanium," Phys. Rev. 87, 387 (1952).

58. Segall, B., and D. T. F. Marple, "Intrinsic Excition Absorption," Physics and Chemistry of II-VI Compounds, Wiley and Sons, New York, 1967.

59. Balkanski, M., and R. D. Waldron, "Internal Photoeffect and Excition Diffusion in CdS and ZnS," Phys. Rev. 112, 123 (1958).

60. Thomas, D. G., and J. J. Hopfield, "Excition Absorption Spectrum in Cadmium Sulfide," Phys. Rev. 116, 573 (1959).

61. Hopfield, J. J., and D. G. Thomas, "Fine Structure and Magneto-Optic Effects in the Excition Spectrum of Cadmium Sulfide," Phys. Rev. 122, 35 (1961).

62. Piper, W. W., and R. E. Halsted, "Intrinsic Electrical Properties of n-type CdS," Proc. Int. Conf. on Semicond. Phys., 1046 (1960).

63. Spear, W. E., and J. Mort, " Electron and Hole Transport in CdS Crystals," Proc. Phys. Soc. London 81, 130 (1963).

64. Czyzak, S. J., et al., "The Study of Properties of Single Crystals For Use as Detectors and Crystal Counters," ASTIA AD 79265.

65. Yamada, S., "On the Electrical and Optical Properties of n-type Cadmium Telluride Crystals," J. Phys. Soc. Japan 17, 645 (1962).

66. Marple, D. T. F., and B. Segall, "Optical Absorption Edge in CdTe: Experimental," Bull. Am.Phys. Soc. 9, 223 (1964).

67. Kanazawa, K. K., and F. C. Brown, "Cyclotron Resonance in Cadmium Telluride," Phys. Rev. 135, A1757 (1964).

68. DeNobel, D., "Phase Equilibria and Semiconducting Properties of Cadmium Telluride," Philips Res. Rept. 14, 361 (1959).

69. Fisher, P., and H. Y. Fan, "Infrared Properties and Effective Ionic Charge of CdTe," Bull. Am. Phys. Soc. 4, 409 (1959).

70. Marple, D. T. F., "Refractive Index of ZnSe, ZnTe, and CdTe," J. Appl. Phys. 35, 539 (1964).

71. Larach, S., R. E. Shrader, and C. F. Stocker, "Anomalous Variation of Band Gap with Composition in Zinc Sulfo- and Seleno-Tellurides," Phys. Rev. 108, 587 (1957).

72. Fischer, A. G., J. N. Carides, and J. Dresner, "Preparation and Properties of n-type ZnTe, Solid State Commun. 2, 157 (1964).

73. Berlincourt, D., H. Jaffe, and L. Shiozawa, "Electroelastic Properties of the Sulfides, Selenides, and Tellurides of Zinc and Cadmium," Phys. Rev. 129, 1009 (1963).

74. Itakura, M., and H. Toyoda, "Surface Properties of CdS Single Crystals," Japan J. Appl. Phys. 3, 197 (1964).

75. Bradberry, C. W., and W. E. Spear, "Electron Mobility and Edge Emission in CdS Crystals," Brit. J. Appl. Phys. 15, 1127 (1964).

76. Buget, U., and G. T. Wright, "Electron Energy Levels in Cadmium Sulfide Single Crystals," Brit. J. Appl. Phys. 16, 1457 (1965).

77. Kulp, B. A., R. M. Detweiler, and W. A. Anders, "Temperature Dependence of Edge Emission in Single Crystal Cadmium Sulfide," Phys. Rev. 131, 2036 (1963).

78. Faeth, P. A., "On the Trapping Level Disposition in Cadmium Sulfide," J. Electrochem. Soc. 115, 440 (1968).

79. Lorenz, M. R., and H. H. Woodbury, "Double Acceptor Defect in CdTe," Phys. Rev.Letters 10, 215 (1963).

80. Lorenz, M. R., and B. Segall, "Deep and Shallow Acceptor States in CdTe," Phys. Letters 7, 18 (1963).

81. Bube, R. H., and E. L. Lind, "Photoconductivity of Zinc Selenide Crystals and a Correlation of Donor and Acceptor Levels in II-VI Photoconductors," Phys. Rev. 110, 1040 (1958).

82. Crowder, B. L., and W. N. Hammer, "Shallow Acceptor States in ZnTe and CdTe," Phys. Rev. 150, 541 (1966).

83. Hartwig, W. H., private communication.

DISTRIBUTION LIST

Current AF-AFOSR Grant

Report on the Joint Services Electronics Program for period ending 31 March 1971

DEPARTMENT OF DEFENSE

Asst Director (Research) (1)
Office of Director of Defense Res. and Eng
Pentagon, Rm 3C128
Washington, D. C. 20301

Technical Library (1)
DDR&E
Room 3C-122, The Pentagon
Washington, D. C. 20301

Director for Materials Sciences (1)
Advanced Research Projects Agency
Room 3D179, Pentagon
Washington, D. C. 20301

Chief, R & D Division (340) (1)
Defense Communications Agency
Washington, D. C. 20305

Defense Documentation Center (50)
Attn: DDC-TCA
Cameron Station
Alexandria, Virginia 22314

Dr. Alvin D. Schnitzler (1)
Institute for Defense Analyses
Science and Technology Division
400 Army-Navy Drive
Arlington, Virginia 22202

Central Intelligence Agency (1)
Attn: CRS/ADD/Publications
Washington, D. C. 20505

M. A. Rothenberg (STEPD-SC (S)) (1)
Scientific Director
Deseret Test Center
Bldg 100, Soldiers' Circle
Fort Douglas, Utah 84113

DEPARTMENT OF THE AIR FORCE

Hq USAF (AFRDDD) (1)
The Pentagon
Washington, D. C. 20330

Hq USAF (AFRDDG) (1)
The Pentagon
Washington, D. C. 20330

Hq USAF (AFRDSD) (1)
The Pentagon
Washington, D. C. 20330
Attn: LTC C. M. Waespy

Colonel E. P. Gaines, Jr (1)
ACDA/FO
1901 Pennsylvania Avenue N. W.
Washington, D. C. 20451

LTC H. W. Jackson (SREE) (5)
Deputy Dir. of Elec. & Solid State Sciences
Air Force Office of Scientific Research
1400 Wilson Boulevard
Arlington, Virginia 22209

Mr. I. R. Mirman (1)
Hq AFSC (SGGP)
Andrews Air Force Base
Washington, D. C. 20331

Rome Air Development Center (1)
Attn: Documents Library (EMTLD)
Griffiss Air Force Base, New York 13440

Mr. H. E. Webb, Jr. (EMBIS) (1)
Rome Air Development Center
Griffiss Air Force Base, New York 13440

Dr. L. M. Hollingsworth (1)
AFCRL (CRN)
L. G. Hanscom Field
Bedford, Massachusetts 01730

Hq ESD (ESTI) (2)
L. G. Hanscom Field
Bedford, Massachusetts 01730

Professor R. E. Fontana, Head (1)
Dept of Electrical Engineering
Air Force Institute of Technology
Wright-Patterson AFB, Ohio 45433

Director (1)
Air Force Avionics Laboratory
Wright-Patterson AFB, Ohio 45433

AFAL (AVTA/R. D. Larson) (1)
Wright-Patterson AFB, Ohio 45433

Director of Faculty Research (1)
Department of the Air Force
U. S. Air Force Academy
Colorado 80840

Academy Library (DFSLB) (1)
USAF Academy, Colorado 80840

Director of Aerospace Mechanics Sciences (1)
Frank J. Seiler Research Laboratory (OAR)
USAF Academy, Colorado 80840

Major Richard J. Gowen (1)
Tenure Associate Professor
Dept. of Electrical Engineering
USAF Academy, Colorado 80840

Director, USAF PROJECT RAND (1)
Via: Air Force Liaison Office
The RAND Corporation
Attn: Library D
1700 Main Street
Santa Monica, California 90406

AFAL (AVT) Dr. H. V. Noble, Chief
Electronics Technology Division
Air Force Avionics Laboratory
Wright-Patterson AFB, Ohio 45433

Hq SAMSO (SMTAE/Lt Belate) (1)
AF Unit Post Office
Los Angeles, California 90045

AUL3T-9663 (1)
Maxwell AFB, Alabama 36112

AFETR Technical Library (1)
(ETV, MU-135)
Patrick AFB, Florida 32925

ADTC (ADBPS-12) (1)
Eglin AFB, Florida 32542

Mr. B. R. Locke (1)
Technical Advisor, Requirements
USAF Security Service
Kelly Air Force Base, Texas 78241

Hq AMD (AMR) (1)
Brooks AFB, Texas 78235

USAFSAM (SMKOR) (1)
Brooks AFB, Texas 78235

Commanding General (2)
Attn: STEWS-RE-L, Technical Library
White Sands Missile Range, New Mexico 88002

Hq AEDC (AETS) (1)
Arnold AFB, Tennessee 37389

European Office of Aerospace Research (1)
Technical Information Office
Box 14
FPO New York 09510

Electromagnetic Compatibility Analysis Center (1)
(ECAC) Attn: ACOAT
North Severn
Annapolis, Maryland 21402

VELA Seismological Center (1)
300 North Washington Street
Alexandria, Virginia 22314

Capt. C. E. Baum (1)
AFWL (WLRE)
Kirtland AFB, New Mexico 87117

DEPARTMENT OF THE ARMY

Director
Physical & Engineering Sciences Division (1)
3045 Columbia Pike
Arlington, Virginia 22204

Commanding General (1)
U. S. Army Security Agency
Attn: IARD-T
Arlington Hall Station
Arlington, Virginia 22212

Commanding General (1)
U. S. Army Materiel Command
Attn: AMCRD-TP
Washington, D. C. 20315

Director (1)
Advanced Materiel Concepts Agency
Washington, D. C. 20315

Commanding General (1)
USACDC Institute of Land Combat
Attn: Technical Library, Rm 636
2461 Eisenhower Avenue
Alexandria, Virginia 22314

Commanding Officer (1)
Harry Diamond Laboratories
Attn: Dr. Berthold Altman (AMXDO-TI)
Connecticut Ave and Van Ness Street N.W.
Washington, D. C. 20438

Commanding Officer (AMXRD-BAT) (1)
U. S. Army Ballistics Research Laboratory
Aberdeen Proving Ground
Aberdeen, Maryland 21005

Technical Director (1)
U. S. Army Land Warfare Laboratory
Aberdeen Proving Ground
Aberdeen, Maryland 21005

U. S. Army Munitions Command (1)
Attn: Science & Technology Information
Branch, Bldg 59
Picatinny Arsenal, SMUPA-RT-S
Dover, New Jersey 07801

U. S. Army Mobility Equipment Research (1)
and Development Center
Attn: Technical Documents Center, Bldg 315
Fort Belvoir, Virginia 22060

Commanding Officer (1)
U. S. Army Engineer Topographic Laboratories
Attn: STINFO Center
Fort Belvoir, Virginia 22060

Dr. Herman Robl (1)
Deputy Chief Scientist
U. S. Army Research Office (Durham)
Box CM, Duke Station
Durham, North Carolina 27706

Richard O. Ulsch (CRDARD-IP) (1)
U. S. Army Research Office (Durham)
Box CM, Duke Station
Durham, North Carolina 27706

Technical Director (SMUFA-A2000-107-1)
Frankford Arsenal (1)
Philadelphia, Pennsylvania 19137

Redstone Scientific Information Center (1)
Attn: Chief, Document Section
U. S. Army Missile Command
Redstone Arsenal, Alabama 35809

Commanding General (1)
U. S. Army Missile Command
Attn: AMSMI-RR
Redstone Arsenal, Alabama 35809

Commanding General (1)
U. S. Army Strategic Communications Command
Attn: SCC-CG-SAE
Fort Huachuca, Arizona 85613

Commanding Officer (1)
Army Materials and Mechanics Research Center
Attn: Dr. H. Priest
Watertown Arsenal
Watertown, Massachusetts 02171

Commandant (1)
U. S. Army Air Defense School
Attn: Missile Science Division, C & S Dept.
P. O. Box 9390
Fort Bliss, Texas 79916

Commandant (1)
U. S. Army Command and General Staff College
Attn: Acquisitions, Lib Div
Fort Leavenworth, Kansas 66027

Mr. Norman J. Field, AMSEL-RD-S (1)
Chief, Science and Technology Division
Research and Development Directorate
U. S. Army Electronics Command
Fort Monmouth, New Jersey 07703

Mr. Robert O. Parker, AMSEL-RD-S (1)
Executive Secretary, TAC-JSEP
U. S. Army Electronics Command
Fort Monmouth, New Jersey 07703

Commanding General (1)
U. S. Army Electronics Command
Fort Monmouth, New Jersey 07703
Attn: AMSEL-SC, DL, GG-DD, XL-D,
XL-DT, BL-FM-P, CT-D, CT-R, CT-S,
CT-L (Dr. W. S. McAfee), CT-O, CT-I
CT-A, NL-D (Dr. H. Bennett), NL-A,
NL-C, NL-P, NL-P-2, NL-R, NL-S,
KL-D, KL-I, KL-E, KL-S, KL-SM, KL-T,
VL-D, VL-F, WL-D

Director (NV-D) (1)
Night Vision Laboratory, USAECOM
Fort Belvoir, Virginia 22060

Commanding Officer (1)
Atmospheric Sciences Laboratory
U. S. Army Electronics Command
White Sands Missile Range, New Mexico 88002

* The Joint Services Technical Advisory Committee has established this list for the regular distribution of reports on the electronics research program of the University of Texas at Austin. Additional addresses may be included on their written request to:

Mr. Robert O. Parker (AMSEL-RD-S)

U. S. Army Electronics Command

Fort Monmouth, New Jersey 07703

An appropriate endorsement by a Department of Defense sponsor is required except on requests from a Federal Agency.

Commanding Officer (AMSEL-BL-WS-R) (1)
Atmospheric Sciences Laboratory
U. S. Army Electronics Command
White Sands Missile Range, New Mexico 88002

Chief (1)
Missile Electronics Warfare Tech. Area (AMSEL-WL-M)
Electronics Warfare Laboratory, USAECOM
White Sands Missile Range, New Mexico 88002

Project Manager NAVCOM (1)
Attn: AMCPM-NS-TM, Bldg 439 (H. H. Bahr)
Fort Monmouth, New Jersey 07703

DEPARTMENT OF THE NAVY

Director, Electronics Programs (3)
Attn: Code 427
Office of Naval Research
800 North Quincy Street
Arlington, Virginia 22217

Commander (1)
Naval Security Group Command
Naval Security Group Headquarters
Attn: Technical Library (G43)
3801 Nebraska Avenue, N.W.
Washington, D. C. 20390

Director
Naval Research Laboratory
Washington, D. C. 20390
Attn: Code 2027 (6)
Dr. W. C. Hall, Code 7000 (1)
Mr. A. Brodzinsky, Supt, Electronics Div (1)

Code 8050 (1)
Maury Center Library
Naval Research Laboratory
Washington, D. C. 20390

Dr. G. M. R. Windkler (1)
Director, Time Service Division
U. S. Naval Observatory
Washington, D. C. 20390

Naval Air Systems Command (2)
AIR 03
Washington, D. C. 20360

Naval Ship Systems Command (1)
Ship 031
Washington, D. C. 20360

Naval Ship Systems Command (1)
Ship 035
Washington, D. C. 20360

U. S. Naval Weapons Laboratory (1)
Dahlgren, Virginia 22448

Naval Electronic Systems Command (2)
ELEX 03, Rm 2534 Main Navy Bldg.
Department of the Navy
Washington, D. C. 20360

Commander (2)
U. S. Naval Ordinance Laboratory
Attn: Librarian
White Oak, Maryland 20910

Director (1)
Office of Naval Research
Boston Branch
495 Summer Street
Boston, Massachusetts 02210

Commander (ADL) (1)
Naval Air Development Center
Attn: NADC Library
Johnsville, Warminster, Pennsylvania 18974

Commander (Code 753) (1)
Naval Weapons Center
Attn: Technical Library
China Lake, California 93555

Commanding Officer (1)
Naval Weapons Center
Corona Laboratories
Attn: Library
Corona, California 91720

Commanding Officer (56322) (1)
Naval Missile Center
Point Mugu, California 93041

W. A. Eberspacher, Associate Head (1)
Systems Integration Division, Code 5340A
U. S. Naval Missile Center
Point Mugu, California 93041

Commander (2)
Naval Electronics Laboratory Center
Attn: Library
San Diego, California 92152

Deputy Director and Chief Scientist (1)
Office of Naval Research Branch Office
1030 East Green Street
Pasadena, California 91101

Library (Code 2124) (1)
Technical Report Section
Naval Postgraduate School
Monterey, California 93940

Glen A. Myers (Code 52 Mv) (1)
Assoc. Professor of Electrical Engineering
Naval Postgraduate School
Monterey, California 93940

Commanding Officer (Code 2064) (1)
Navy Underwater Sound Laboratory
Fort Trumbull
New London, Connecticut 06320

Commanding Officer (1)
Naval Avionics Facility
Indianapolis, Indiana 46241

Director (2)
Naval Research Laboratory
Attn: Library, Code 2029 (ONRL)
Washington, D. C. 20390

Director (1)
Office of Naval Research Branch Office
219 South Dearborn Street
Chicago, Illinois 60604

OTHER GOVERNMENT AGENCIES

Dr. H. Harrison Code RRE (1)
Chief, Electrophysics Branch
National Aeronautics and Space Administration
Washington, D. C. 20546

NASA Lewis Research Center (1)
Attn: Library
21000 Brookpark Road
Cleveland, Ohio 44135

Los Alamos Scientific Laboratory
Attn: Reports Library
P. O. Box 1663
Los Alamos, New Mexico 87544

Mr. M. Zane Thornton, Chief
Network Engineering, Communications and Operations Branch
Lister Hill National Center for Biomedical Communications
8600 Rockville Pike
Bethesda, Maryland 20014

U. S. Post Office Department (1)
Library - Room 6012
12th & Pennsylvania Ave. N. W.
Washington, D. C. 20260

Dr. J. Ryland Mundie (HRBB) (1)
Chief, Neurophysiology Branch
Biodynamics & Bionics Division
6570th Aerospace Medical Research Labs.
Wright-Patterson AFB, Ohio 45433

NON-GOVERNMENT AGENCIES

Director (1)
Research Laboratory of Electronics
Massachusetts Institute of Technology
Cambridge, Massachusetts 02139

Mr. Jerome Fox, Research Coordinator (1)
Polytechnic Institute of Brooklyn
333 Jay Street
Brooklyn, New York 11201

Director (1)
Columbia Radiation Laboratory
Columbia University
538 West 120th Street
New York, New York 10027

Director (1)
Coordinated Science Laboratory
University of Illinois
Urbana, Illinois 61801

Director (1)
Stanford Electronics Laboratories
Stanford University
Stanford, California 94305

Director (1)
Microwave Physics Laboratory
Stanford University
Stanford, California 94305

Director (1)
Electronics Research Laboratory
University of California
Berkeley, California 94720

Director (1)
Electronics Sciences Laboratory
University of Southern California
Los Angeles, California 90007

Director (1)
Electronics Research Center
The University of Texas at Austin
Austin, Texas 78712

Division of Engineering and Applied Physics (1)
210 Pierce Hall
Harvard University
Cambridge, Massachusetts 02138

Dr. G. J. Murphy (1)
The Technological Institute
Northwestern University
Evanston, Illinois 60201

Dr. John C. Hancock, Head (1)
School of Electrical Engineering
Purdue University
Lafayette, Indiana 47907

Dept. of Electrical Engineering (1)
Texas Technological College
Lubbock, Texas 79409

Aerospace Corporation (1)
P. O. Box 95085
Los Angeles, California 90045
Attn: Library Acquisitions Group

Airborne Instruments Laboratory (1)
Deerpark, New York 11729

The University of Arizona (1)
Dept. of Electrical Engineering
Tucson, Arizona 85721

Chairman, Electrical Engineering (1)
Arizona State University
Tempe, Arizona 85281

Engineering & Mathematical Sciences Library (1)
University of California at Los Angeles
405 Hilgred Avenue
Los Angeles, California 90024

Sciences - Engineering Library (1)
University of California
Santa Barbara, California 93106

Professor Nicholas George (1)
California Institute of Technology
Pasadena, California 91109

Aeronautics Library (1)
Graduate Aeronautical Laboratories
California Institute of Technology
1201 E. California Blvd.
Pasadena, California 91109

Hunt Library (1)
Carnegie-Mellon University
Schenley Park
Pittsburgh, Pennsylvania 15213

Dr. A. G. Jordon (1)
Head of Dept. of Electrical Engineering
Carnegie-Mellon University
Pittsburgh, Pennsylvania 15213

Case Institute of Technology (1)
Engineering Division
University Circle
Cleveland, Ohio 44106

Hollandar Associates (1)
P. O. Box 2276
Fullerton, California 92633
Attn: Librarian

Dr. Sheldon J. Welles (1)
Electronic Properties Information Center
Mail Station E-175
Hughes Aircraft Company
Culver City, California 90230

Illinois Institute of Technology (1)
Department of Electrical Engineering
Chicago, Illinois 60616

Government Documents Dept. (1)
University of Iowa Libraries
Iowa City, Iowa 52240

New York University (1)
Engineering Library
Bronx, New York 10453

Utah State University (1)
Dept. of Electrical Engineering
Logan, Utah 84321

Professor James A. Godzow (1)
Dept. of Electrical Engineering
State University of New York at Buffalo
Buffalo, New York 14214

Dept. of Electrical Engineering (1)
Clippinger Laboratory
Ohio University
Athens, Ohio 45701

Raytheon Company (1)
Research Division Library
28 Seyon Street
Waltham, Massachusetts 02154

Dept. of Electrical Engineering (1)
Rice University
Houston, Texas 77001

Dr. Leo Young (1)
Stanford Research Institute
Menlo Park, California 94025

The Johns Hopkins University (1)
Applied Physics Laboratory
Attn: Document Librarian
8621 Georgia Avenue
Silver Spring, Maryland 20910

Lehigh University (1)
Department of Electrical Engineering
Bethlehem, Pennsylvania 18015

Lenkurt Electric Co., Inc. (1)
1105 County Road
San Carlos, California 94070
Attn: Mr. E. K. Peterson

Lincoln Laboratory (1)
Massachusetts Institute of Technology
P. O. Box 73
Lexington, Massachusetts 02173

Miss. R. Joyce Harmon (1)
Project MAC, Room 810
545 Main Street
Cambridge, Massachusetts 02139

Professor R. H. Rediker (1)
Electrical Engineering, Professor
Mass. Institute of Technology
Building 13-3050
Cambridge, Massachusetts 02139

Professor Joseph E. Rowe (1)
Chairman, Dept. of Electrical Engineering
The University of Michigan
Ann Arbor, Michigan 48104

Sylvania Electronic Systems (1)
Applied Research Laboratory
Attn: Documents Librarian
40 Sylvan Road
Waltham, Massachusetts 02154

Syracuse University (1)
Dept. of Electrical Engineering
Syracuse, New York 13210
Attn: Dr. W. R. LePage, Chairman

Dr. F. R. Charvat (1)
Union Carbide Corporation
Materials Systems Division
Crystal Products Department
8888 Balboa Avenue
P. O. Box 23017
San Diego, California 92123

Research Laboratories for the Engineering Sciences (1)
School of Engineering and Applied Science
University of Virginia
Charlottesville, Virginia 22903

Yale University (1)
Engineering Department
New Haven, Connecticut 06520

UNCLASSIFIED
Security Classification

DOCUMENT CONTROL DATA - R&D

(Security classification of title, body of abstract and indexing annotation must be entered when the overall report is classified)

1 ORIGINATING ACTIVITY (Corporate author)	2a. REPORT SECURITY CLASSIFICATION
The University of Texas at Austin Electronics Research Center Austin, Texas 78712	UNCLASSIFIED
	2b. GROUP

3. REPORT TITLE

ANALYSIS OF LOW TEMPERATURE TRAPPING AND RECOMBINATION IN II-VI COMPOUNDS USING PHOTODIELECTRIC TECHNIQUES

4. DESCRIPTIVE NOTES (Type of report and inclusive dates)

Scientific Interim

5. AUTHOR(S) (Last name, first name, initial)

James J. Hinds
William H. Hartwig

6. REPORT DATE	7a. TOTAL NO. OF PAGES	7b. NO. OF REFS
19 June 1970	156	83

8a. CONTRACT OR GRANT NO.	9a. ORIGINATOR'S REPORT NUMBER(S)
AFOSR 69-1792	JSEP, Technical Report No. 90
b. PROJECT NO. 4751	
c. 61102F	9b. OTHER REPORT NO(S) (Any other numbers that may be assigned this report) AFOSR-70-
d. 681305	

10. AVAILABILITY/LIMITATION NOTICES

1. This document has been approved for public release and sale; its distribution is unlimited.

11. SUPPLEMENTARY NOTES	12. SPONSORING MILITARY ACTIVITY
TECH, OTHER	JSEP through AF Office of Scientific Research (SREE) 1400 Wilson Boulevard Arlington, Virginia 22209

13. ABSTRACT

In II-VI compounds at cryogenic temperatures, the photodielectric (PD) effect is the result of optically-induced changes in the densities of free and trapped carriers. Changes in both the real and imaginary parts of the complex dielectric constant are observable when the semiconductor is placed in a superconducting microwave cavity and irradiated with light. A change in the real part of the dielectric constant results in a sizeable change in the cavity resonant frequency, while a change in the imaginary part of the dielectric constant produces a change in the microwave power absorbed by the semiconductor. Equations are presented which relate the frequency change and power absorption change to the densities and binding energies of trapped carriers, and to the density of free carriers. The PD technique gives a direct measurement of both the free carrier density and the trapped carrier density.

Models involving trapping and recombination centers with selected properties are analyzed to reveal the relations between carrier densities and other physical characteristics of the sample. Equations are written in forms which allow capture cross sections, recombination cross sections, trap ionization energies, and trap densities to be calculated from the time and temperature variations of the free and trapped carrier densities.

Samples of CdS:Al, CdS:Ag, CdTe, and ZnTe are analyzed, both with PD techniques and with other techniques such as thermally stimulated conductivity, and values for trap depths, densities, and capture cross sections are obtained and compared. In most cases where a comparison of methods is possible, results from the different techniques agree. In the remainder of the cases, photodielectric data, which gives a direct observation of trapped carrier behavior, gives significantly improved accuracy compared to the other techniques where trapped carrier behavior is only obtained indirectly. Results presented demonstrate that PD response spectra yield values for bandgaps and trap ionization energies. The time variation of the photodielectric response is used to reveal several traps which exist in one sample, and to separate trapped carrier effects from free carrier behavior. The direct observation of trap filling and emptying yields sufficient data to calculate trap depths, densities, and cross sections. The temperature dependence of the PD response gives additional information concerning trap ionization energies and cross sections. Data from the variation of the response with respect to light intensity greatly simplifies the choice of an energy band model.

It is demonstrated that in some cases, a photodielectric experiment is clearly more sensitive than other techniques, such as photoconductivity analysis, applied to the same material. The PD method is contactless, eliminating all of the problems associated with making ohmic contacts. The successful application of PD techniques to a powdered sample is demonstrated. Even when the PD method is applied to single crystal samples, the fact that the behavior of trapped carriers is directly observed means that the method greatly improves an experimenter's ability to analyze and measure trapping and recombination parameters.

DD FORM 1473 JAN 64

UNCLASSIFIED
Security Classification

14. KEY WORDS	LINK A		LINK B		LINK C	
	ROLE	WT	ROLE	WT	ROLE	WT
CRYOGENIC PROPERTIES						
PHOTODIELECTRIC EFFECT						
OPTICAL PROPERTIES						
SEMICONDUCTOR PARAMETERS						
TRAPPING AND RECOMBINATION						
II-VI COMPOUNDS						

INSTRUCTIONS

1. ORIGINATING ACTIVITY: Enter the name and address of the contractor, subcontractor, grantee, Department of Defense activity or other organization *(corporate author)* issuing the report.

2*a*. REPORT SECURITY CLASSIFICATION: Enter the overall security classification of the report. Indicate whether "Restricted Data" is included. Marking is to be in accordance with appropriate security regulations.

2*b*. GROUP: Automatic downgrading is specified in DoD Directive 5200.10 and Armed Forces Industrial Manual. Enter the group number. Also, when applicable, show that optional markings have been used for Group 3 and Group 4 as authorized.

3. REPORT TITLE: Enter the complete report title in all capital letters. Titles in all cases should be unclassified. If a meaningful title cannot be selected without classification, show title classification in all capitals in parenthesis immediately following the title.

4. DESCRIPTIVE NOTES: If appropriate, enter the type of report, e.g., interim, progress, summary, annual, or final. Give the inclusive dates when a specific reporting period is covered.

5. AUTHOR(S): Enter the name(s) of author(s) as shown on or in the report. Enter last name, first name, middle initial. If military, show rank and branch of service. The name of the principal author is an absolute minimum requirement.

6. REPORT DATE: Enter the date of the report as day, month, year; or month, year. If more than one date appears on the report, use date of publication.

7*a*. TOTAL NUMBER OF PAGES: The total page count should follow normal pagination procedures, i.e., enter the number of pages containing information.

7*b*. NUMBER OF REFERENCES: Enter the total number of references cited in the report.

8*a*. CONTRACT OR GRANT NUMBER: If appropriate, enter the applicable number of the contract or grant under which the report was written.

8*b*, 8*c*, & 8*d*. PROJECT NUMBER: Enter the appropriate military department identification, such as project number, subproject number, system numbers, task number, etc.

9*a*. ORIGINATOR'S REPORT NUMBER(S): Enter the official report number by which the document will be identified and controlled by the originating activity. This number must be unique to this report.

9*b*. OTHER REPORT NUMBER(S): If the report has been assigned any other report numbers *(either by the originator or by the sponsor)*, also enter this number(s).

10. AVAILABILITY/LIMITATION NOTICES: Enter any limitations on further dissemination of the report, other than those imposed by security classification, using standard statements such as:

(1) "Qualified requesters may obtain copies of this report from DDC."

(2) "Foreign announcement and dissemination of this report by DDC is not authorized."

(3) "U. S. Government agencies may obtain copies of this report directly from DDC. Other qualified DDC users shall request through _____."

(4) "U. S. military agencies may obtain copies of this report directly from DDC. Other qualified users shall request through _____."

(5) "All distribution of this report is controlled. Qualified DDC users shall request through _____."

If the report has been furnished to the Office of Technical Services, Department of Commerce, for sale to the public, indicate this fact and enter the price, if known.

11. SUPPLEMENTARY NOTES: Use for additional explanatory notes.

12. SPONSORING MILITARY ACTIVITY: Enter the name of the departmental project office or laboratory sponsoring *(paying for)* the research and development. Include address.

13. ABSTRACT: Enter an abstract giving a brief and factual summary of the document indicative of the report, even though it may also appear elsewhere in the body of the technical report. If additional space is required, a continuation sheet shall be attached.

It is highly desirable that the abstract of classified reports be unclassified. Each paragraph of the abstract shall end with an indication of the military security classification of the information in the paragraph, represented as *(TS)*, *(S)*, *(C)*, or *(U)*.

There is no limitation on the length of the abstract. However, the suggested length is from 150 to 225 words.

14. KEY WORDS: Key words are technically meaningful terms or short phrases that characterize a report and may be used as index entries for cataloging the report. Key words must be selected so that no security classification is required. Identifiers, such as equipment model designation, trade name, military project code name, geographic location, may be used as key words but will be followed by an indication of technical context. The assignment of links, rules, and weights is optional.

GPO 886-551